Structural and functional characterization of the HPV16 entry platform on the cell surface

Dissertation

zur

Erlangung des Doktorgrades (Dr. rer. nat)

der

Mathematisch-Naturwissenschaftlichen Fakultät

der

Rheinischen Friedrich-Wilhelms-Universität Bonn

vorgelegt von

Jérôme Finke

aus

Hoya

Bonn 2020

Angefertigt mit Genehmigung der Mathematisch-Naturwissenschaftlichen Fakultät der Rheinischen Friedrich-Wilhelms-Universität Bonn

1. Gutachter: Prof. Dr. Thorsten Lang

2. Gutachter: Prof. Dr. Eva Kiermaier

Tag der Promotion: 30.10.2020

Erscheinungsjahr: 2020

Eidesstattliche Erklärung

Hiermit versichere ich, dass ich die vorliegende Dissertation eigenständig und ohne unerlaubte Hilfe angefertigt habe. Es wurden keine anderen als die angegebenen Hilfsmittel verwendet. Direkt oder indirekt übernommenes Gedankengut wurde nach bestem Wissen und Gewissen kenntlich gemacht. Die Arbeit liegt in dieser oder ähnlicher Form keiner anderen Prüfungsbehörde vor.

_____

(Datum) (Unterschrift)

Anmerkung

Teile dieser Arbeit wurden bereits in folgenden Publikationen veröffentlicht:

Mikuličić, S., **Finke, J.**, Boukhallouk, F., Wüstenhagen, E., Sons, D., Homsi, Y., Reiss, K., Lang, T., Florin, L. ADAM17-dependent signaling is required for oncogenic human papillomavirus entry platform assembly. *eLife* **8**; 10.7554/eLife.44345 (2019).
In Teilen verwendet in Methoden (Abschnitt 4.2.11) und Ergebnissen (Abschnitt 5.1.1, 5.1.4 und 5.3.3).

Finke, J., Mikuličić, S., Loster, A-L., Gawlitza, A., Florin, L., Lang, T. Anatomy of a viral entry platform differentially functionalized by integrins α3 and α6. *Scientific reports* **10,** 5356; 10.1038/s41598-020-62202-9 (2020).
In Teilen verwendet in Methoden (Abschnitt 4.2.1 – 4.2.11), Ergebnissen (Abschnitt 5.1 und 5.2) und Diskussion.

Finke, J., Hitschler, L., Boller, K., Florin, L. & Lang, T. HPV caught in the tetraspanin web? *Medical microbiology and immunology*; 10.1007/s00430-020-00683-1 (2020).
In Teilen verwendet in Methoden (Abschnitt 4.2.1, 4.2.2, 4.2.10 und 4.2.11), Ergebnissen (Abschnitt 5.3) und Diskussion.

Table of contents

List of Figures

List of Tables

Abbreviations

a.u.	arbitrary units
A2t	annexin A2 heterotetramer
ADAM	a disintegrin and metalloprotease
BSA	bovine serum albumin
CFP	cyan fluorescent protein
CHAPS	3-[(3-cholamidopropyl)dimethyl-ammonio]-1-propanesulfonate
CMV	cytomegalovirus
D	diffusion coefficient
$_{dd}H_20$	double distilled water
DMEM	Dulbecco's Modified Eagle Medium
DMSO	dimethyl sulfoxide
DNA	deoxyribonucleic acid
DPBS	Dulbecco's phosphate-buffered saline
ECM	extracellular matrix
EdU	5-Ethinyl-2'-desoxyuridine
EGF	epidermal growth factor
EGFR	epidermal growth factor receptor
EM	electron microscopy
ER	endoplasmatic reticulum
ESCRT	endosomal sorting complexes required for transport
FAK	focal adhesion kinase
FWHM	full width at half maximum
GFP	green fluorescent protein
GFR	growth factor receptor
HCV	hepatitis C virus
HIV	human immunodeficiency virus
HPV	human papillomavirus
HS	heparan sulfate
HSPG	heparan sulfate proteoglycan
HSV	herpes simplex virus
IF	immunofluorescence
KGFR	keratinocyte growth factor receptor

LEL	large extracellular loop
mAbs	monoclonal antibodies
MEM	Minimum Essential Medium Eagle
MERS	Middle East respiratory syndrome
mRNA	messenger ribonucleic acid
MSD	mean square displacement
OBSL1	obscurin-like protein 1
ori	origin of replication
PBS	phosphate buffered saline
PBS-T	phosphate buffered saline with 0.1 % Tween-20
PCC	Pearson correlation coefficient
PFA	paraformaldehyde
PI3K	phosphoinositide-3 kinase
PLL	poly-L-lysine
PSF	point spread function
PsV	pseudovirus
RFP	red fluorescent protein
ROI	region of interest
RT	room temperature
RT-PCR	reverse transcription polymerase chain reaction
SD	standard deviation
SDS	sodium dodecyl sulfate
SDS-PAGE	sodium dodecyl sulfate polyacrylamide gel electrophoresis
SEL	small extracellular loop
SEM	standard error of the mean
siRNA	small interfering ribonucleic acid
STED	stimulated emission depletion
TEM	tetraspanin enriched microdomain
TIRF	total internal reflection fluorescence
TMA-DPH	1-(4-tri-methyl-ammonium-phenyl)−6-phenyl-1,3,5-hexatriene p-toluene-sulfonate
UV	ultraviolet
vge	viral genome equivalents
WB	Western blot

1 Summary

Human papillomaviruses (HPV) are small, non-enveloped DNA viruses that infect skin and mucosa tissues. Among the family, HPV16 is one of the most oncogenic subtypes responsible for a variety of cancers, including cervical, anal and head and neck cancers. HPV internalization is a slow and asynchronous process involving many steps and host cell factors. Among these factors is the tetraspanin CD151, which is essential for HPV infection. In microscopy, it colocalizes with viral particles on the cell surface. Moreover, CD151 associates with other host cell factors, notably laminin-binding integrins. While integrin α6 is accepted to have a role during infection, the involvement of integrin α3 remains controversial.

In this study, HPV16 pseudoviruses (PsVs) associated with large assemblies of CD151 at the plasma membrane were studied. Superresolution microscopy revealed that those assemblies are crowds of closely arranged CD151 nanodomains. It could also be observed that integrin α3 and integrin α6 clusters both associate with these nanodomains. CD151 and integrin nanodomains segregate with only their margins being in contact with each other rather than concentrating in the same cluster to form a homogenous protein mixture. In line with this, integrin clusters were similarly densely packed in the PsV associated CD151 assemblies.

Moreover, the functionality of integrin α3 and integrin α6 for HPV infection was verified in a keratinocyte cell model. As in accordance with literature, integrin α6 is a proviral factor mediating host cell binding. More importantly, a role in HPV entry was demonstrated for integrin α3 as well. Integrin α3 mediates internalization rather than virus binding, as knockdown of the protein hardly affected PsV binding but all analysed post-binding steps were reduced. The CD151 assemblies were sites of actin accumulation. Overexpression of tetraspanins seemed to enhance the occurrence and size of the assemblies, possibly by enhancing the availability of TEM components at the cell surface.

Viral entry platforms were shown to be enriched with another tetraspanin, CD63, which is required for intracellular trafficking of the virus. These platforms seem to be very variable in size, invaginating to the cell interior and reaching up to a few micrometres under overexpressing conditions. Moreover, the cytoskeletal adaptor protein OBSL1 was identified as a putative platform component possibly acting as a linker of the platform to cytoskeletal dynamics needed for internalization. Preliminary data indicate that OBSL1 may be recruited to early endocytic structures at the plasma membrane.

Thus, it was concluded that CD151 organizes viral entry platforms containing integrin α3 and α6, forming cluster crowds that associate with viral particles, while both integrins have different functions in viral entry. The crowds also contain additional components like CD63 and actin and may be linked to the cytoskeleton via OBSL1. Since numerous viruses utilize TEMs for viral entry, the concept of a tetraspanin scaffolding several host cell factors to build up an entry platform could be a general model for cell surface architectures utilized by viral particles.

2 Introduction

2.1 Viruses

Viruses are parasitic biological entities that are not considered to be living organisms by most definitions and are very diverse in their characteristics. They can have a DNA or RNA based genome with single- or double-stranded nucleic acids, which is encapsidated by a protein shell called viral capsid. Some viruses have an additional envelope composed of a lipid bilayer and viral membrane proteins. Viruses can be quite variable in size and range from the very small 17 nm sized porcine circovirus [1] to the recently discovered tupanviruses with mean sizes of 1.2 µm [2], which is bigger than numerous bacteria. Regardless of their structural feature, all viruses have one thing in common: they have no metabolism of their own and rely on host cells for their replication.

Viruses are known to infect all domains of life. However, their origin remains controversial. Three models for their evolution are currently discussed [3]. The “virus-first” hypothesis, which is based on the lack of cellular homologues for genes of most viruses, claims that viruses were already present before the emergence of cellular organisms. The “reduction hypothesis” states that viruses were originally parasitic cellular organisms that lost their own metabolic activity during their evolution, an assumption supported by the recent discovery of giant viruses that share features of some known parasitic bacteria. The last hypothesis, called “escape hypothesis”, postulates that viruses were once a part of the host cell genome that escaped cellular control and evolved by getting new genes via horizontal gene transfer.

No matter of their evolutionary origin or their structural characteristics, all viruses need to bind to their host cell, get access to the cell interior for replication and escape from their host in order to infect new cells. For all these steps, they also rely on a distinct set of host cell factors.

2.2 The HPV life cycle

All HPVs (human papilloma viruses) are small non-enveloped viruses containing a double stranded DNA genome that encodes for six non-structural proteins (E1, E2, E4, E5, E6 and E7) and two structural proteins (L1 and L2) that form the viral capsid. To date, more than 150 HPV types have been identified in humans. Additionally, dozens of PVs are known to infect other vertebrates. They were classified into five genera based on their DNA sequence homology (see Figure 2.1). Many of these viruses were observed to cause only asymptomatic or benign infections in healthy individuals, indicating that those HPV types are well-adapted to their human host [4]. This characteristic suggests that PVs have evolved with their hosts over a very long period of time. A recent phylogenetic analysis indicates that the most recent common ancestor of the PV backbone, consisting of E1, E2, L1 and L2, can be dated back to 424 million years ago [5].

Within the phylogenetic tree, the genus Alpha papillomavirus comprises some of the best studied genotypes. This genus includes low-risk and high-risk HPVs. HPVs infect epithelial cells with genotype specific tropism with most types infecting cutaneous or mucosal tissues. Low-risk HPVs are associated with asymptomatic infections and benign tissue lesions such as different types of warts and other skin abnormities [6]. These cutaneous lesions are quite common but in general self-limiting, not life threatening and can be cleared by the immune system. In contrast to high-risk HPVs, these viruses are not linked with malignant transformation, except for some immunosuppressed individuals [6]. A report from 2017 estimated that HPVs contribute to 4.5 % of all cancers worldwide [7]. The overwhelming majority of all cervical cancers is attributed to HPVs, with high-risk types HPV16 and HPV18 together causing 71 % of all cervical carcinoma.

Productive infection of HPVs is thought to require a microwound of the multi-layered epithelium in order for the viral particles to get access to the basal cell layer where

they infect basal keratinocytes [8]. After binding to host cells, the viral capsid undergoes conformational changes. A complex cascade of events, involving numerous host cell factors, precedes the formation of an entry receptor complex and endocytosis of the viral particles [9].

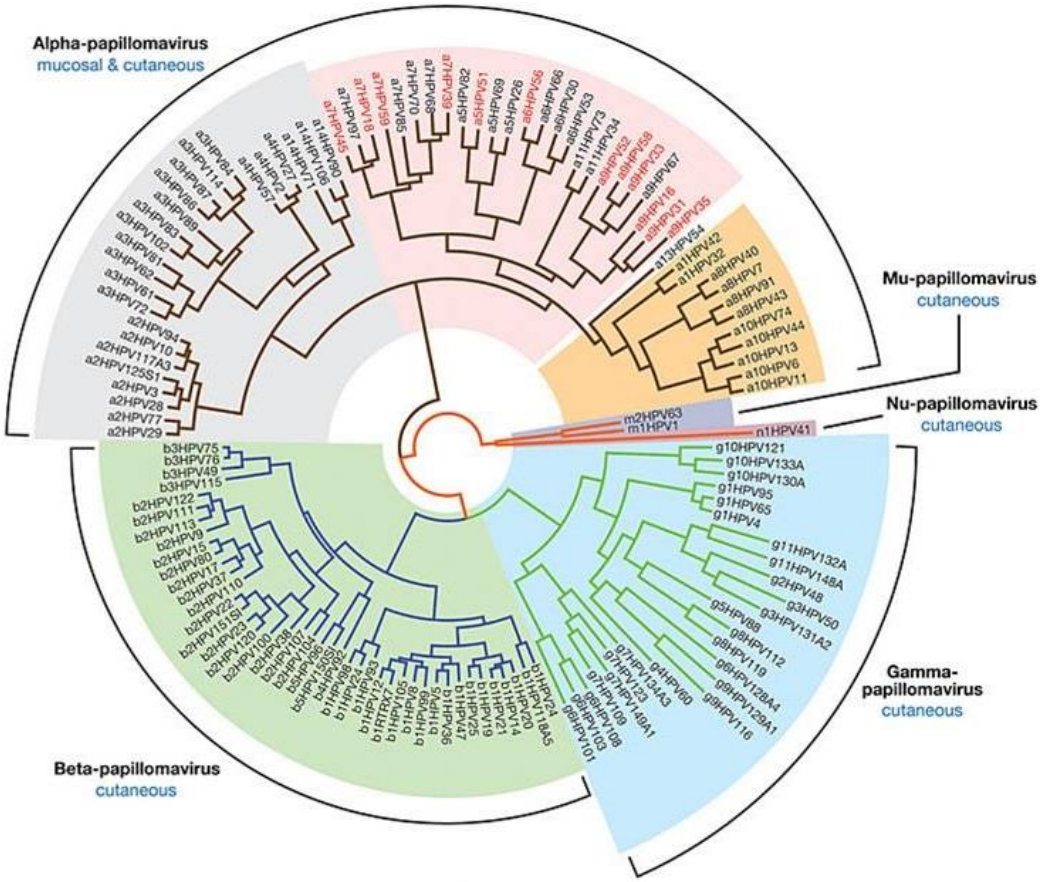

Figure 2.1 The Phylogenetic tree of human papillomaviruses
Human papillomaviruses are classified in five genera. The Alpha genus is the largest group. Strains from this genus can be divided into low-risk cutaneous and mucosal types, and high-risk types like HPV16, which are represented in grey, orange and pink, respectively. Figure taken and modified from reference [10].

After endocytosis, viral particles are directed to multivesicular bodies [9] for capsid disassembly. For HPV to get access to the nucleus where viral replication and transcription occurs, infected cells need to undergo cell cycle progression with breakdown of the nuclear envelope [11,12]. Hence, productive infection (see Figure 2.2) requires uptake of viruses into mitotically active cells.

Genome replication is initiated via E1, the only HPV protein displaying enzymatic activity. E1 assembles at the viral origin of replication (ori) [13]. Efficient genome amplification requires the presence of E2, which acts as a loading factor by simultaneously binding to E1- and E2-binding sites in the viral genome. E1 then initiates genome replication via helicase activity by unwinding the DNA strand [13]. In addition, E1 binds to several proteins of the host cell replication machinery to enable viral DNA amplification [13]. Beside its role in initiating genome replication, E2 also has a major role in regulating viral gene transcription.

The viral gene expression is tightly controlled by the keratinocyte differentiation status. Two main viral promoters have been identified: the early promoter within the regulatory and non-coding long control region that appears to be constitutively active and the late promoter located within the E7 ORF, which is regulated by the cell differentiation status. Beside these two dominant promoters, several other promoters have been found in various HPVs, which highlights the complexity of the viral transcription regulation [14].

The E6 and E7 proteins are expressed soon after infection from the early promoter in the lower epithelial layers [15]. In high-risk HPVs, E6 and E7 are thought to drive cell cycle progression and proliferation and to bind tumour suppressor proteins, which in turn induce their degradation [16]. By driving cell proliferation, they promote viral genome amplification. HPV genome can integrate into the host cell DNA, occasionally disrupting the E2 gene, which normally represses the expression of E6 and E7. In turn, the oncogenic proteins E6 and E7 accumulate, promoting cancer formation [10].

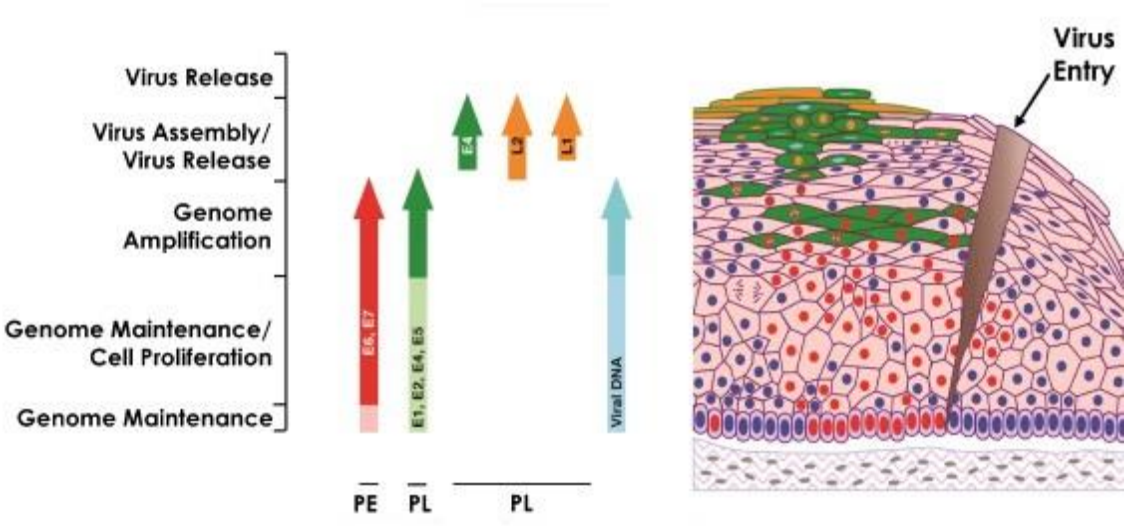

Figure 2.2 The productive life cycle of high-risk HPVs
A microwound allows HPV to access the basal cells of a multi-layered epithelium. In the infected basal cells, the viral genome is maintained at low copy numbers. Subsequent cellular division pushes daughter cells to the above lying epithelial layers. The migration process leads to life cycle progression of the virus. In the lower epithelial layers, cell cycle progression and division is triggered by the expression of viral E6 and E7 genes (cells marked by red nuclei). Genome amplification takes place in mid layers, as proteins from the DNA replication machinery and E4 accumulate (E4 expressing cells marked in green). In the E4-positive cells of the uppermost epithelial layers, the structural capsid proteins L2 and L1 proteins are produced and the viral genomes are packed into the capsid. The arrows on the left side of the figure mark the site of the epithelium where viral proteins are expressed and the different events of the HPV life cycle are listed alongside. The main promotors involved in HPV gene expression are PE: Early promoter, also known as p97 and PL: late promoter, also known as p670. Figure taken and modified from reference [4].

As keratinocyte differentiation is progressing, expression of the E4 protein becomes upregulated [15]. It is thought to facilitate genome amplification, virus assembly and release [17]. Just like E4, the production of E5 is upregulated during tissue differentiation but at much lower concentrations. E5 is a transmembrane protein that predominantly localizes to ER and Golgi membranes [18] and is thought to be oncogenic. However, E5 is not expressed in all HPV types.

Production of the capsid proteins L1 and L2 takes place in the terminally differentiating keratinocytes of the uppermost epidermal layers. The production is thought to be dependent on upregulation of the late promoter and more importantly on a switch in the splice sites of the polycistronic mRNA [10,15]. L1 and L2 translocate to the nucleus where genome amplification takes place and the viral genome is packed into the self-assembling viral capsid [19]. The oxidative environment in the upper epithelial layer then allows for the formation of the stabilizing disulphide bonds in the viral capsid [20].

2.3 Structure of the human papillomavirus

The L1 protein has a size of approximately 55 kDa. It has the ability to spontaneously form pentamers, which in turn self-assemble to form the viral capsid comprising 72 pentamers. This assembly process is solely dependent on the presence of L1 molecules and does not require any activity of chaperones or other molecules [21]. The capsid is approximately 60 nm in diameter and displays an icosahedral structure [22].

High-resolution cryoelectron microscopy reveals that the capsid has a knobby surface (see Figure 2.3) with each knob representing one L1 pentamer [23]. The N- and C-terminal ends of the L1 molecule form the valley between the pentameric knobs [24,25]. Each C-terminus wraps up the surface of a neighbouring pentamer, forming a so-called invading arm. In consequence, each pentamer receives and donates five C-terminal arms from and to neighbouring pentamers, respectively [24]. The capsid of most papillomaviruses is stabilized by disulphide bonds between the pentamers [26,27].

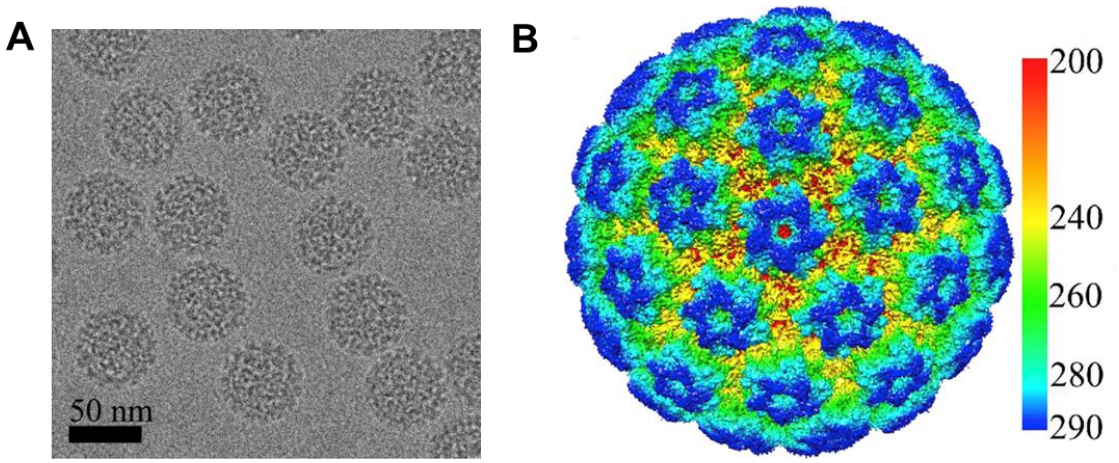

Figure 2.3 High resolution cryo-EM reconstruction of the HPV16 capsid
(A) Representative cryo-EM micrograph of the HPV16 capsid. The particles display a homogenous size of approximately 60 nm. (B) Surface rendered 3D-reconstruction of the HPV16 capsid. The colour indicates the distance from the capsid centre in angstroms. L1-pentamers are visible as knobs protruding from the capsid surface. Figure taken and modified from reference [28].

The L1 protein forms an 8-stranded β-jelly roll structure with prominent loops connecting the individual β-strands (see Figure 2.4). These loop structures are found on the outward top of the pentameric knob and contain the epitopes for most neutralizing antibodies [29]. However, some antibodies were described that detect L1 only after conformational changes or disassembly of the capsid [30,31].

While the majority of the viral capsid is composed of L1, it also contains the minor capsid protein L2, which is also ~ 55 kDa in size but lacks the ability to self-assemble to form viral particles. However, it is co-assembled with L1 in the viral capsid. The HPV capsid can contain up to 72 copies of L2, but naturally produced virions seem to contain substantially lower amounts [32]. It is assumed that most parts of the L2-molecule are hidden under the surface of native viral particles [32].

Both capsid proteins display DNA binding activity. They have short conserved sequences of positively charged amino acids that can interact with negatively charged DNA in the C-terminus of L1 and in the C- and N-termini of L2. However, this DNA-

binding activity does not seem to be sequence specific, enabling package of a reporter construct in the viral capsid in order to create so-called pseudoviruses (PsVs) [33]. While it is possible to pack DNA into HPV16 L1-only capsids, L2 seems to be required for intracellular-trafficking of the packaged DNA to the *trans*-Golgi network [34] and subsequent accumulation in the nucleus [35]. The L2-DNA interaction appears to be important for the viral genome to escape from late endosomes, which is an important step in HPV infection [36]. This escape is achieved by a membrane-destabilizing peptide within the C-terminus of L2 [37].

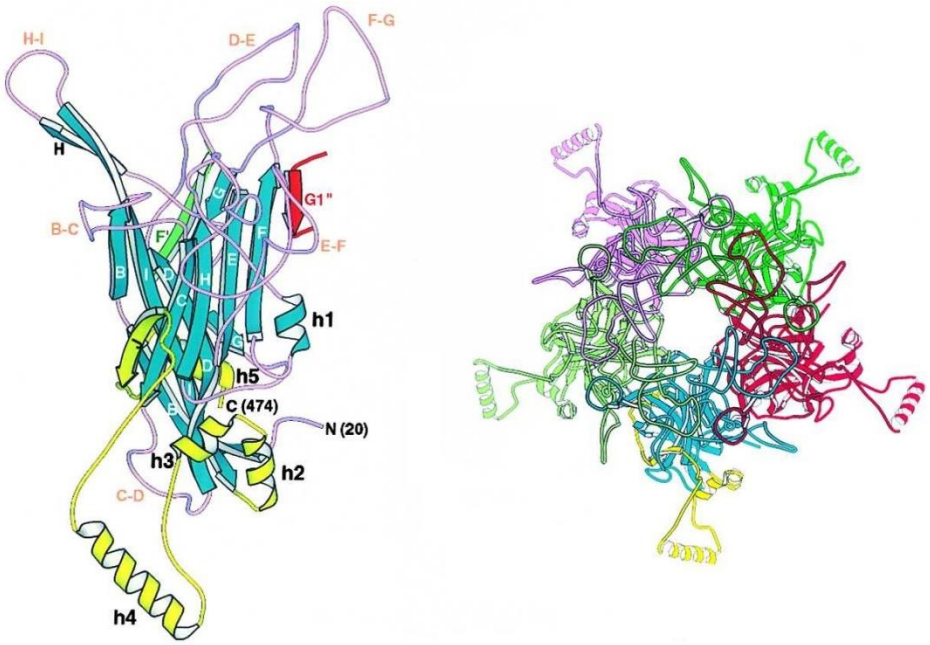

Figure 2.4 Structure of the L1 monomer and pentamer
The N- and C-terminal residues of the monomer (left image) are labelled N(20) and C(474), respectively. The β-jelly roll is represented in blue and is composed of 8 β-strands marked by capital letters. The individual β-strands are connected by loops represented in pink and labelled according to the strands they connect. Helices are labelled from h1 to h5. The C-terminal arm is represented in yellow. Five monomers assemble to form a pentamer (right image, top view). Each monomer within the pentamer connects to an adjacent pentamer through its so-called invading C-terminal arm. Figure taken and modified from reference [29].

2.4 HPV binding to host cells and early extracellular events

Over the years, many host molecules were identified to be involved in the infectious entry of HPVs into cells. After initial binding to the cell surface, the viral capsid is assumed to undergo conformational changes and to be transferred to an entry receptor complex for endocytosis. However, the timing of the complex sequence of events at the cell surface and the interplay between the molecules is poorly understood (for a model based on the current knowledge, see Figure 2.5).

HPVs are thought to bind to host cells mainly via heparan sulfate proteoglycans (HSPGs) present in the secreted extracellular matrix (ECM) or in the epithelial plasma membrane [38,39]. In particular, syndecan-1 and syndecan-4 were shown to bind HPV16 PsVs in HaCaT keratinocytes [40]. The interaction between the HPV capsid and HSPGs is thought to occur via ionic interactions between negatively charged heparan sulphate chains and positively charged residues within the major capsid protein L1 [41,42]. However, several other cell surface molecules were shown to be able to bind HPV particles, including EGFR and KGFR [43], laminin-5 [44] and integrin α6 [45]. Especially integrin α6 proved to be important for HPV infection or binding in several studies [46–48], even leading some authors to speculate it may be the main receptor for HPV binding [49]. However, it remains unclear to what extent each of the involved HPV binding partners contributes to initial binding and there may be some variations between different HPV subtypes. Moreover, the contribution of these molecules could vary between cell types, as different expression patterns may influence their availability.

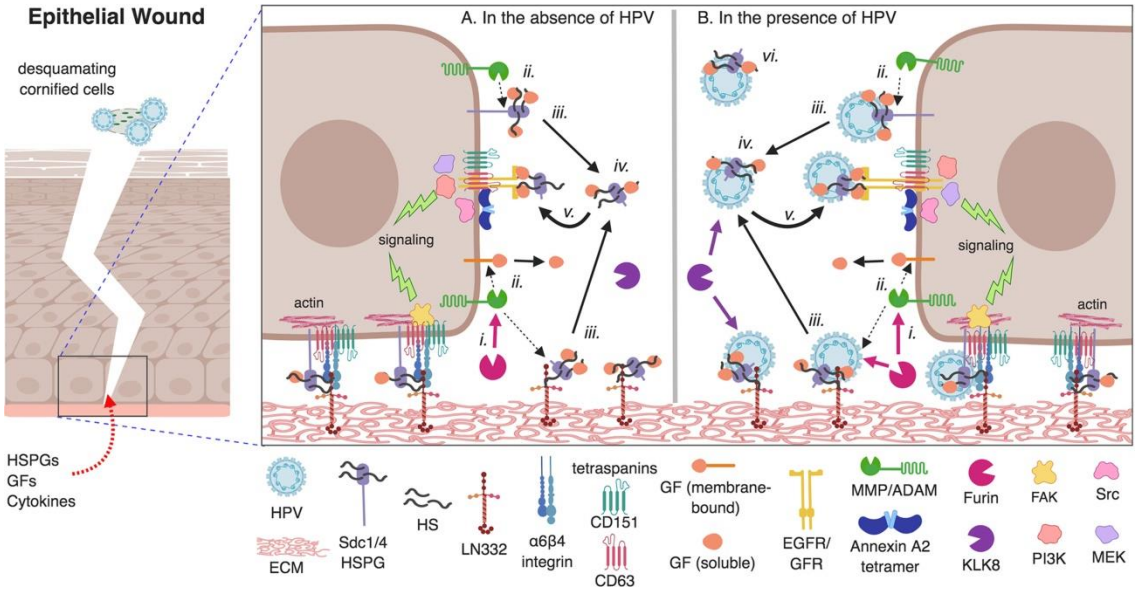

Figure 2.5 Model for HPV extracellular interactions in a dynamic wounded microenvironment

(A). Endogenous cellular functions occurring in the absence of HPV. Complexes on the surface of basal epithelial cells, containing Sdc1, CD151 tetraspanin and α6β4 integrin, interact with LN332 (also called laminin-5) and thereby provide anchorage to the ECM. (i.) MMPs and ADAM proteases are activated via proprotein convertases like furin. (ii) These proteases in turn release membrane-bound GFs and extracellular domains of HSPG, including Sdc1 and Sdc4 present on the cell surface or in the ECM (dotted arrows). (iii.) The HSPG ectodomains can bind soluble GFs, which are released by (iv.) heparanases and proteolytic cleavage of LN332. (v.) Signalling pathways are activated via GFR-GF binding. For example, the trafficking of A2t to the cell surface is triggered by the activity of Src, which is mediated via EGFR activation. (B). HPV makes use of cellular fuctions. After HSPG binding, viral capsid proteins are cleaved by KLK8 and furin. Bound viruses are supposed to be released by sheddase activity. Released capsids are coated by GFs and HS (iv.) and interact with the secondary receptor complex (v.). Alternatively, viruses may associate directly with soluble HS-GF complexes and bind directly to the secondary receptor complex bypassing primary receptors (vi.). Figure taken from reference [39].

Matrix metalloproteinases (MMPs), a disintegrin and metalloproteinases (ADAMs) and heparinases proved to be important for HPV infection, due to their activity in cleaving and releasing HS-containing ectodomains of HSPGs and growth factor (GF) precursors [39,43,50], a process called "ectodomain shedding". ECM and cell-bound HPV particles are released by this shedding activity and remain associated with HS and GFs. Interestingly, shedded virions, which are coated with these HS-GF-complexes, can infect cells lacking HSPGs [43], indicating that HS-GF-HPV association render virions infectious. The precise sheddases that release HSPG associated viral particles are not known. However, ADAM17 was shown to be required for shedding GFs and thereby modulating HPV infection indirectly [51]. Some studies suggest that HPV virions obtained from organotypic derived tissues [52] or pre-treated with conditioned medium from furin-overexpressing cells [53] do not need cell-bound HSPGs for infection. This may be due to HS and GFs being present in the viral inoculum [39]. Therefore, the precise role of target cell HSPGs for the infectivity of HPV released from lesions in vivo needs to be investigated.

It is believed that the viral capsid undergoes conformational changes mediated by initial cell-surface binding that results in exposure of the N-terminus of the minor capsid protein [54,55]. These conformational changes are believed to be induced by L1-binding to HSPGs and are required for efficient infectious endocytosis [56,57]. In these studies, evidence for the conformational changes mainly comes from binding of monoclonal antibodies raised against L1 and L2 epitopes only accessible after virus binding to HS or to the cell-surface. Moreover, subsequent proteolytic capsid processing was shown to be facilitated by capsid interactions with HS, suggesting a facilitated exposure of cleavage sites [58]. These HS binding sites are scattered across the surface loops of L1 [59] (see L1 structure, Figure 2.4). More recently, a cryo-EM study confirmed that L2, which is predominantly buried below the capsid surface (see section 2.3), becomes more exposed on the capsid-surface after treatment of viral

particles with heparin [28]. However, the study only found minor alterations in the L1 conformation, suggesting that L2 contributes to heparin binding and initial conformational changes. Capsid conformational changes resulting in L2 exposure were shown to also be facilitated by the activity of cyclophilins, which are peptidyl-prolyl cis/trans isomerases [58,60]. Extracellular alterations of the capsid also involve the activity of kallikrein-8, which cleaves the L1-molecule, and are required as well for L2 exposure and proper endocytosis [58,61].

After undergoing these conformational changes, it is assumed that HPV particles are transferred to a non-HSPG secondary or co-receptor complex possibly involving GFs and GFRs [43,62,63], either by shedding of HS-GF-coated capsids [39] or by reduced capsid affinity to primary HS-binding sites [56]. However, the nature of this secondary receptor complex remains poorly understood, but seems to involve tetraspanin enriched microdomains (TEMs) [9].

2.5 Tetraspanin enriched microdomains

Tetraspanins are a family of small membrane proteins mainly localizing to the plasma membrane. They consist of four transmembrane domains that give tetraspanins their name, a small and a large extracellular loop (SEL and LEL), a short intracellular loop and C- and N-terminal cytoplasmic tails (see example depicted in Figure 2.6). Tetraspanins are expressed in nearly all multicellular organisms. In humans, 33 tetraspanins have been identified [64].

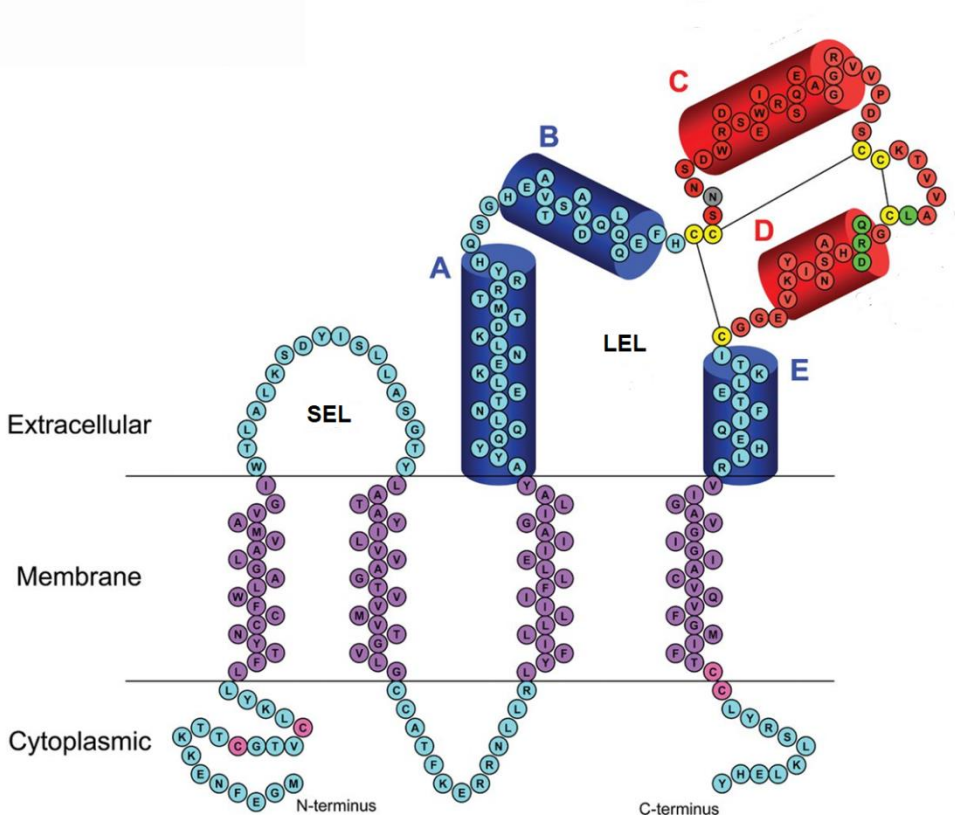

Figure 2.6 Structure of tetraspanin CD151
Schematic representation of the tetraspanin CD151. Tetraspanins have four name-giving transmembrane domains (purple). The LEL is supposed to be responsible for most direct protein-protein interactions and contains a constant region (helices A, B, E; in blue) and a variable region (helices C, D; in red). Key amino acid residues responsible for CD151-integrin interactions are marked in green. The LEL is stabilized by three disulphide bonds between cysteine residues (in yellow). Cytoplasmic tails contain N-glycosylation (in grey) and palmitoylation sites (in pink). Figure taken and modified from reference [65].

Their most prominent characteristic is the ability to laterally interact with one another and numerous other partner proteins in high copy number, forming large networks of interaction called tetraspanin enriched microdomains or tetraspanin web [66]. This concept initially comes from biochemical experiments, showing that some complexes involving tetraspanins were resistant to certain detergents [67,68]. Based on their resistance to these detergents, the formation of the tetraspanin web was initially proposed to rely on three levels of interaction [69]. The first level of interaction refers to

direct interactions, which are maintained in stringent detergents and comprise tetraspanin-tetraspanin associations as well as associations of tetraspanin with other transmembrane proteins. These heteromeric interactions for example include the association of CD151 with laminin-binding integrins [68,70], CD9 and CD81 with EWI-proteins [71] and CD81 with CD19 [72]. The second level of interaction refers to protein-protein interactions only maintained in less stringent detergents. Here, primary complexes are thought to mutually assemble into higher order secondary networks. This web formation is based on the ability of different types of tetraspanins to associate with each other. By recruiting different primary complexes into TEMs, tetraspanin could organize different components into a functional platform. The last or tertiary level of interaction involves very weak interactions, which are only detectable in very weak detergents like CHAPS. These interactions may be dependent on lipids as tetraspanins were shown to associate with cholesterol or ganglioside [73]. However, the contribution of lipids to tetraspanin web formation is unclear, although they may be involved in its stabilization [74].

In any case, this is a rather descriptive classification with little information about the functionality of the interactions. Therefore, a more recent model proposes the classification of tetraspanin interaction with respect to their contribution to tetraspanin web formation: intramolecular interactions necessary to maintain tetraspanin structure, interactions that support tetraspanin web formation and interactions that add functional partners to the web [66].

Within the intramolecular interactions, the correct folding of the LEL, which is stabilized by the formation of disulphide bridges and hydrophobic interactions within the LEL, is of particular importance as most intermolecular interactions of tetraspanins are thought to be mediated via this domain [66]. It was also proposed, that binding of cholesterol in a pocket formed by the transmembrane domains has an influence on the conformation of the LEL [75].

Intermolecular interactions of tetraspanins can be classified into three different types as shown in Figure 2.7. Specific tetraspanin-tetraspanin interactions were shown to be mediated by the short δ-domain within the LEL for CD81 [76,77]. In the case of CD9, it was demonstrated that transmembrane domains 1 and 2 contribute to CD9-CD9 interactions [78]. Palmitoylation of cytoplasmic cystein residues of tetraspanin also contributes to tetraspanin-tetraspanin interactions, as removal of palmitoylation sites proved to reduce association of different tetraspanins [79,80] . Moreover gangliosides and cholesterol also seem to have a role in promoting tetraspanin-tetraspanin interactions [81].

Due to their association with numerous partner proteins, including integrins and IgG superfamily members, and their broad expression range, tetraspanins are involved in a broad range of cellular processes like signal transduction, cell proliferation, adhesion, and migration [64,82]. In order to associate with specific sets of partners, there must be a great variability between individual tetraspanins. The most variable part in the tetraspanin structure is the LEL, as was established by comparing sequences of different tetraspanins [83]. Indeed, it was demonstrated that CD151 binds to integrin α3 via its LEL in a very stable and stoichiometric manner [70,84]. This supports the notion that the specificity of primary interactions is mainly modulated via the LEL. A recent study employing superresolution stimulated emission depletion (STED) microscopy found that several tetraspanins formed individual nanocluster in the plasma membrane with diameters of about 100 – 200 nm [85]. Interestingly, these tetraspanin nanodomains were closer to domains containing their reported interaction partner than to nanodomains from different tetraspanins [85], which could reflect the different strength of the interactions mentioned above. However, it should be noted that beside their role in tetraspanin-tetraspanin interactions, palmitoylation, cholesterol and gangliosides were also shown to stabilize tetraspanin-partner interactions [81,86,87].

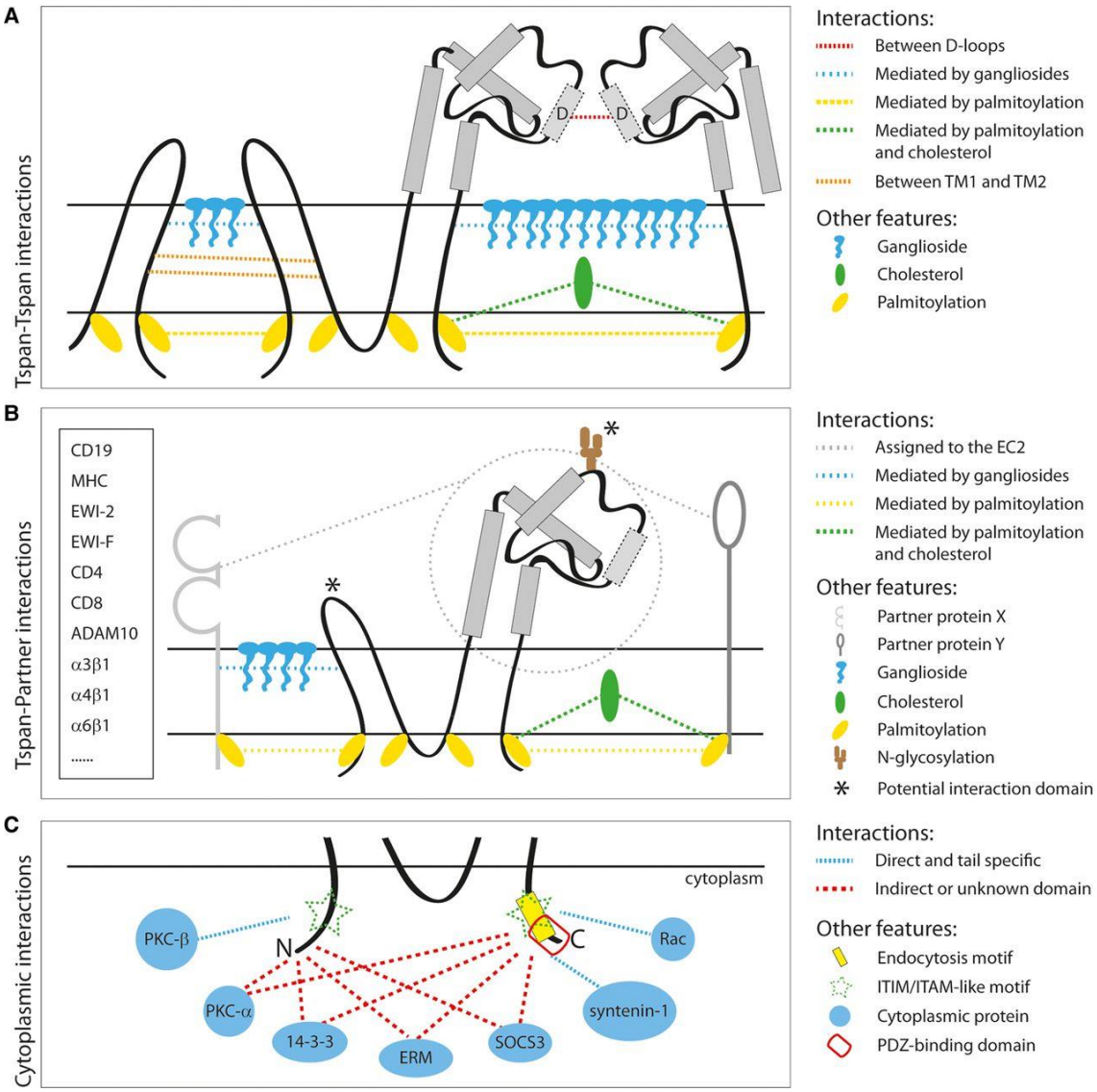

Figure 2.7 Model for intermolecular interactions of tetraspanins
(A) Different factors contribute to the stability of tetraspanin–tetraspanin interactions. Interactions include direct protein-protein interactions between the δ-loops and transmembrane domains of individual tetraspanins, palmitoylation of cytoplasmic tails, cholesterol and gangliosides. (B) The LEL is supposed to mediate most tetraspanin–partner interactions (a few examples of tetraspanin partners are indicated on the left). Palmitoylation, cholesterol and gangliosides stabilize interactions of tetraspanin with their non-tetraspanin partners. (C) Tetraspanins were shown to interact with cytosolic proteins via their N- and C-terminal cytoplasmic tails. Some examples for interactions of tetraspanins with cytoplasmic proteins (blue) are indicated. Figure taken from reference [66].

In addition to their role in organizing partner molecules in the plasma membrane, tetraspanins were further shown to exhibit some cytoplasmic interactions. Examples of such direct interactions include the interaction of the N-terminus of CD53 with PKC-β, which is important for B-cell receptor signalling [88], the association of Rac GTPase with the C-terminus of CD81, an important step in cell migration [89], and the association of syntenin with the C-terminus of CD63 [90]. These examples point out that tetraspanins not only organize plasma membrane events but also scaffold cytosolic factors making them key regulator of signalling and trafficking processes.

With respect to their broad and ubiquitous expression in a great variety of tissues, it is not surprising that tetraspanins were soon found to be associated with numerous pathological processes, like host-pathogen interactions [91]. There, the role of tetraspanins is best characterized for viral infections [92]. TEMs were found to modulate viral binding and entry directly or via TEM associated proteins for numerous viruses, including coronavirus [93], influenza A virus [94], hepatitis C virus (HCV) [95,96], human immunodeficiency virus (HIV) [97,98] and notably HPV [48].

2.6 Tetraspanins in endocytosis and trafficking

A few tetraspanins were identified that seem to have a key role during the endocytosis and cellular trafficking of their associated partner proteins. An example is the tetraspanin CD63 that has a tyrosine based sorting motif within its C-terminal cytoplasmic tail, which confers a fast rate endocytosis from the cell surface and a predominant localization to late endosomes and lysosomes [99]. Synaptotagmin VII is a partner protein of CD63 [100] and localizes to lysosomes where it regulates their exocytosis [101]. It does not have an own lysosomal sorting motif and requires association with CD63 in order to reach lysosomes. Mutation of the CD63 sorting-motif causes both proteins to accumulate at the plasma membrane [100]. CD63 was also shown

to promote HIV cell entry [98], possibly by targeting HIV co-receptors like CXCR4 to the plasma membrane [102]. Moreover, the internalization of the H,K-ATPase β-subunit relies on its interaction with CD63 [103].

CD151 was also shown to be present in intracellular compartments [104]. Notably, CD151 was found to co-accumulate in the same endocytic compartments as its associated laminin-binding integrins [105]. Similarly to CD63, CD151 has a endocytosis/sorting motif within its C-terminal cytoplasmic tail and mutation of this motif attenuates CD151 internalization [105]. Noteworthy, this reduced CD151 endocytosis is accompanied by a lowered internalization of integrins [105], indicating that this tetraspanin modulates integrin trafficking and function.

TSPAN15 and other so-called C8 tetraspanins were observed to regulate the cellular distribution and maturation of their partner protein ADAM10 [106]. Overexpression of TSPAN15 was associated with promotion of ADAM10 cell surface localization, its exit from the ER and stabilization of its active form. Knockdown of TSPAN15 on the other hand is associated with a reduction in ADAM10 maturation and cell surface localization [107].

These examples show that tetraspanins are involved in the trafficking and internalization of molecules that are associated with them. Thereby, they could regulate the availability of cell surface receptors required for virus binding or promote the endocytosis of viral particles, which are associated with TEMs, making them key regulators of viral entry.

2.7 The tetraspanin web in HPV infection: an entry and trafficking platform?

As mentioned above, tetraspanins are suspected to be part of the secondary receptor complex. The involvement of TEMs in HPV infection initially derives from studies analysing the unusual endocytic pathway of HPV [31,108]. The studies found similar

endocytic requirements for several oncogenic HPV subtypes. Knockdown of clathrin, which controls many endocytic pathways, and dominant inhibitors of clathrin-mediated endocytosis had no effect on viral endocytosis [31]. Likewise, caveolin, another protein commonly mediating endocytosis, does not seem to be involved in the process. Viral particles did not colocalize with caveolae structures on the cell surface, cells with low levels of caveolin were efficiently infected and an inhibitory caveolin mutation as well as caveolin knockdown did not prevent infection [31]. In line with this, inhibition and knockdown of dynamin, which is a GTPase required for caveolae and clathrin mediated endocytosis, did not inhibit HPV infection. However, actin polymerization is required for infection and scission of endocytic vesicles, as cytochalasin D was observed to block this process [108,109].

These studies found that knockdown of tetraspanins and antibodies raised against tetraspanins inhibited infection by HPV, which was confirmed by subsequent investigations [48,110]. HPV was found to colocalize with domains containing CD151 and CD63 on the cell surface, while colocalization increased with incubation time [31]. HPV was observed to colocalize with large assemblies of CD151 [48], CD63 [111] and CD81 [77]. However, CD81 plays a less important role for infection [31,110]. Subsequent analyses showed that CD151 was required for endocytosis and TIRF-measurements indicate that only viruses, which are associated with CD151 assemblies, undergo endocytosis [48]. The functionality of the tetraspanin seems to rely on its association with integrins, as CD151-mutants that are unable to associate with integrins fail to support infection [48]. This could support the notion that CD151 controls the formation of an integrin-containing tetraspanin web that is utilized by HPV. On the other hand, CD63 interacts with the major capsid protein L1 but is dispensable for endocytosis and seems to be required for intracellular virus trafficking in a complex with syntenin [112]. Following endocytosis, HPV is found in CD63-positive vesicles recruiting syntenin [112]. The association of CD63 with syntenin is crucial for HPV intracellular trafficking, as CD63

mutants that are impaired in their ability to interact with syntenin are unable to support infection [112]. Syntenin mutants that do not interact with CD63 are likewise inhibitory for infection. This CD63-syntenin complex was observed to control the routing of internalized HPV to multivesicular bodies [112] before viral DNA gets to the trans-Golgi network [34]. However, CD63 already colocalizes with CD151 as well as with HPV at the plasma membrane [31], which may indicate that both tetraspanins could be incorporated in the same tetraspanin web.

CD151 was shown to regulate cytoskeletal actin reorganization with a possible involvement of integrin signalling [113,114]. This is particularly interesting, as integrin signalling involving focal adhesion kinase (FAK) and phosphoinositide-3 kinase (PI3K) is activated during HPV infection [47,115]. Actin polymerization has been shown to be required for scission of endocytic vesicles from the plasma membrane [109]. However, some kind of molecule has to connect the actin cytoskeleton to the entry complex in the plasma membrane, similarly to ezrin-radixin-moesin (ERM) proteins that connect CD81 and tetraspanin interaction partners to the actin cytoskeleton [116]. The cytoskeletal adaptor obscurin-like protein 1 (OBSL1) [117] could be such a molecular linker, as it colocalizes with CD151, interacts with the minor capsid protein L2 and is required for HPV endocytosis [118]. However, it is not known if OBSL1/L2 interaction occurs at the cell surface or intracellularly and its function in connecting the tetraspanin web to intracellular dynamics remains to be demonstrated.

As mentioned earlier, HPV was found to bind KGFR and EGFR. Moreover, GFR signalling is required for infection [43,51] and EGFR colocalizes and directly interacts with CD151 [51,119]. Colocalization of HPV with EGFR (and CD151) was shown to be promoted by ADAM17 activity, probably via shedding of growth factors [51]. This further suggests that EGFR is part of the secondary receptor complex alongside with CD151.

For a long time, the minor capsid protein L2 was not known to have a role in events on the cell surface, despite its critical role for infection [38]. This changed with the discovery

of the annexin A2 heterotetramer (A2t) as an additional host cell factor that binds to L2 and proved to be required for HPV infection [120]. A2t is composed of two annexin A2 and two S100A10 subunits and is proposed to have roles in numerous cellular processes, including exocytosis, endocytosis, membrane organization and linking of the cytoskeleton to the plasma membrane [121]. Virus contact to host cells results in the activation of EGFR signalling [43] that in turn leads to the phosphorylation and translocation of annexin A2 to the plasma membrane where HPV binds to A2t [122]. A2t seems to have a dual role during infection, as antibodies raised against the annexin A2 subunit prevent virus internalization while antibodies raised against the S100A10 subunit block infection at the level of intracellular trafficking. Interestingly, the colocalization of A2t and CD63 was recently shown to increase upon incubation with HPV particles [123], indicating that the tetraspanin and A2t may be cointernalized from the plasma membrane via HPV endocytosis. This could point to the possibility that A2t is also part of the tetraspanin web or that it may be recruited there by binding to HPV particles. It is possible that additional components of the endocytic trafficking machinery could also be recruited by tetraspanins, for instance components of the ESCRT sorting machinery, which were shown to be required for HPV infection [124,125]. Noteworthy, the routing of tetraspanins to exosomes was recently shown to be dependent on ESCRT-sorting [126], pointing towards the possibility of interactions between tetraspanins and ESCRT components.

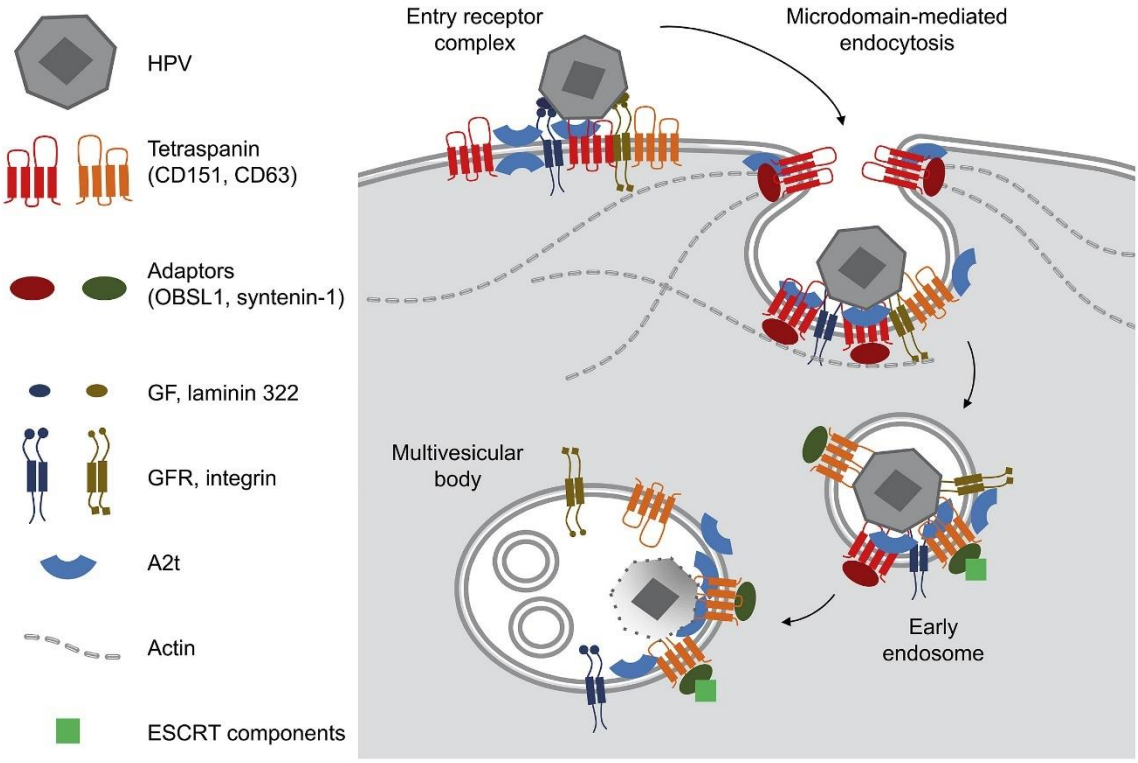

Figure 2.8 HPV16 endocytosis and trafficking to multivesicular bodies
The entry receptor complex contains tetraspanins, annexins, integrins and growth factor receptors. After binding to the complex, HPV16 is internalized via a poorly characterized clathrin-, caveolin-, dynamin-independent endocytic process, which is dependent on actin dynamics. Endocytosis requires the presence of the cytoskeletal adaptor protein OBSL1, annexin A2 heterotetramer and tetraspanin CD151. Endosomes traffic to multivesicular bodies in a CD63- and syntenin-1-dependent manner, also involving ESCRT components. Figure taken from reference [9].

In summary, all these observations suggest that numerous HPV associated host cell factors can be related to TEMs. The tetraspanin web could be organized by tetraspanin CD151 as the central key player, which recruits the functional factors for viral binding and endocytosis (see Figure 2.8), and tetraspanin CD63 that could organize the components of the intracellular trafficking machinery. However, it remains unknown how all these components coordinate in time and space during HPV entry thereby shaping the architecture of the viral entry platform.

3 Aim of the study

The cell-surface binding and internalization process of human papillomaviruses is a complex multi-step process that is not yet fully understood. To date, numerous host cell factors were identified that are required for mediating host cell binding and virus endocytosis. However, little is known about how these molecules are coordinated in time and space on the cell surface. It is possible that the virus associates with specific domains on the plasma membrane.

Among the proviral host cell factors is the tetraspanin CD151, which is known to interact with laminin-binding integrins.

i) The first aim was to study the nano-architecture of CD151 domains at superresolution. It was verified if integrins can be found in these domains and how the molecules assemble with each other in the plasma membrane. Moreover, it was investigated whether HPV particles associate with specific domains of the host cell membrane that can be identified as viral entry platforms.

ii) The second aim of the study was to establish if integrin α3 has a role in binding or internalization of HPV16 pseudovirions in our keratinocyte cell-line model, comparing it to integrin α6, which is known to contribute to HPV cell-surface binding.

iii) Finally, it was investigated if the viral entry platforms are linked to the actin cytoskeleton and if additional components can be found in these structures.

4 Materials and Methods

4.1 Material

If not stated otherwise, standard chemicals, reagents and consumables used in this study were obtained from Carl Roth (Karlsruhe, Germany), Merck (Darmstadt, Germany), Sigma-Aldrich (Hamburg, Germany), Biochrom (Berlin, Germany), Thermo Fisher Scientific (Waltham, MA), PAN Biotech (Aidenbach, Germany), Sarstedt (Nümbrecht, Germany), Invitrogen (Carlsbad, CA), VWR (Darmstadt, Germany), Labomedic (Bonn, Germany), Eppendorf (Hamburg, Germany), or Bio-Rad (Hercules, CA).

4.1.1 Appliances

Table 4.1 Appliances

Name	Supplier	Application
Inverted microscope CLIPSE TS100, CFI60 Infinity Optical System	Nikon, Tokyo, Japan	Brightfield microscope for cell culture purpose
Olympus IX81-ZDC fluorescence microscope, MT20E illumination system	Olympus, Tokyo, Japan	Epifluorescence microscopy
easy3D STED module coupled to Olympus IX83 confocal microscope	Abberior Instruments, Göttingen, Germany / Olympus	STED and confocal microscopy
Odyssey® CLx Imaging System	Li-Cor, Lincoln, NE	Western Blot Imaging
Sonopuls HD 2070	Bandelin, Berlin, Germany	Sonifier for membrane sheet generation

4.1.2 Buffers and solutions

All buffers and solutions were prepared using double distilled water ($_{dd}H_2O$) and autoclaved or sterile filtered if necessary.

Table 4.2 Compositions of buffers and solutions

Name	Composition
Phosphate buffered saline (PBS)	137 mM NaCl, 2.7 mM KCl, 1.76 mM KH_2PO_4, 10mm Na_2HPO_4, pH 7.4
Sonication buffer	120 mM potassium glutamate, 20 mM potassium acetate, 10 mM EGTA, 20 mM HEPES, pH 7.2
Cytomix solution	20 mM KCl, 10 mM KH_2PO_4, 0.15 mM $CaCl_2$, 2 mM EGTA, 5 mM $MgCl_2$, 25 mM HEPES-KOH, pH 7.6
SDS sample buffer	63 mM Tris-HCl, 2% w/v SDS, 10% w/v Glycerol, pH 6.8
SDS running buffer	25 mM Tris, 0.1% w/v SDS, 192 mM glycine, pH 8.3
Towbin buffer	25 mM Tris, 192 mM glycine, 20% v/v MeOH, pH 8.3
Blocking buffer for Western blot / antibody dilution for Western blot	50 % (v/v) Odyssey blocking buffer (cat# 927-40000,Li-Cor, Lincoln, NE) in PBS, 0.1 % (v/v) Tween-20 were added for antibody dilution
Western blot washing buffer	0.1 % Tween (v/v) in PBS
Poly-L-Lysine (PLL) stock solution (20x)	2 mg/mL PLL in $_{dd}H_2O$
Paraformaldehyde (PFA) stock solution / fixative solution	16 % (w/v) PFA in $_{dd}H_2O$, adjusted with 10x PBS and $_{dd}H_2O$ to get fixative solution (4 % PFA in 1x PBS, pH adjusted to 7.4)
Permeabilization buffer	0.2 % (v/v) Triton X-100 in PBS

Blocking buffer for immunostaining / antibody dilution buffer	3 % BSA in PBS

4.1.3 Cell culture media and reagents

Table 4.3 Cell culture media and reagents

Name	Supplier
DMEM high glucose (4.5 g/l)	cat# P04-03550, PAN Biotech
MEM	cat# P04-08509, PAN Biotech
Fetal bovine serum	cat# S0615, Biochrom
Penicillin-streptomycin solution (10,000 U/ml Penicillin, 10 mg/ml Streptomycin)	cat# P06-07100, PAN Biotech
Trypsin solution	cat# P10-0231SP, PAN Biotech
DPBS	cat# P04-36500, PAN-Biotech
RNAiMAX Lipofectamine transfection reagent	cat# 13778100, Invitrogen

4.1.4 Kits

Table 4.4 Kits

Name	Supplier
Neon™ Transfection System 100 µL Kit	cat# MPK10096, Thermo Fisher Scientific
EdU Click-488	cat# 7773.1, Carl Roth

4.1.5 Plasmids

Table 4.5 Plasmids

Name of construct	Origin	Backbone	Description
CD151-GFP	Reference [48]	pEGFP-C1, Clontech Laboratories, Mountain View, CA	CD151 N-terminally tagged with EGFP
CD151-RFP	Reference [76]	pEGFP-C1, Clontech Laboratories	CD151 C-terminally tagged with RFP*
CD63-GFP	Reference [112]	pEGFP-C1, Clontech Laboratories	CD63 N-terminally tagged with EGFP
V5-OBSL1	Reference [127]	pCDNA3.1, Invitrogen	OBSL1 N-terminally tagged with V5

* here, CD151 was fused at its C-terminus to RFP via PCR, EGFP was removed from pEGFP-C1 via restriction enzymes

4.1.6 Primary antibodies and nanobodies

Table 4.6 Primary antibodies and nanobodies, IF: immunofluorescence; WB: western blot

Tame / name	Host species / clonality	Origin / supplier	Application / dilution
HPV16 L1, K75	Rabbit, polyclonal	Reference [128]	IF, 1:1000
HPV16 L1, 16L1-312F	Mouse, monoclonal	Reference [41]	IF, 1:200
HPV16 L1, L1-7	Mouse, monoclonal	Reference [129]	IF, 1:500
HPV16 L1, CamVir1	Mouse, monoclonal	cat# NB100-2732, Novus Biologicals, Centennial, CO	WB, 1:2000
CD151, 11G5A	Mouse, monoclonal	cat# MCA1856, Bio-Rad, Hercules, CA	IF, 1:100

CD151, E9M8T	Rabbit, monoclonal	cat# 81626, Cell Signaling Technology, Danvers, MA	IF, 1:500
Integrin α3, A-3	Mouse, monoclonal	cat# sc-374242, Santa Cruz, Dallas, TX	IF, 1:100 WB, 1:1000
Integrin α6	Rabbit, polyclonal	cat# PA5-12334, Thermo Fisher Scientific	IF, 1:200 WB, 1:1000
β-Actin, 13E5	Rabbit, monoclonal	cat# 4970, Cell Signaling Technology	WB, 1:4000
V5-tag	Rabbit, monoclonal	cat# ab9116, Abcam, Cambridge, UK	IF, 1:5000
GFP, 9F9.F9	Mouse, monoclonal	cat# ab1218, Abcam	IF, 1:100
GFP, GFP-Booster Atto488	Alpaca, monoclonal, coupled to Atto488	cat# gba488, Chromotek, Planegg-Martinsried, Germany	IF, 1:200
RFP, RFP-Booster Atto594	Alpaca, monoclonal, coupled to Atto594	cat# rba594, Chromotek	IF, 1:200

4.1.7 Secondary antibodies

Table 4.7 Secondary antibodies, IF: immunofluorescence; WB: western blot

Target species	Host species	Flurophore	Supplier	Application / dilution
Mouse	Donkey	AlexaFluor488	cat# A-21202, Invitrogen	IF, 1:200
Mouse	Donkey	AlexaFluor594	cat# A-21203, Invitrogen	IF, 1:200

Mouse	Goat	STAR RED	cat# STRED-1001, Abberior GmbH, Göttingen, Germany	IF, 1:200
Rabbit	Goat	AlexaFluor488	cat# A-11034, Invitrogen	IF, 1:200
Rabbit	donkey	AlexaFluor594	cat# ab150064, Abcam	IF, 1:200
Rabbit	Goat	STAR RED	cat# STRED-1002, Abberior GmbH	IF, 1:200
Rabbit	Goat	Atto647N	cat# 40839, Sigma-Aldrich	IF, 1:200
Mouse	Goat	IRDye 800CW	cat# 925-32210, Li-Cor	WB, 1:10000
Rabbit	Goat	IRDye 680RD	cat# 925-68071, Li-Cor	WB, 1:10000
Rabbit	Goat	IRDye 800CW	cat# 925-32211, Li-Cor	WB, 1:10000

4.1.8 Pseudoviruses

PsVs and EdU-PsVs were kindly provided by Luise Florin and produced as described in reference [130]. Very briefly: expression plasmids containing HPV16 L1 and L2 proteins were cotransfected with a luciferase reporter plasmid into HEK 293TT cells. For EdU-PsVs, culture medium was supplemented with 5-ethynyl-2'-deoxyuridine (EdU) to enable the staining of the reporter plasmid DNA employing click-chemistry. The reporter plasmid is encapsidated by the HPV16 capsid proteins L1 and L2. Cells are lysed, PsVs/EdU-PsVs are purified via gradient centrifugation and PsVs are quantified via RT-PCR of the reporter plasmid and the amount is expressed as viral genome equivalents (vge).

4.1.9 Software

Table 4.8 Software

Name	Supplier	Application
ImageJ	Wayne Rasband, National Institute of Health, USA (open source)	Image analysis
Microsoft Excel	Microsoft Corporation, Redmond, WA	Data analysis and organization
Graphpad Prism	GraphPad Software Inc., San Diego, CA	Data plotting
OriginPro	OriginLab Corporation, Northampton, MA	Data plotting
Adobe Illustrator	Adobe Inc., San José, CA	Assembly of Figures

4.2 Methods

4.2.1 Cell culture

Passaging and cultivation of HaCaT and HepG2 cells

In this study, HaCaT and HepG2 cells were employed. The HaCaT human immortalized keratinocyte cell-line was obtained from Cell Lines Services (Eppelheim, Germany). HaCaT cells were cultivated using high glucose (4.5 g/l) DMEM (cat# P04-03550 PAN Biotech, Aidenbach, Germany) supplemented with 10 % fetal bovine serum (cat# S0615, Biochrom, Berlin, Germany) and 1 % penicillin-streptomycin working solution (cat# P06-07100, PAN Biotech). HepG2 cells (Cell Lines Services) were cultivated in MEM (cat# P04-08509, PAN Biotech) supplemented with 10 % fetal bovine serum and 1 % penicillin-streptomycin. Both cell lines were kept at 37 °C and 5 % CO_2. Cells were grown to confluence and passaged by trypsination. For this, cells were incubated with 1-3 ml trypsin solution (cat# P10-0231SP, PAN Biotech) for approximately 10 min (HaCaT) or 2 min (HepG2) at 37 °C. Trypsin activity was arrested by adding 4 - 12 ml of the respective growth medium and the cells were vigorously resuspended. Cells were split approximately 1:5 - 1:10 for HaCaT and 1:8 - 1:16 for HepG2. Cells were passaged every 3-4 days.

Cleaning of coverslips

For microscopic experiments, cells were grown on high precision glass coverslips (cat# 0117650, Paul Marienfeld GmbH, Lauda-Königshofen, Germany) placed in six-well plates. Coverslips were cleaned and sterilized. To achieve this, coverslips were incubated in 1M HCl for 1 h under constant agitation. Afterwards, HCl was discarded and coverslips were extensively washed with distilled H_2O, followed by incubation with 1M NaOH under constant agitation. Coverslips were washed again and incubated with 100 % ethanol for 1 h. Coverslips were then either baked at 180 °C and kept sterile or

kept in 70 % ethanol until they were placed in six-well plates and coated with PLL solution (0.1 mg/ml) for 30 min. Afterwards, the solution was removed and coverslips were dried for at least 1 h, followed by 20 min sterilization via UV light. Coverslips were kept at 4°C until further processing.

Freezing and thawing of cells

Cells were trypsinated (see above) and resuspended at a concentration of $2*10^6$ cells per ml in growth medium without antibiotics but supplemented with 10 % DMSO. The cell suspension was then transferred to cryovials (1 ml per vial), placed in a "Mr. Frosty" freezing container (cat# 5100-0001, Thermo Fisher Scientific) filled with isopropanol and frozen by storing the container at -80 °C for 24 h. Afterwards, cryovials were transferred to a liquid nitrogen tank for long-term storage.

For thawing, cryovials were quickly warmed up in a water bath at 37°C. Immediately after thawing, the cell suspension was transferred to a falcon tube containing growth medium without antibiotics before being mixed and centrifuged. Supernatant was discarded, cells were resuspended in normal growth medium and transferred to cell-culture flasks for cultivation.

4.2.2 Transfection of plasmids

For transfection, cells were detached using trypsin solution as described above. HaCaT cells were transfected using the Gene pulser Xcell electroporation system (Bio-Rad). HaCaT cells were centrifuged, washed using DPBS (cat# P04-36500, PAN-Biotech) and resuspended in cytomix solution. For each transfection, $2*10^6$ cells were used and supplemented with 15 µg plasmid DNA, yielding a final volume of 400 µL. For double transfection, 15 µg of each construct were used (30 µg total DNA amount). The cell suspension was transferred to a 4 mm electroporation cuvette and electroporated

employing the following settings: 200 V, 950 µF and 200 Ω. After electroporation, cells were diluted in growth medium without antibiotics, seeded onto PLL-coated glass-coverslips (~3*10^5 cells/coverslip) and allowed to recover for about 30 min at 37 °C before adding growth medium with antibiotics. Cells were incubated approximately 24 h at 37 °C before start of experiments.

HepG2 cells were electroporated using the Neon® electroporation system (Thermo Fisher Scientific) following the manufacturer's instructions. The cells were centrifuged, washed with DPBS and resuspended in buffer R (Thermo Fisher Scientific). For each transfection, 2*10^6 cells were used and supplemented with 12.5 µg plasmid DNA in a final volume of 120 µL. The cell suspension was transferred to a 100 µL gold tip and electroporated with a single pulse of 50 ms and 1200 V. The cells were diluted in growth medium without antibiotics, seeded onto PLL-coated glass-coverslips (~3*10^5 cells/coverslip) and allowed to recover for about 30 min at 37 °C before adding growth medium with antibiotics. The cells were incubated approximately 24 h at 37 °C before start of experiments.

4.2.3 Transfection of siRNA

For siRNA transfection, RNAiMAX Lipofectamine transfection reagent (Invitrogen) was used. HaCaT cells were seeded in six-well plates or on PLL-coated glass coverslips at a concentration of approximately 10^5 cells/well or coverslip and incubated in growth medium at 37 °C overnight. Thereafter, cells were incubated for two days with 30 nM of the respective siRNA using RNAiMAX Lipofectamine transfection reagent according to the manufacturer's instructions. For each integrin, a pool of two siRNAs with dT-dT overhangs was used; for integrin α3: α3#1 (GCUACAUGAUUCAGCGCAA[dT][dT]) and α3#2 (GUUUGAAGGCUUGGGCAAA[dT][dT]), and for integrin α6: α6#1 (GGAUAUGCCUCCAGGUUAA[dT][dT]) and α6#2 (CUGUAAGGAUCCGGAAAGA[dT][dT]).

AllStars negative control siRNA (Qiagen, Hilden, Germany) was used as a non-silencing control. After incubation with siRNA, cells were used for subsequent experiments. For assessing the knockdown efficiency, cells were lysed directly in SDS sample buffer supplemented with 5% β-mercaptoethanol. Lysates were vortexed thoroughly, heated for 10 min at 95 °C and stored at -20 °C until being processed for SDS-PAGE and Western blot analysis, analyzing for the content of integrin proteins.

4.2.4 SDS-PAGE

Protein samples were analyzed using a stacking gel containing 4 % acrylamide and a running gel containing 8 % acrylamide (for integrin detection and PsV binding assay) or 12 % acrylamide (for L1 cleavage assay). For each gel, samples were loaded together with NEB broad range protein ladder (cat# P7712, New England Biolabs, Ipswich, MA) as a reference for protein sizes. Gels were run in a MiniPROTEAN Tetra Cell unit (Bio-Rad) in SDS running buffer. Gel electrophoresis started at 70 V until samples had left the stacking gel. Afterwards, voltage was raised to 150 V and gels were run until the reference bands of the protein ladder were properly separated. The stacking gel was discarded and the running gel was transferred to ice-cold Towbin buffer until being processed for Western blotting.

4.2.5 Western blotting

After SDS-PAGE, gels were equilibrated for at least 10 min in ice-cold Towbin buffer. Whatman paper and nitrocellulose membrane were incubated in Towbin buffer for 30 min at 4°C. Gels and membranes were mounted in a MiniPROTEAN Tetra Cell equipped with Mini Trans-Blot Module (Bio-Rad) in cooled Towbin buffer under constant buffer agitation. Proteins were transferred for 45 min (L1-cleavage assay and PsV-binding

assay) or for 2 h (integrin detection) at 100 V. After blotting, the membrane was washed for ~ 5 min in PBS and blocked for 1 h using Odyssey blocking buffer (Li-Cor, cat# 927-40000) diluted 1:2 in PBS. Afterwards, nitrocellulose membranes were incubated with primary antibodies diluted in Odyssey blocking buffer diluted 1:2 in PBS-T (PBS supplemented with 0.1 % Tween-20) for 1 h at RT or overnight at 4 °C under constant agitation. Afterwards, membranes were washed four times for about 10 min with PBS-T. Subsequently, membranes were incubated with secondary antibodies (dilution 1:10000 in Odyssey blocking buffer diluted 1:2 with PBS-T) for 1 h at RT under constant agitation. Finally, nitrocellulose membranes were washed three times with PBS-T and one time with PBS for about 10 min, respectively. Blots were imaged using the Li-Cor Odyssey Classic Imaging System employing near-infrared fluorescence imaging (700 nm and 800 nm channels).

4.2.6 L1 cleavage assay

HaCaT cells were seeded in six-well plates at a concentration of approximately 10^5 cells/well and incubated in growth medium at 37 °C overnight. Then, cells were transfected with either integrin α3 siRNA, integrin α6 siRNA or AllStars Negative control siRNA as described above (section 4.2.3). Two days after transfection, supernatant was removed and cells were incubated in growth medium without antibiotics supplemented with PsVs ($4*10^7$ vge per well) for 24 h at 37 °C. After incubation, supernatant was removed and cells were washed extensively three times with ice-cold PBS. Cells were lysed directly in SDS sample buffer supplemented with 5 % β-mercaptoethanol. Lysates were vortexed thoroughly, heated for 10 min at 95 °C and stored at -20 °C until being processed for SDS-PAGE and Western blot analysis. For Western blot, the primary antibodies CamVir1 and 13E5 were used for L1 and actin detection, respectively. In the images, the 25 kDa L1 cleavage product was quantified.

Actin was used as standard for relating the amount of L1 cleavage product to the cell number.

4.2.7 PsV binding assay

HaCaT cells were seeded in six-well plates at a concentration of approximately 10^5 cells/well and incubated in growth medium at 37 °C overnight. Thereafter, cells were transfected with either integrin α3 siRNAs, integrin α6 siRNAs or AllStars Negative control siRNA as described above. Two days after transfection, supernatant was removed and cells were incubated in ice-cold growth medium without antibiotics supplemented with PsVs ($2*10^7$ vge per well). Cells were incubated for 1 h at 4 °C to allow PsV binding in the absence of internalization. After incubation, supernatant was removed and cells were washed extensively three times with ice-cold PBS. Afterwards, cells were scraped from the six-well plate, transferred to a reaction tube and washed three times with ice-cold PBS to remove unbound PsVs. Cells were lysed directly in SDS sample buffer supplemented with 5 % β-mercaptoethanol. Lysates were vortexed thoroughly, heated for 10 min at 95 °C and stored at -20 °C until being processed for SDS-PAGE and Western blot analysis. For Western blot, the primary antibodies CamVir1 and 13E5 were used for L1 and actin detection, respectively. In the images, the ~55 kDa L1 protein was quantified. Actin was used as standard for relating the amount of L1 protein to the cell number.

4.2.8 Sample preparation for microscopy

Knockdown cells, overexpressing cells, or untransfected cells grown on glass coverslips were processed directly for sample preparation or after incubation with growth medium without antibiotics supplemented with or without PsVs/EdU-PsVs ($4*10^7$ vge per well) for different incubation times, ranging from 15 min to 5 h.

Membrane sheet generation

Cells grown on PLL-coated glass coverslips were washed with DPBS and transferred to a Petri dish containing ice-cold sonication buffer. The tip of a sonifier was placed in the buffer right above the coverslip (at a distance of approximately 0.5 cm). Membrane sheets were generated by applying a 100 ms ultrasound pulse at the center of the coverslip, using 100 % and 75 % pulse power for HaCaT and HepG2 cells, respectively. For HaCaT cells, several ultrasound pulses were applied at different coverslip locations, as this cell-line was quite resistant to membrane sheet generation. Afterwards, membrane sheet samples were processed for fixation.

Fixation, permeabilization and blocking

Cells were washed with DPBS and either fixed directly or after membrane sheet generation. Samples were fixed in 4 % PFA in PBS for 30 min at RT. Afterwards, fixative solution was discarded and remaining PFA was quenched with 50 mM NH_4Cl in PBS for 30 min at RT. Permeabilization was performed with 0.2 % Triton X-100 in PBS for 2 min (intact cells) or 1 min (membrane sheets) at RT. Samples were blocked employing 3 % BSA in PBS for 30 min at RT.

In experiments employing the rabbit monoclonal anti-CD151 antibody (section 5.3.2), methanol fixation was employed by incubation with 100 % methanol at -20 °C for 15 min, washed extensively three times with PBS and blocked directly as described above, as methanol fixation bypasses the need for permeabilization. Fixed and blocked

samples were then processed for immunostaining. In experiments where EdU-PsVs were used, an additional step was performed just before blocking the sample. Here, the EdU Click 488 kit (Carl Roth, cat# 7773.1) was used for click-labelling the encapsidated plasmid DNA with fluorescein for 30 min at RT according the manufacturer's instructions.

Immunostaining

Immunostaining was performed on samples blocked as described above. All antibodies were diluted using 3 % BSA in PBS as dilution buffer. Dilutions of primary and secondary antibodies are indicated in Table 4.6 and Table 4.7, respectively. Incubation with primary antibodies took place for 1 h at RT or in the case of knockdown experiments and CD151-GFP/integrin α3/integrin α6 triple staining overnight at 4 °C. Incubation with secondary antibodies took place for 1 h at RT. Nanobodies and Phalloidin-iFluor647 (used for F-actin staining, diluted 1:100 from a 100x stock solution in DMSO, cat# ab176759, Abcam) were added during the secondary antibody incubation. If nanobodies were used in the absence of primary/secondary antibody combination, the primary antibody incubation step was omitted. Samples were washed three times with PBS after primary and secondary antibody incubation, respectively. For Epifluorescence microscopy, washed samples were kept at 4 °C in PBS until being imaged. For STED and confocal microscopy, samples were mounted on microscopy slides employing ProLong® Gold antifade mounting medium (Invitrogen, cat# P36930), cured overnight at RT and sealed with nail varnish

Samples for determination of the point spread function

Approximately $2*10^7$ vge were added per ml of DMEM and vortexed vigorously. One ml of the solution was added per poly-L-lysine coated glass-coverslip placed in a six-well plate. Coverslips were incubated overnight at 4°C to allow adsorption of PsVs. The

samples were washed with PBS and fixed with PFA and quenched as described above. Immunostaining was performed employing the 16L1-312F antibody omitting the permeabilisation step.

4.2.9 Epifluorescence microscopy

Stained samples were imaged directly in microscopy chambers containing PBS supplemented with 1-(4-tri-methyl-ammonium-phenyl)−6-phenyl-1,3,5-hexatriene *p*-toluene-sulfonate (TMA-DPH; cat# T-204, Invitrogen). TMA-DPH is incorporated in lipid bilayers and therefore enables visualization of cell membranes. Imaging was performed with an Olympus IX81 fluorescence microscope (Olympus) equipped with an 60x 1.49 NA Apochromat oil immersion objective coupled to a 16-bit EMCCD camera (ImagEM C9100-13, Hamamatsu Photonics, Japan) employing an additional 4x lens. The microscope is equipped with a MT20E illumination system (Olympus) with a 150W xenon lamp using the filter sets DAPI HC (F36-500) for TMA-DPH, EGFP HC (F36-525) for GFP and TRITC HC (F36-503) for Alexa 594 (all filter sets: AHF Analysentechnik, Tuebingen, Germany). Images were acquired using the CellR® (Olympus) software.

4.2.10 STED and confocal microscopy

Confocal and STED microscopy were both performed using the same microscope, which was an Olympus IX83 confocal microscope (Olympus) equipped with an UPlanSApo 100x (1.4 NA) objective (Olympus). Pinhole size was adjusted to 60 µm for all experiments and the pixel size was adjusted to 20-50 nm depending on the experiment.

The antibody L1-7 detects an L1 epitope buried under the surface of the capsid that becomes accessible to immunostaining after intracellular capsid disassembly.

Therefore, for quantification of L1-7 positive intracellular compartments, images were acquired in the focal plane of the cell body where most vesicles displaying L1-7 staining were visible. For visualization of the 3-D extension of large tetraspanin/actin assemblies, z-stacks were acquired recording an image every 400 nm starting from the basal plane of the cell up to 1600 nm above the basal plane. For all other experiments, the focal plane was adjusted to the basal plasma membrane or membrane sheet.

A 485 nm laser was employed for exciting Atto488, Alexa488 and fluorescein. Detection of those fluorophores was achieved with the combination of 500-520 nm and 532-558 nm filters. A 561 nm laser was employed for exciting Alexa594 and Atto594. Detection of those fluorophores was achieved with a 580-630 nm filter. A 640 nm laser was employed for exciting Atto647N, STAR RED and iFluor647. Detection of those fluorophores was achieved with a 650-720 nm filter.

For STED microscopy, the confocal microscope is equipped with a 4-channel easy3D super-resolution STED optics module (Abberior Instruments) and a time-gated detection with 0.75 ns delay and 8 ns gate width was used. Depletion of fluorophores was performed using pulsed STED lasers 595 nm (Alexa488, Atto488, and fluorescein) and 775 nm (Alexa594, Atto647N, and STAR RED).

4.2.11 Image analysis

Image analysis of micrographs and Western blot images was performed using ImageJ software. For analysis, rectangular/squared regions of interest (ROIs) were used, if not specifically stated otherwise. ROIs were placed in one reference channel and, if needed, propagated to the other respective channels. Freehand ROIs were used, for quantifying total number of PsVs or vesicles per cell base, analyzing fractional overlap between CD151-GFP and actin, calculating intensity and Pearson correlation

coefficient (PCC) of CD63-GFP/CD151-RFP/actin triple-assemblies or measuring band intensities in Western blots.

Average fluorescence intensity

For measuring the average fluorescence intensity, ROIs were placed on cells or membrane sheets. The mean signal intensity within this ROI was quantified and corrected for background. Background intensity was taken from ROIs placed outside of the cell or membrane sheet.

Maxima analysis

A custom ImageJ macro (developed by Dr. Jan-Gero Schloetel) was used for analyzing maxima or vesicle parameters (size, distance, density, or fluorescence intensity). All maxima parameters were averaged for each individual cell or membrane sheet.

Before analysis, images were processed by applying a Gaussian blur with $\sigma = 1$. This procedure reduces pixel noise in the background and therefore improves identification of maxima. A threshold of 1-3 a.u. (depending on the experiment) was set for the detected maxima to be considered for analysis in order to further reduce the chance of including maxima that arise from background signal. The macro uses the ImageJ function “Find maxima” that detects local maxima in a given ROI. The coordinates of those spots were extracted and used for further analysis.

The maxima density was calculated by relating the number of detected maxima to the analyzed area.

The macro places a circular ROI with a radius of 2 pixels centered to the maxima position and measures the average intensity within this ROI. This value is taken as the maxima mean intensity. The distance between maxima was calculated as follows: for each maximum, the nearest neighboring maximum is determined and the distance between them is calculated and taken as the inter maxima distance. This procedure is

applied for calculating distances within the same channel as well as for distances between different channels.

The size of the maxima was calculated as follows: a vertical and a horizontal 31 × 3 pixels line scan were respectively placed centered to the maxima locations. For each maximum, a Gaussian function was fitted to the intensity profile of both line scans, respectively. Only the fit with the best quality was considered for the determination of the size of the maximum. The full width at half maximum (FWHM) of the Gaussian fits was taken as the size of the maximum. If maxima are very close to each other, it is possible that their size is misinterpreted by this procedure. Therefore, only maxima where the peak of the Gaussian fit was located within the central third of the line scan and that have a fit quality of $R^2 \geq 0.8$ were considered.

The viral entry platform (see section 5.3) was characterized using the algorithm described above. Therefore, a 1 µm x 1 µm ROI was placed and centered to the PsV position. As it is possible that dimmer maxima originate from single molecules or unspecific signal, only bright maxima, considered to potentially be protein clusters, were counted, setting 8, 11, 15, and 14 intensity counts as a threshold for CD151-rabbit antibody-, CD151-mouse antibody-, integrin α3-antibody- and integrin α6-antibody stained maxima, respectively.

Western blot analysis

In Western blot images, freehand ROIs were drawn around the bands of interest. The band intensity was quantified by measuring the integrated fluorescence intensity within this ROI. Intensities were corrected for background by measuring the intensity in the same ROI moved in a region within the same lane with no visible band and subtracting this background intensity from the respective band intensity. Band signals were normalized to the cell number by relating the intensity of the protein of interest to background corrected actin band signal.

Pearson correlation coefficient (PCC)

A custom ImageJ macro (developed by Dr. Jan-Gero Schloetel) was used for calculating the PCC. ROIs were placed in one reference channel and propagated to the other respective channel. The PCC between the channels was calculated within these ROIs. For creating random relationships between the channels, the image of one of the channels was flipped vertically and horizontally within the ROI.

Fractional signal overlap

Fractional overlap was calculated using the ImageJ built-in autothresholding function. A value of three intensity counts was subtracted from the image in order to avoid selecting background in images with weak staining. A Gaussian blur ($\sigma = 1$) was applied to the image in order to enhance edge detection of structures. The image was segmented by using the autothresholding function “Mean”. The segmented area from one channel was compared to the segmented area from a second (for double colocalization) or a second/third channel (for triple colocalization) and the number of pixels overlapping between the channels was determined. The ratio of pixels of one channel that overlapped with those in the other channel(s) was taken as colocalization (ratio overlapping pixels to total pixels).

Tracking of PsVs and CD151

For this analysis, five TIRF movies were kindly provided by Luise Florin from an experiment described and published in reference [48]. HPV16 PsVs and CD151-CFP positive particles were tracked with the built-in ImageJ function "Find maxima”. A circular ROI with a diameter of 5 pixels was placed and centered at the location of detected maxima and the center of mass of the fluorescence within the ROI was measured for determining the exact object position. The objects were tracked manually over a period of maximally 180 s with a time interval of 6 s between frames

in order to get the x- and y-positions of the objects over time. The mean of the squared displacements (MSDs) was calculated for each time interval and plotted against the time intervals. For CD151-CFP, this plot indicated unidirectional flow, which was ignored when calculating the diffusion coefficient D. D was calculated by fitting a linear regression line to the MSD vs. time interval plot. The slope was equal to four times the apparent diffusion coefficient. D was calculated for each single track and an average diffusion coefficient was calculated.

5 Results

5.1 Organization of integrin α3, integrin α6 and CD151 in the plasma membrane

CD151 is required for efficient HPV infection [48] and HPV16 PsVs colocalize with CD151 during infection [31]. The laminin binding integrins α3 and α6 have been shown to interact in biochemical experiments with the tetraspanin CD151 [70,84,131]. The interaction is particularly strong for integrin α3 [84]. Therefore, it is tempting to speculate that these proteins assemble with each other and form complexes in the plasma membrane.

5.1.1 Membrane sheets and STED microscopy

The membrane sheet preparation is a useful tool to study plasma membrane organizations of proteins. By applying a short ultrasound pulse to cells, which adhere to a substrate, it is possible to rip off the apical cell membrane. Thereby, the cytosolic content, such as cytosolic proteins or organelles, can be removed, leaving behind the basal membrane. Figure 5.1 illustrates the preparation of membrane sheets and shows an example of a HaCaT membrane sheet expressing CD151-GFP (Figure 5.1 B). This method facilitates imaging of the plasma membrane with high-signal-to-noise ratio and without background from cytosolic structures close to the basal membrane.

Classical confocal and epifluorescence microscopy are not suitable for studying the nanoscopic organization of proteins due to their diffraction-limited resolution. Therefore, STED microscopy was employed. A STED-microscope is based on a confocal microscope that is equipped with a donut-shaped STED-laser in addition to an excitation laser. After excitation, fluorophores are depleted by the STED-laser.

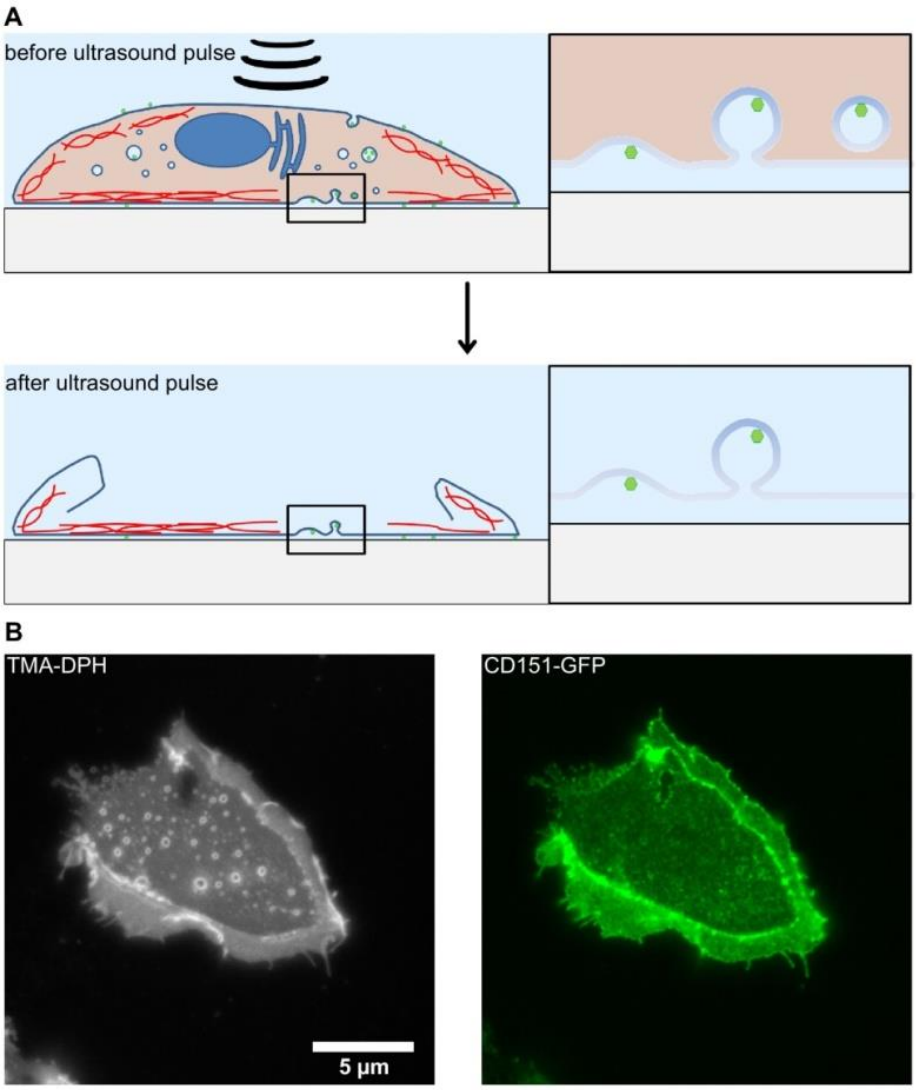

Figure 5.1 Illustration of the membrane sheet preparation
(A) By applying an ultrasound pulse, the apical membrane and cytosolic structures are ripped off, leaving behind the basolateral membrane. Intracellular compartments and cytosolic content are removed. Only membrane bound invaginations, cytoskeletal elements and other membrane-anchored structures remain. (B) Exemplary image of a plasma membrane sheet generated from a HaCaT cell expressing CD151-GFP. The left panel shows membrane staining with TMA-DPH. The right panel shows overexpressed CD151-GFP. Notably, double membranes are visible at the edges. Figure taken, legend taken and modified from reference [51].

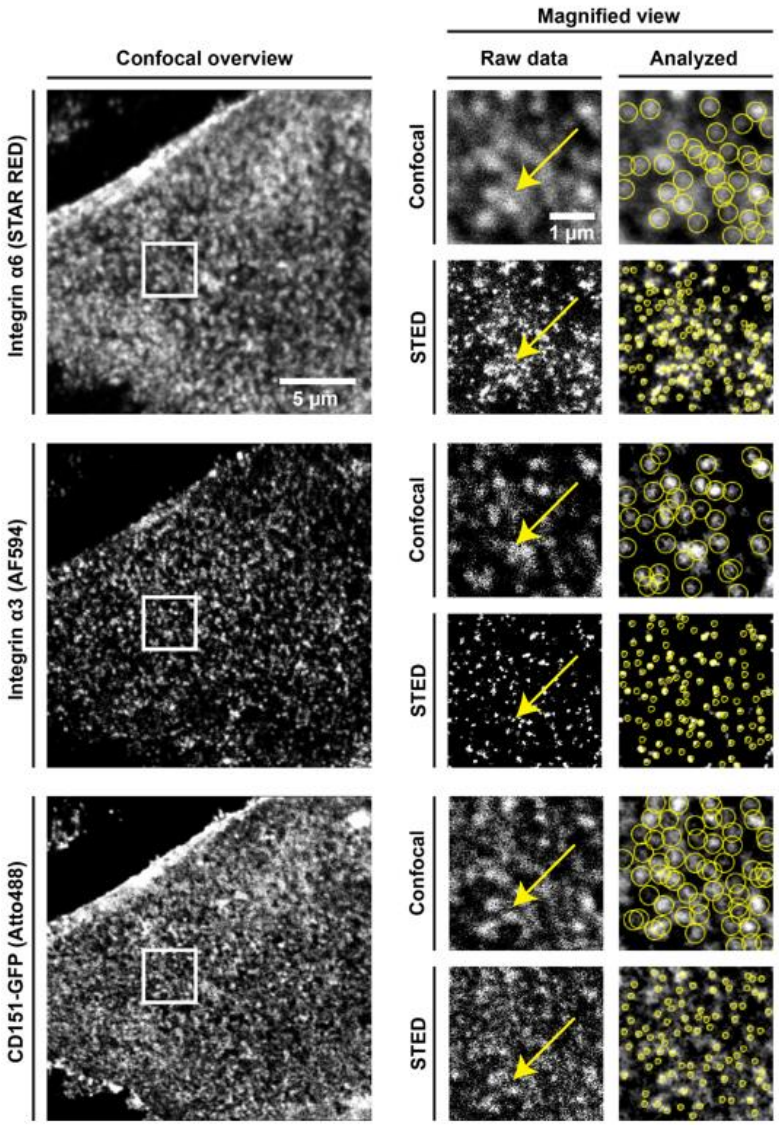

Figure 5.2 Illustration of the increase in resolution by STED microscopy
Membrane sheets from cells overexpressing CD151-GFP were fixed and stained for integrin α3 and integrin α6. CD151-GFP fluorescence was enhanced by nanobodies. For the confocal channels, overviews and magnified views are shown. Magnified views are further given for STED micrographs. Magnified views in the left column show raw data, the right column illustrates smoothed images that were used for maxima detection. Circles indicate locations of detected maxima. Images are shown using a linear greyscale lookup table employing an arbitrary scaling. As visible, STED microscopy allows for resolution of larger spots into smaller entities (arrows point to an assembly that is better resolved in the integrin channels). Figure and legend both taken from reference [130].

Only fluorophores in the centre of the ring remain excited. This effect diminishes the size of the excitation point spread function (PSF) and allows getting resolutions below the diffraction limit. The difference between standard confocal and STED imaging of the microscope used in this study is illustrated in Figure 5.2. As can be seen in the STED channel, fluorescent signal is resolved into more but smaller entities, in particular concerning the integrins. Structures that appear to be continuous in diffraction limited images turn out to be closely associated signal maxima. However, it must be kept in mind that the gain in resolution is of course dependent on the imaging conditions like the fluorophore, the signal-to-noise ratio and the power of the depletion laser. In any case, this experimental condition was used for studying the distribution of CD151, integrins and PsVs in the plasma membrane.

5.1.2 Plasma membrane distribution of CD151 and integrins

While suitable antibodies are available for staining endogenous CD151, it was still necessary to turn to overexpressed CD151-GFP for analyzing the organization of the tetraspanin in combination with the integrins. This necessity arises because the available antibodies raised against the integrins originate from the same species as the well working anti-CD151 antibodies. Therefore, it was not possible to perform a triple immunostaining of the endogenous proteins. To exclude certain overexpression artefacts, control experiments performed in collaboration with the Florin group could demonstrate that CD151-GFP is as functional in supporting HPV infection as wildtype CD151 [130]. However, it was still unclear how well the construct blends with endogenous CD151. To clarify this issue, HaCaT cells were transfected with CD151-GFP, membrane sheets were generated, fixed, permeabilized, immunostained with anti-CD151 antibody and imaged by epifluorescence microscopy. Only membrane sheets with a distinct GFP fluorescence intensity were recorded (Figure 5.3 A). If CD151-GFP

does not blend into the same domains, GFP and antibody signal will not overlap very well. For analysis, the PCC between GFP fluorescence and antibody staining was calculated (0.75 ± 0.09). This value is higher than a value obtained previously for a double tagged protein (0.63) [132] and can be taken as a reference. Therefore, it can be concluded that CD151-GFP is incorporated in the same domains as endogenous CD151.

Since overexpression was used to study the distribution of CD151 and integrins, the amount of CD151 added to the system is important. Therefore, supplementary membrane sheets, also without visible GFP signal, were included in the analysis, in addition to those used for calculation of the PCC. The antibody staining intensity of the membrane sheets without GFP marks the level of endogenous CD151. The antibody staining intensity was plotted versus GFP signal intensity (Figure 5.3 B). Compared to the membrane sheet population without visible GFP signal, overexpression increased the CD151 level by about 2.5-fold. However, the individual expression level was highly variable, reaching 5-fold stronger expression level. These values are likely an upper estimate, as membrane sheets with a higher GFP signal were preferentially imaged in order to properly assess the colocalization between GFP signal and antibody signal.

To study the distribution of CD151 and integrins in the plasma membrane, HaCaT cells were transfected with CD151-GFP. Membrane sheets were generated by applying several short ultrasound pulses at different coverslip locations. Afterwards, samples were fixed, permeabilized and immunostained. Integrin α3 and α6 were stained with a primary-secondary antibody combination, while CD151-GFP was enhanced with a nanobody raised against GFP. Membrane sheets exhibiting CD151-GFP staining were subsequently imaged using STED-microscopy.

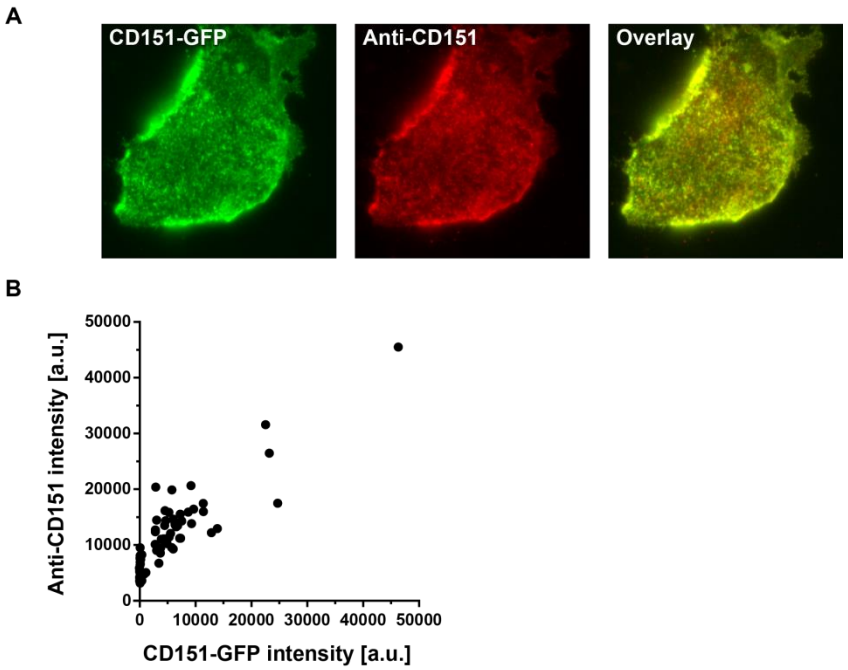

Figure 5.3 Overexpressed and endogenous CD151 localize to the same domains
(A) CD151-GFP was transfected into HaCaT cells. After one day, membrane sheets were generated, fixed, permeabilized, immunostained for CD151 and imaged by epi-fluorescence microscopy. Images are displayed with linear green (CD151-GFP) and red (anti-CD151) lookup tables at arbitrary intensity scalings. The Pearson correlation coefficient between the two channels was calculated (0.75 ± 0.09; value is given as mean ± SD; n = 36 membrane sheets collected from three biological replicates). (B) Plotting of CD151 immunostaining intensity versus GFP fluorescence intensity. In addition to the 36 membrane sheets analysed in A, supplementary membrane sheets, also without CD151-GFP, were included. The average immunostaining intensity of these membrane sheets marks the endogenous CD151. Figure and legend both taken and modified from reference [130].

Local signal maxima of integrin α3 and α6 appeared rather spherical and were sharply defined (Figure 5.4 A). Nanobodies are directly coupled with a fluorophore and therefore do not have the same signal strength as a combination of primary and secondary antibodies. This could be the reason why CD151 GFP nanodomains are more diffuse and more background can be distinguished. Hence, maxima number is likely underestimated. As stated in the methods, maxima sizes were determined by centrally placing a line scan on the detected maxima and applying a Gaussian fit to its

intensity profile. Sizes were included in analysis if their fit had a R^2 value > 0.8 and if the position of the Gaussian peak was in the central third of the line scan. This filtering process reduces the inclusion of falsified sizes originating from merged maxima structures where maxima are very close to each other and poorly separated. Therefore, the data regarding maxima sizes include only 42.7% (8300 maxima), 62.2% (22623 maxima) and 39.1% (20209 maxima) of all initially detected CD151-GFP, integrin α3 and integrin α6 maxima, respectively. As stated above, CD151 level is substantially increased under overexpression conditions. Hence, it is possible that increasing the protein level has an influence on the maxima characteristics. For verification, the CD151-GFP maxima size and maxima density of individual membrane sheets were plotted against the overall CD151-GFP staining intensity, respectively (Figure 5.4 B, C). Both parameters increased with rising CD151 level. However, the maxima density exhibited a stronger dependency on the expression level than the maxima size.

Analysing the raw data, maxima displayed average sizes of 106 nm, 157 nm and 209 nm for integrin α3, integrin α6 and CD151-GFP, respectively (Figure 5.4 D). As a next step, the relationship between the different proteins was investigated. Nearly half of the integrin α3 signal overlapped with signal from both other components (Figure 5.4. E). The fraction of integrin α6 or CD151-GFP, which overlaps with the respective other two components, was substantially lower. The question arises whether the overlap originates from evenly mixed components or from closely associated but distinct protein clusters. A distance analysis is suitable for tackling this issue, as evenly mixed components would exhibit inter maxima distances close to zero. Clearly segregated maxima, however, would exhibit distances in the range of the maxima sizes.

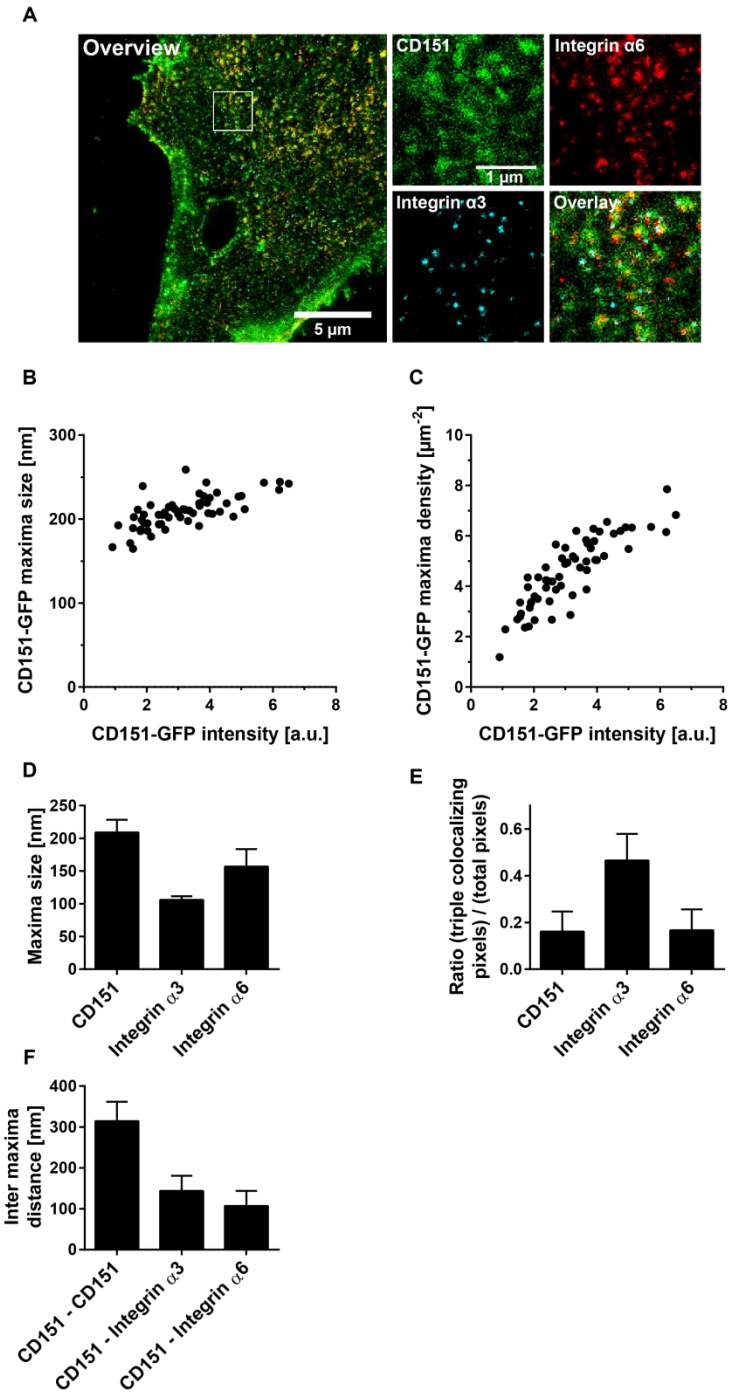

Figure 5.4 Characteristics of CD151 and integrin maxima
CD151-GFP was transfected into HaCaT cells. One day after transfection, cells were treated for 5 h without or with PsVs (see Figure 5.8), washed, membrane sheets were generated, stained and analysed by three channel STED microscopy. Green lookup table, CD151-GFP visualized by nanobodies (Atto488); red and cyan

lookup tables, integrin α6 and integrin α3 stained by antibody labelling (STAR RED and AF594, respectively). Images are displayed at arbitrary intensity scalings (linear lookup tables). (A) Large panel, membrane sheet (channel overlay). The white box marks an area from which magnified views of the individual channels are shown. (B and C) Maxima size (B) and density (C) of individual sheets were plotted against the average CD151 intensity. The average (D) maxima size and signal overlap (E) was measured. For (E), for all three channels within a ROI the pixels with an intensity higher than the average ROI intensity were selected. The number of pixels positive in all three channels was related to the number of all positive pixels in one specific channel as indicated. (F) Shortest inter-maxima distances of CD151-GFP to CD151-GFP, integrin α3 or integrin α6. Values are given as means ± SD (n = 60 membrane sheets collected from three biological replicates). Figure and legend both taken and modified from reference [130].

The average distance between the centre of a CD151-GFP maximum to the centre of the next integrin α6 maximum was only 107 nm, whereas distances to the next integrin α3 or CD151-GFP maximum were higher: 144 nm and 315 nm, respectively (Figure 5.4 F). These distances, which rather are in the range of the maxima sizes than close to zero, as well as the comparatively low triple overlap of CD151-GFP and integrin α6 signal point to closely associated but segregated structures rather than to evenly mixed proteins.

5.1.3 Maxima size distribution of integrin α3, integrin α6 and CD151

In Figure 5.4, signal maxima sizes were averaged for each membrane sheet. However, this approach does not allow distinguishing between populations. Are maxima sizes defined or do they cover a wide size range? Are there differences between the three maxima types? To tackle these questions, all individual maxima sizes were pooled and the size distribution for each protein was plotted into histograms (Figure 5.5). As can be seen, CD151-GFP and integrin α6 (Figure 5.5 A, C) cover a wide size range while integrin α3 has a sharper peak, concentrating at smaller maxima sizes (Figure 5.5 B). All three maxima types show a lognormal distribution, in particular for integrin α3 and no

maxima sizes below 50 nm were detected. This might indicate that the used STED-system cannot resolve the sizes of the smallest maxima. Therefore, maxima sizes may be overestimated, especially the size of integrin α3. In addition, maxima are enlarged due to the PSF.

To estimate the PSF of the microscope, PsVs were used. Papillomaviruses have a constant diameter of approximately 60 nm [22]. This makes them a suitable nanoscopic ruler to determine the resolution achieved by the STED-system. It was estimated that the primary-secondary antibody complex increases the diameter of the capsid by roughly 20 nm, as has been observed before in nanoscopy images of microtubuli [133]. Therefore, 80 nm were taken as the physical size. For this reason, HPV16 PsVs were adhered overnight to PLL-coated glass coverslips. Samples were fixed and immunostained. The same dyes and laser powers as in Figure 5.4 were used and confocal and STED images were recorded. In confocal images, the apparent particle size ranges from 236 nm to 315 nm depending on the fluorophore, in accordance with the Abbe diffraction limit (Figure 5.6). In the STED images, the apparent particle sizes are reduced to 121 nm (Atto488), 103 nm (AF594) and 126 nm (STAR RED) (Figure 5.6). Point spread functions (PSFs) were calculated using the following formula:

$$PSF = \sqrt{measured\ size^2 - physical\ size^2}$$

Consequently, the signals in the CD151-GFP, integrin α3 and integrin α6 channels in Figure 5.4 are blurred by PSFs of 91 nm, 64 nm and 97 nm, respectively. Correcting for these effects yields average maxima sizes of 189 nm for CD151-GFP, 84 nm for integrin α3 and 123 nm for integrin α6.

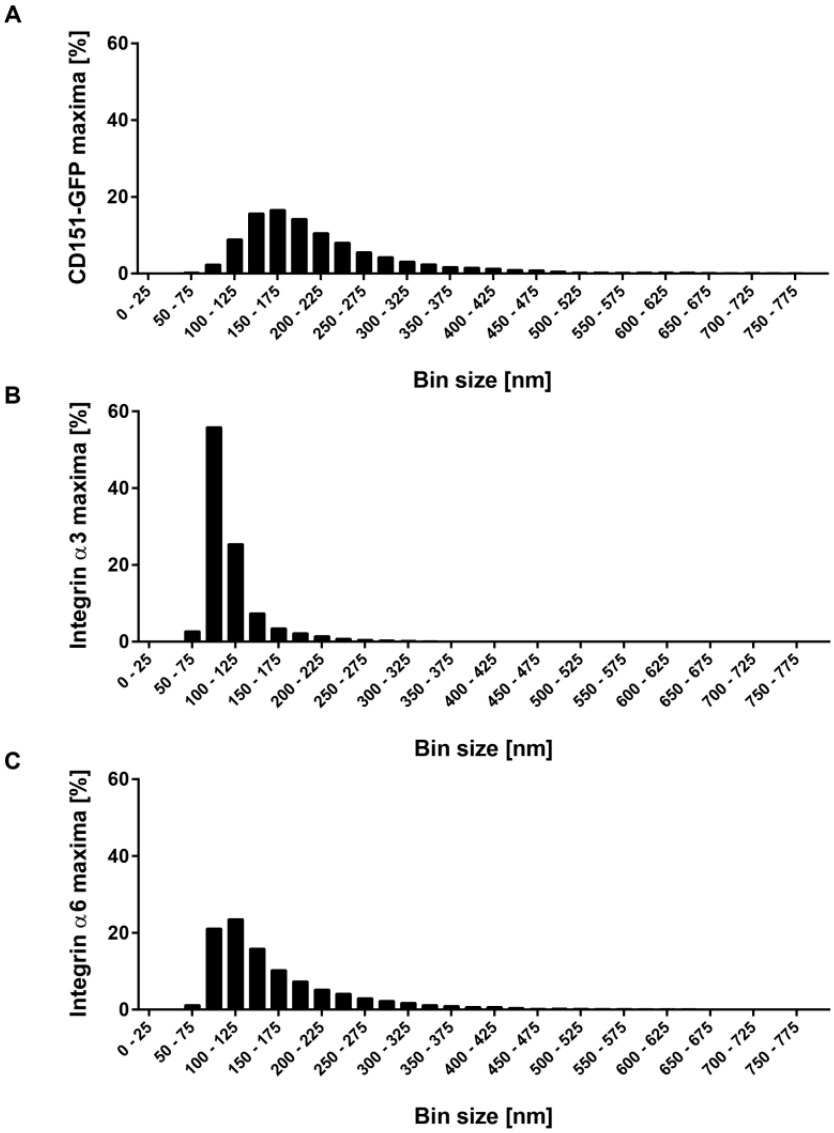

Figure 5.5 Histogram of maxima sizes for CD151, integrin α3 and integrin α6
Based on Figure 5.4, the size distribution of all analysed CD151-GFP maxima (A), integrin α3 maxima (B) and integrin α6 maxima (C) was plotted in histograms (bin size: 25 nm). To ensure proper size determination, maxima sizes were filtered for fit quality of the Gaussian function (see methods). Figure taken from reference [130].

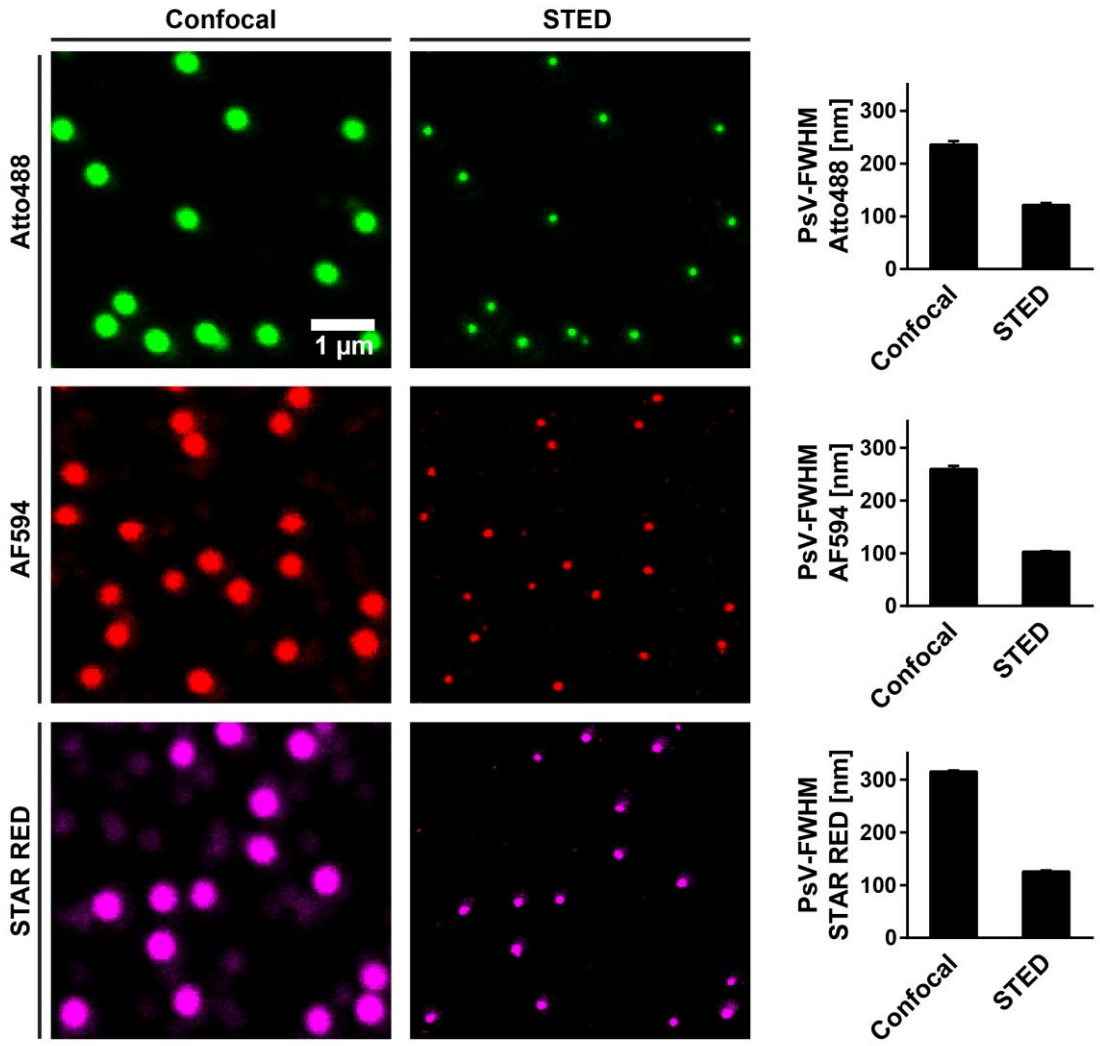

Figure 5.6 Determination of the point spread functions of the STED system
PsVs were adhered to PLL-coated glass coverslips and immunostained using the dyes Atto488 (used in Figure 5.4 for CD151-GFP labelling; linear green lookup table), AF594 (used in Figure 5.4 for integrin α3 labelling; linear red lookup table) and STAR RED (used in Figure 5.4 for integrin α6 labelling; linear magenta lookup table). All Images are displayed at arbitrary intensity scalings. Maxima were analyzed as in Figure 5.4. Maxima sizes were used for estimation of PSFs. Values are given as means ± SD (n = 10 images per dye, each obtained from one coverslip; in total, the analysis includes 582 - 1461 maxima per dye). Figure taken, legend taken and modified from reference [130].

5.1.4 Impact of PsV incubation on the organization of TEM components

Using STED microscopy, it was possible to show that integrin α3 and α6 are closely associated with CD151 maxima on the cell surface as they exhibit short inter-maxima distances. Regarding the functional relevance of CD151 for HPV infection, it is likely that viruses associate with such integrin-rich assemblies defined by CD151. First, the relationship between CD151 maxima and PsVs was studied. HaCaT cells were incubated with PsVs for 15 min. After extensive washing, cells were subsequently further incubated for up to additional 4 h 45 min. Afterwards, cells were washed, fixed, permeabilized, immunostained for CD151 and PsVs and imaged via STED microscopy (Figure 5.7 A).

The fraction of PsVs that was within a distance of 150 nm to the next CD151 maximum was quantified for different time points. A distance of 150 nm was selected for the following reason: considering the average size of a CD151 maximum with ~190 nm (after PSF correction) and PsVs with a size of ~60 nm, a distance of ~150 nm (centre to centre) would still allow for direct contact between CD151 and PsVs. Directly after 15 min incubation time, roughly 30 % of all viral particles were already located within this distance (Figure 5.7 B). This fraction gradually increased with further incubation time, reaching almost 50 % five hours after adding PsVs to the cells. In parallel, the staining intensity of CD151 at the PsV location increased over time (Figure 5.7 C). The staining intensity reached 140 % five hours after initial PsV addition when compared to the value after 15 min incubation time. Therefore, it can be concluded that HPV16 associates with maxima defined by tetraspanin CD151 during the infection process.

A previous study employing TIRF microscopy suggests that CD151 and HPV16 cointernalize at the cell surface [48]. Hence, incubation with PsVs is likely to reduce the cell surface level of TEM components. Figure 5.8 shows the condition applied in the experiment mentioned in the legend in 5.4 where HaCaT cells were incubated with PsVs for 5 h prior to membrane sheet preparation. Here, the staining intensity of

CD151-GFP was indeed slightly dimmer when compared to the condition without PsVs (22 % reduction, Figure 5.8 B). Integrins were diminished as well, but the effect was only significant for CD151-GFP. Interestingly, an increased occurrence of large CD151-GFP assemblies, which also contained signals of both integrins, was observed after incubation with PsVs (Figure 5.8 A, magnified view). This suggests that HPV16 is able to aggregate TEM components on the plasma membrane. However, as PsVs were not visualized in this experiment, it is unclear whether they colocalize with the large assemblies.

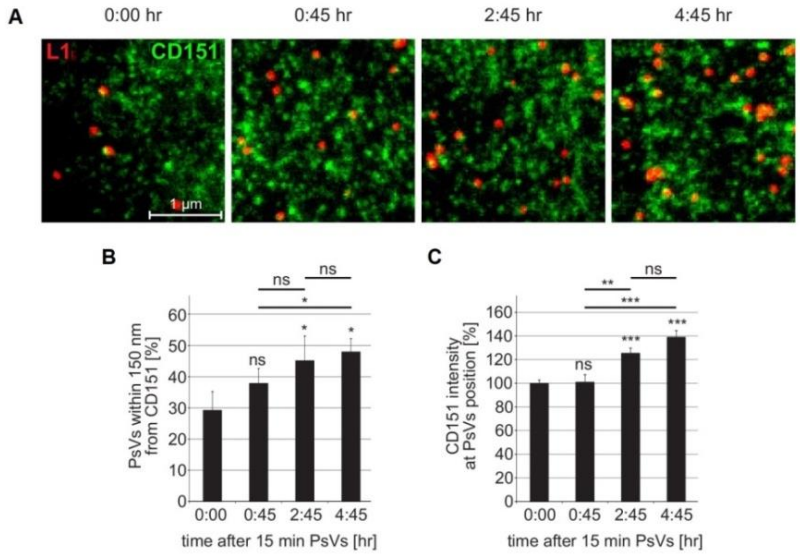

Figure 5.7 Association of PsVs with CD151 maxima
HaCaT cells were incubated for 15 min with HPV16 PsVs, washed, either fixed directly or after incubation for the indicated time and stained for CD151 (green) and PsVs (red) and imaged via STED microscopy. (A) Representative images for the different time points are shown (linear lookup tables, same arbitrary scalings). (B) Increase of the fraction of HPV16 PsVs that are closer than 150 nm to the next CD151 maximum (n = 3 biological replicates). Values for every sample were expressed as percentage of the total number of PsVs in the given sample. (C) The CD151 intensity at the HPV16 PsV position increases over time (n = 60–65 cells collected from 3 biological replicates). 15 min time point (0:00) was normalized to 100%. All values are given as means ± SD. Unpaired Student's t-test, comparing control to conditions as indicated (***p < 0.001; **p < 0.01; *p < 0.05). Figure taken, legend taken and modified from reference [51]. Microscopy of the samples and parts of data analysis were performed by Dominik Sons (AG Thorsten Lang).

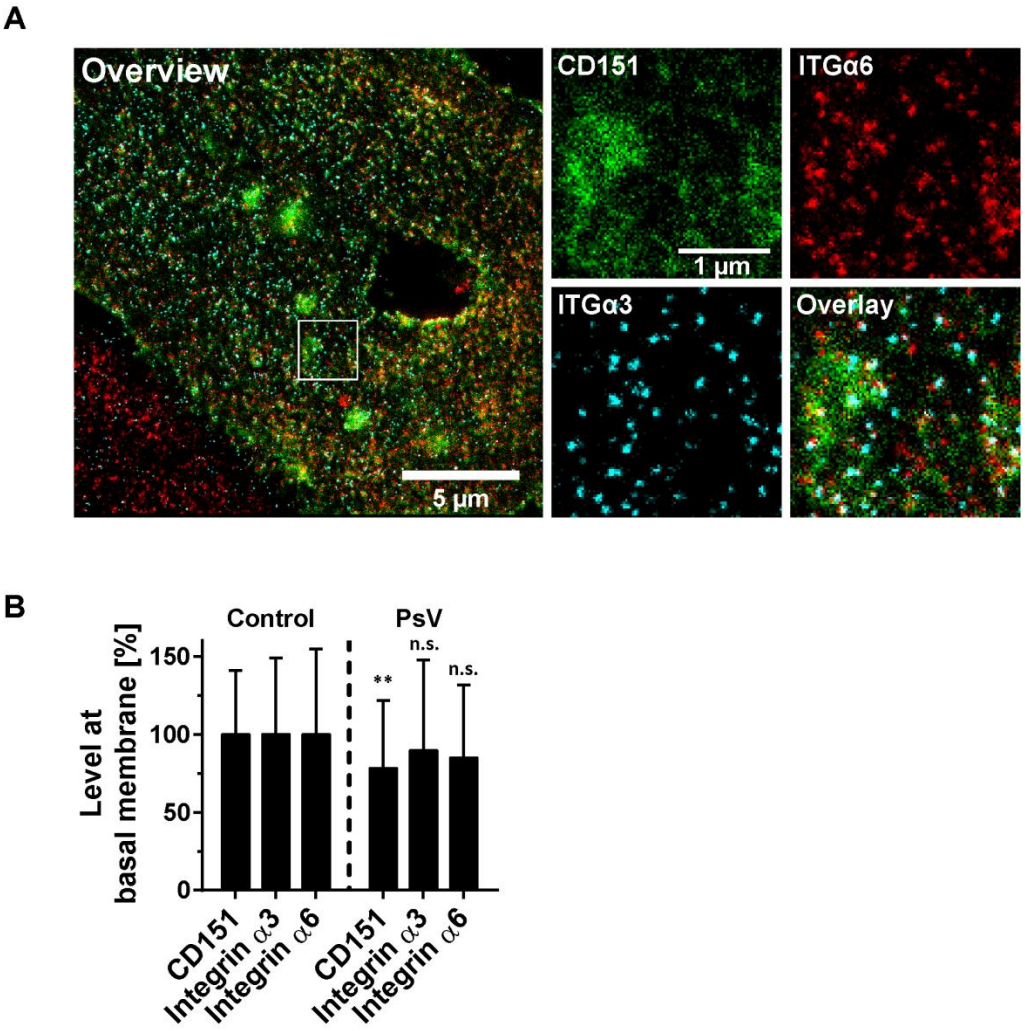

Figure 5.8 PsVs induce assemblies of CD151-GFP
Experiment from Figure 5.4, showing the condition with PsVs. (A) Large panel, channel overlay showing a membrane sheet generated from a cell incubated with PsVs. Several CD151 assemblies are visible that are less frequent in the absence of PsVs (compare Figure 5.4 A). The white box marks an area from which magnified views from the individual channels are shown. Images are displayed with the same lookup tables and scalings as in Figure 5.4. (B) Mean staining intensities of CD151-GFP, integrin α3 and integrin α6 quantified from membrane sheets generated from cells previously incubated for 5 h without (control) or with PsVs. Values are given as means ± SD (n = 60 membrane sheets collected from three biological replicates). Unpaired Student's t-tests compare control to PsV (**, $p < 0.01$). Figure and legend both taken from reference [130].

5.1.5 Influence of integrin knockdown on CD151 distribution and PsV density on the cell surface

As has been shown above, CD151, integrin α3 and integrin α6 maxima associate with each other in the plasma membrane. Moreover, interaction of the laminin-binding integrins with CD151 was previously suggested by biochemical pulldown experiments [70,84,131]. Hence, it was speculated that expression of integrins might have an influence on CD151 transport to the plasma membrane. To test this hypothesis, HaCaT cells were knocked down for integrin α3 or integrin α6, respectively. The expression of the integrins was silenced using mixtures of two different siRNAs for each integrin. As a non-silencing control, AllStars Negative control siRNA (see methods) was used.

In a first step, the knockdown efficiency of the siRNA mixtures was assessed. HaCaT cells were transfected with the respective siRNAs and cultivated for 48 h. Then, cells were lysed and knockdown efficiencies were quantified using SDS-PAGE followed by Western blotting (Figure 5.9 A, B). Integrin band intensities were normalized to their actin loading control and the value for the control siRNA was set to 100 %. As can be seen, knockdown of both integrins resulted in a very efficient reduction of the protein level by 97 % and 87 % for integrin α3 and α6, respectively (Figure 5.9 C, D). This high knockdown efficiency was used to test how specific the anti-integrin antibodies are in immunofluorescence (the same antibodies were used as in Western blot). For this purpose, membrane sheets were employed (see Figure 5.1). As can be seen, hardly any signal was detected in plasma membrane preparations originating from integrin knockdown cells (Figure 5.9 E, F).

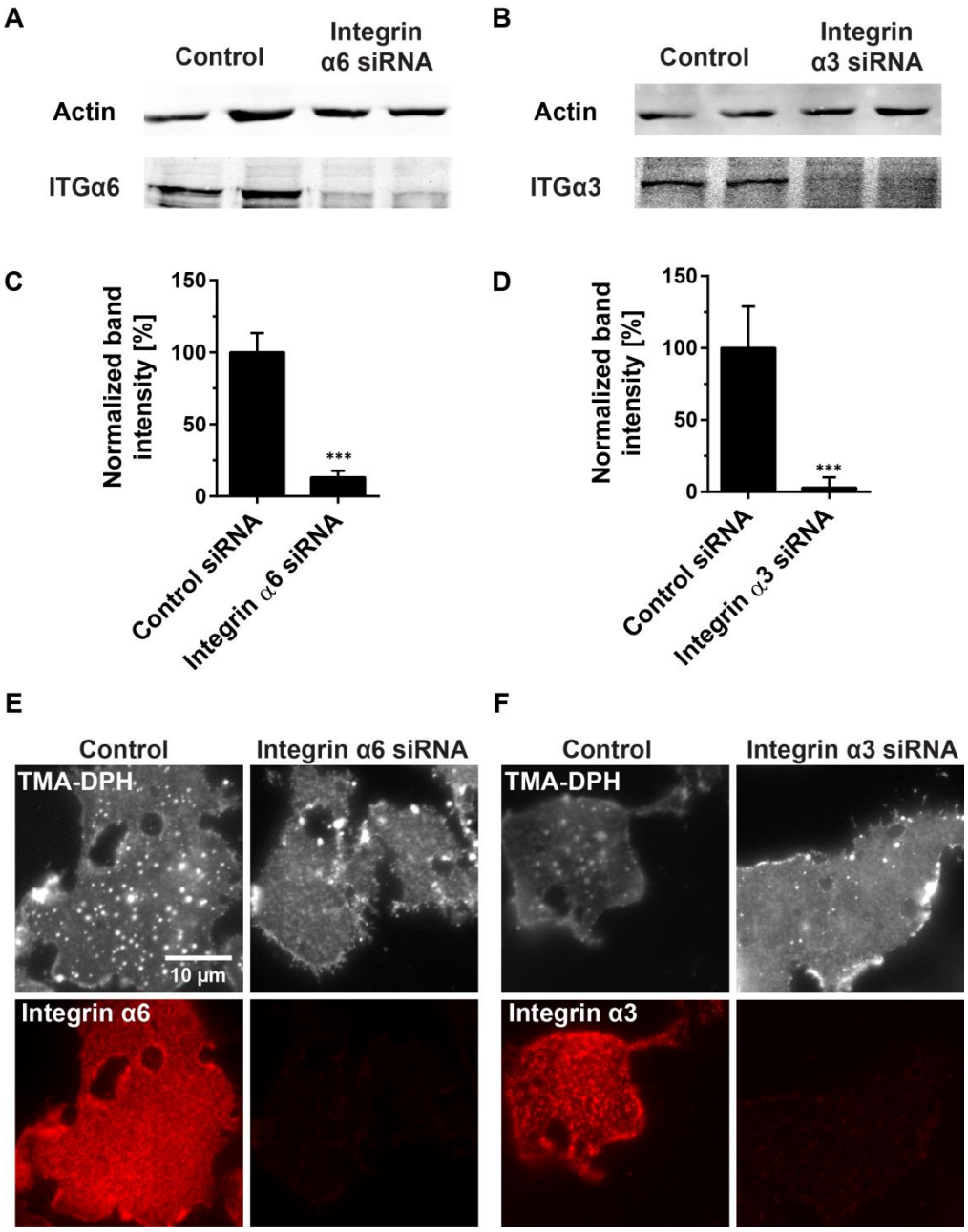

Figure 5.9 Integrin knockdown efficiency

(A - D) HaCaT cells were transfected with control, integrin α6 or integrin α3 siRNA. After 2 days, cell lysates were analyzed for integrin α6(A and C) or integrin α3 (B and D) by Western blot analysis using actin as loading control. Two lysates per condition are shown. Integrin band intensities were related to actin band intensities. The average of the control lysates for each biological replicate was set to 100%. Values are given as means ± SD (n = 6 - 8 lysates collected from 3 - 4 biological replicates). The unpaired Student's t-test compares the control to

the knockdown (***, $p < 0.001$). (E and F) Example images from an experiment in which membrane sheets from control and knockdown cells were generated and immunostained for (E) Integrin α6 or (F) integrin α3. Upper panels show membranes visualized by the membrane dye TMA-DPH, lower panels the respective integrin immunostainings. Images are displayed employing greyscale (TMA-DPH) and red (integrins) linear lookup tables. For E and F different scalings were applied, although all panels from one channel in E or F have the same arbitrary scaling. After knockdown, the integrin antibodies hardly recognize any protein. Figure and legend both taken from reference [130].

After knockdown, HaCaT cells were incubated with or without PsVs for 5 h in order to see if integrin knockdown has an influence on the HPV mediated reduction of CD151 at the cell surface. Cells were fixed, permeabilized and immunostained for CD151 and PsVs. Images were recorded via STED microscopy in the focal plane of the basal membrane.

The knockdown of integrin α3 had no influence on the level of CD151 at the basal membrane (Figure 5.10 A, B). In cells treated with control siRNA, incubation with PsVs reduced the cell surface level of CD151 to roughly 77 %. Interestingly, in integrin α3 knockdown cells no significant reduction of CD151 occurred after PsV addition. Moreover, the number of PsV particles at the cell body was counted. No significant change in the PsV density was observed after integrin α3 knockdown when compared to control cells (Figure 5.10 C).

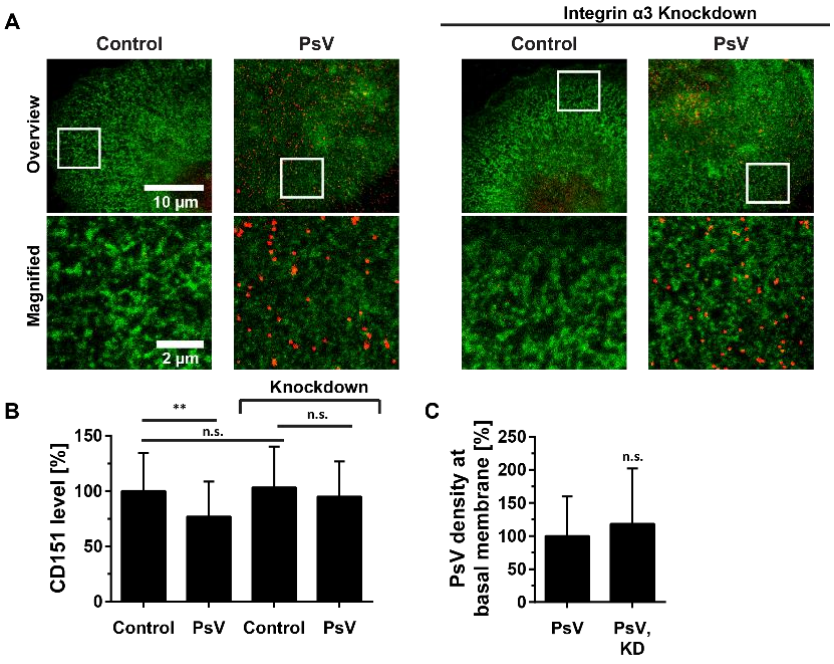

Figure 5.10 Integrin α3 knockdown does not affect the level of CD151 and the PsV density at the plasma membrane
HaCaT cells were transfected with integrin α3 siRNA and two days later incubated without or with HPV16 PsVs for 5 h. Cells were fixed, permeabilized, immunostained for CD151 (green) and L1 (red), and imaged by STED microscopy. Images are displayed employing linear lookup tables with the same scaling. (A) For each condition, overlays from an overview and a magnified view are shown. (B) Average CD151 immunostaining intensity and (C) the PsV particle density (100% PsV density correspond to 1.2 particles/µm^2). Values are shown as means ± SD (n = 60 cells collected from three biological replicates). The unpaired Student's t-tests compare the conditions as indicated by the bars (B) or PsV to PsV and knockdown (C) (**p < 0.01). Figure and legend both taken and modified from reference [130].

In integrin α6 knockdown cells, a huge impact on the CD151 level at the basal membrane was observed, as opposed to integrin α3 knockdown. Compared to control treated cells, integrin α6 depleted cells had only ~ 67 % CD151 staining intensity (Figure 5.11 A, B). The small reduction in CD151 level induced by PsV incubation was abolished in integrin α6 knockdown cells. The knockdown effect on the PsV density was even more prominent. The particle concentration at the cell body was reduced by ~ 55 % in integrin α6 depleted cells (Figure 5.11 C).

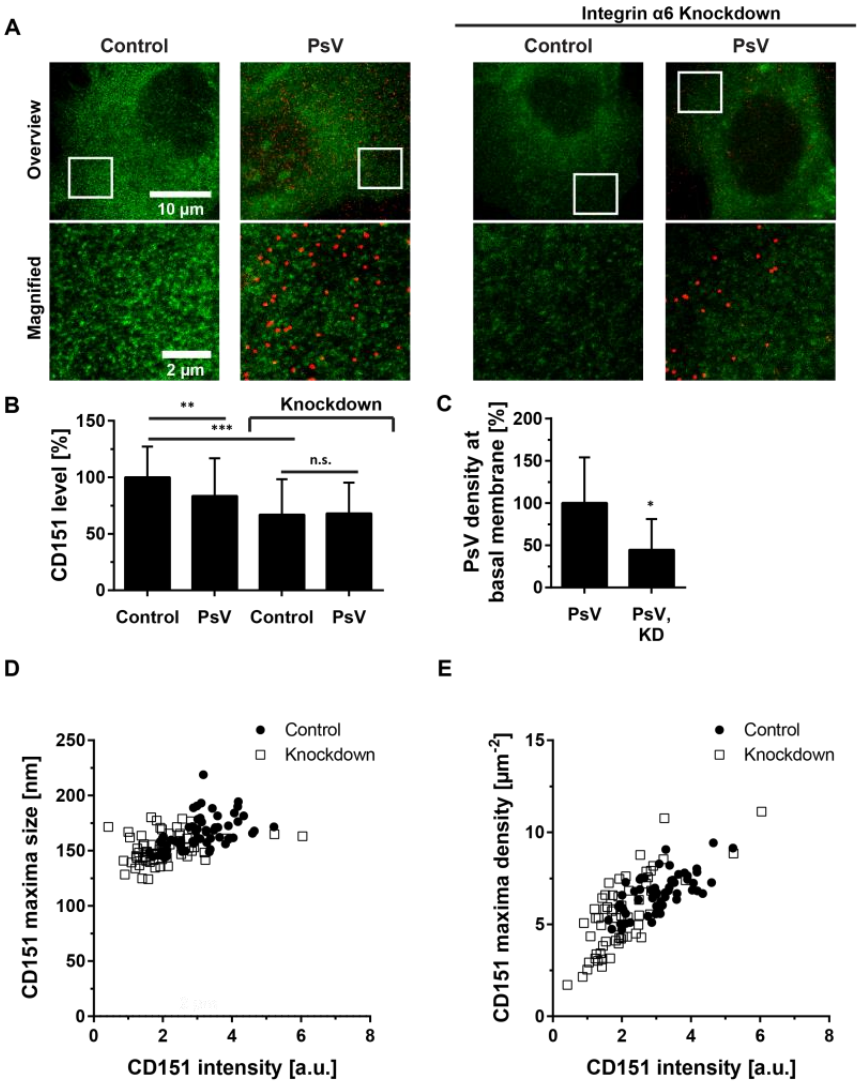

Figure 5.11 Integrin α6 knockdown reduces CD151 level and PsV density at the plasma membrane

HaCaT cells were transfected with integrin α6 siRNA and two days later incubated without or with HPV16 PsVs for 5 h. Cells were fixed, permeabilized, immunostained for CD151 (green) and L1 (red), and imaged by STED microscopy. Images are displayed employing linear lookup tables with constant scaling. (A) For each condition, overlays from an overview and a magnified view are shown. (B) Average CD151 immunostaining intensity and (C) the PsVs particle density (100% PsV density correspond to 1.4 particles/µm^2). (D and E) Maxima size (D) and density (E) of individual cells were plotted against the average CD151 intensity. Values are shown as means ± SD (n = 60 cells collected from three biological replicates). The unpaired Student's t-tests compare the conditions as indicated by the bars (B) or PsV to PsV and knockdown (C) (***p < 0.001; **p < 0.01; *p < 0.05). Figure and legend both taken and modified from reference [130].

Moreover, integrin α6 depletion has a strong effect on the basal membrane level of CD151 while integrin α3 knockdown has no effect. However, knockdown of both integrins abolished the PsV induced reduction of cell-surface CD151. Taken together, the data underline that, despite both integrins being required for infection and associating with CD151, they contribute differently to CD151 level and PsV-binding to the basal membrane.

When looking at the average cluster size and the density of CD151 in the cells, it can be noted that both parameters increase with rising CD151 level in the plasma membrane (Figure 5.11 D, E). This indicates that endogenous CD151 displays similar clustering dynamics as overexpressed CD151-GFP (Figure 5.4).

Since integrin α6 seems to influence the CD151 concentration in the plasma membrane, the question arises if CD151 in turn also influences the level of integrin α6 in the plasma membrane. Therefore, HaCaT cells were transfected with CD151-GFP and membrane sheets were generated. As a control, cells were electroporated without adding plasmid DNA. Membrane sheets were fixed, permeabilized and stained for GFP and integrin α6. Here, GFP was stained using a primary-secondary antibody combination to ensure signal amplification, giving a better signal compared to the use of nanobodies. Images were recorded using STED microscopy (Figure 5.12 A).

When CD151 was overexpressed, the average integrin α6 staining intensity increased by about 25 % (Figure 5.12 B). This suggests that overexpressing CD151 resulted in more integrin α6 protein reaching the plasma membrane.

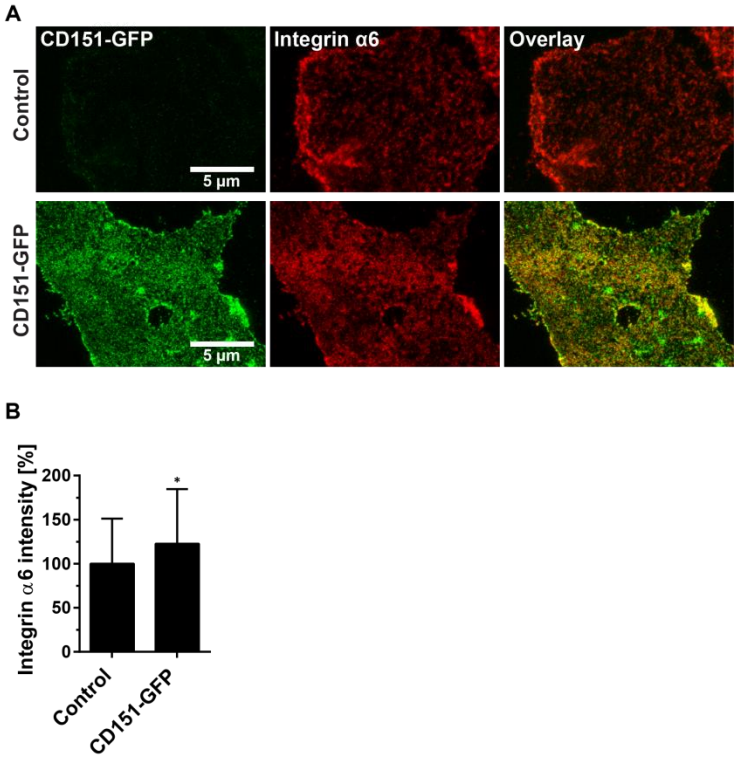

Figure 5.12 CD151-GFP overexpression increases the level of cell surface integrin α6

(A) Membrane sheets from control and CD151-GFP overexpressing HaCaT cells, stained with antibodies for GFP (green) and integrin α6 (red). Images are displayed at arbitrary intensity scalings (linear lookup tables). (B) Average integrin α6 staining in membrane sheets from control and overexpression condition. Values are shown as means ± SD (n = 59 membrane sheets collected from three biological replicates). The unpaired Student's t-test compares control to overexpression (***, $p < 0.001$; *, $p < 0.05$). Figure and legend both taken and modified from reference [130].

5.2 Roles of integrin α3 and α6 in HPV16 infection

The second aim of the study was to test whether integrin α3 and α6 have a functional role during the infection of a human keratinocyte cell line (HaCaT). While integrin α6 was already shown to be important for infection of various cell lines with papillomaviruses [47,48], the involvement of integrin α3 is less clear because of two inconsistent studies implying a role in HeLa cells but not in HaCaT cells. Therefore, we assessed the impact of the integrins in our HaCaT based infection model.

5.2.1 Impact of integrin knockdown on lysosomal capsid processing

After cell entry, the HPV capsid is trafficked to lysosomes where it becomes processed and degraded. Among others, lysosomal processing of the HPV16 L1 protein leads to one characteristic cleavage product of about 25 kDa [58]. This degradation product can be used to quantify the amount of viral particles taken up by the cell. Throughout the study, HPV16 PsVs were used instead of native viruses, as only early steps of the viral infection were investigated that do not need the viral genome or viral replication.

To test the influence of integrins on viral uptake, HaCaT cells were depleted of integrins and incubated with HPV16 PsVs for 24 h. Afterwards, cells were extensively washed to remove unbound PsVs. The cells were lysed and the cleavage product was quantified by Western blot detection of the L1 protein. The knockdown of both integrins resulted in a strong depletion of the ~25 kDa L1 cleavage product. The relative band intensities were reduced by 73 % and 44 % in integrin α3 and α6 knockdown cells, respectively (Figure 5.13). As lysosomal degradation of the capsid protein L1 was severely reduced in the absence of both integrins, both proteins apparently play a role in the uptake of HPV16.

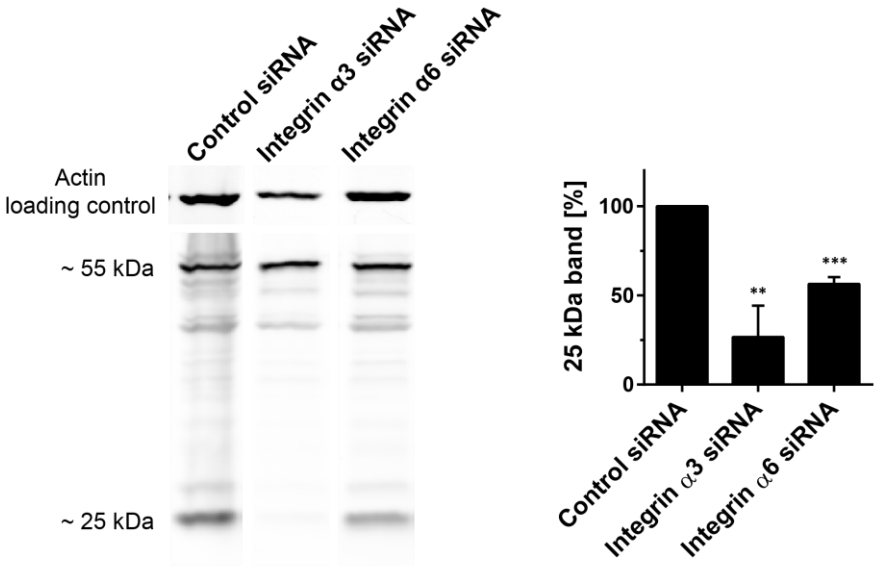

Figure 5.13 Less lysosomal capsid processing after integrin α3 or integrin α6 knockdown
Integrin α3 or integrin α6 were knocked down in HaCaT cells by siRNA transfection (for knockdown efficiency see Fig. 5.9). Two days after transfection, cells were incubated for 24 h with HPV16 PsVs, washed, lysed and analyzed by Western blot for the viral protein L1 and its ~25 kDa cleavage product. Values were related to the control which was set to 100% and are given as means ± SD (n = 3 independent experiments). Figure and legend both taken and modified from reference [130].

5.2.2 Impact of integrin knockdown on capsid disassembly

In a second approach, the cell entry of HPV16 PsVs was quantified by using the antibody L1-7 as a probe for capsid disassembly. This antibody binds to an epitope buried deep inside the viral capsid which becomes accessible only after capsid disassembly [31]. HaCaT cells were treated with control or integrin siRNA and incubated with PsVs for 5 h. To study the effect of integrins on capsid disassembly, immunostaining followed by confocal microscopy was employed. Cells were also stained for actin, allowing the identification of cells (Figure 5.14 A). Optical sections were recorded in the cell body plane where most L1-7 staining was visible using actin

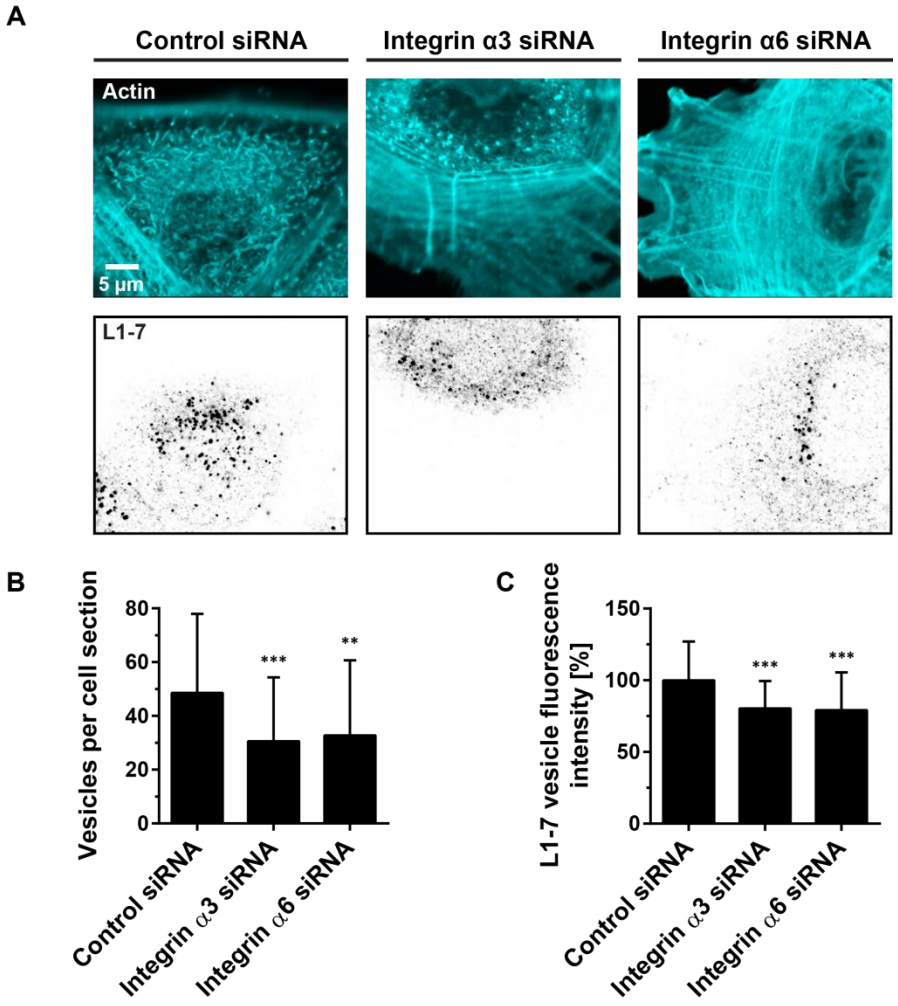

Figure 5.14 Integrin α3 or integrin α6 knockdown prevents capsid disassembly
Two days after transfection, cells were incubated for 5 h with HPV16 PsVs, washed, fixed, stained with an antibody (L1-7) that recognizes L1 after capsid disassembly, and imaged by confocal microscopy taking an optical section from the cell body. (A) Actin (cyan) and L1–7 (inverted greyscale) are each displayed at the same arbitrary scaling (linear lookup tables). From the optical section (A), an image analysis algorithm counted the number of detected vesicles per cell (B) and quantified the vesicle staining intensity (C). Values are given as means ± SD. For (B): n = 60 analysed cells collected from three biological replicates. For (C): individual vesicle intensity values were averaged per cell; cells without vesicles were excluded from the analysis (n = 58 - 60 cells collected from three biological replicates). Unpaired Student's t-test, comparing control to knockdown conditions (***, $p < 0.001$; **$p < 0.01$). Figure and legend both taken and modified from reference [130].

staining as a reference for cell outlines. The number of L1-7-positive vesicles per cell was reduced by about a third in integrin knockdown cells (Figure 5.14 B). Additionally, fluorescence intensity of the vesicles was about 25 % lower in these cells, suggesting that the viral load per vesicle was also diminished (Figure 5.14 C). This indicates that viral endocytosis, resulting in capsid disassembly in lysosomes, is diminished after knockdown of both integrins.

Taken together, the results indicate that both integrins have a critical role in promoting HPV16 cell entry into HaCaT cells.

5.2.3 Contribution of integrins to cell-binding of HPV16 PsVs

The results above suggest that integrin α3 and α6 both have a role in promoting HPV cell entry to keratinocytes. Moreover, the functional relevance was verified in collaboration with the Florin group (University of Mainz, Germany) in a luciferase-based infection assay. The knockdown of both integrins resulted in less expression of the luciferase reporter plasmid, which is encapsidated by the HPV16 PsVs [130]. Together, these findings underline the importance of both integrins for HPV infection.

After confirming that both integrins are functionally involved in HPV cell entry, the exact role of each integrin in this process needs to be determined. In principle, at least two scenarios are conceivable: the proteins can either promote PsV-binding to host cells or mediate endocytosis of cell-bound viral particles. Previous studies indicate that integrin α6 is involved in binding [45,46,49]. For integrin α3, there is no evidence on its function yet. Therefore, the role of integrin α3 in cell binding was tested. To this end, HaCaT cells were depleted of integrins, incubated with PsVs for 1 h at 4 °C and extensively washed. However, PsVs that unspecifically adsorb to the substrate are a problem when lysing cells directly and trypsin treatment was shown to remove bound PsVs from cells [49]. Therefore, cells were collected by direct mechanical scraping from

the substrate followed by extensive washing and lysing. The amount of cell-bound PsVs was quantified by Western blotting and detection of the L1-protein (Figure 5.15). When compared to control cells, the amount of PsVs bound to integrin α6 knockdown cells is strongly reduced by 40 % (Figure 5.15). Integrin α3 knockdown only has a minor effect, suggesting it has a role different from promoting PsV-binding to host cells. These results are in line with the PsV densities found in knockdown cells in immunofluorescence experiments (Figure 5.10 and 5.11).

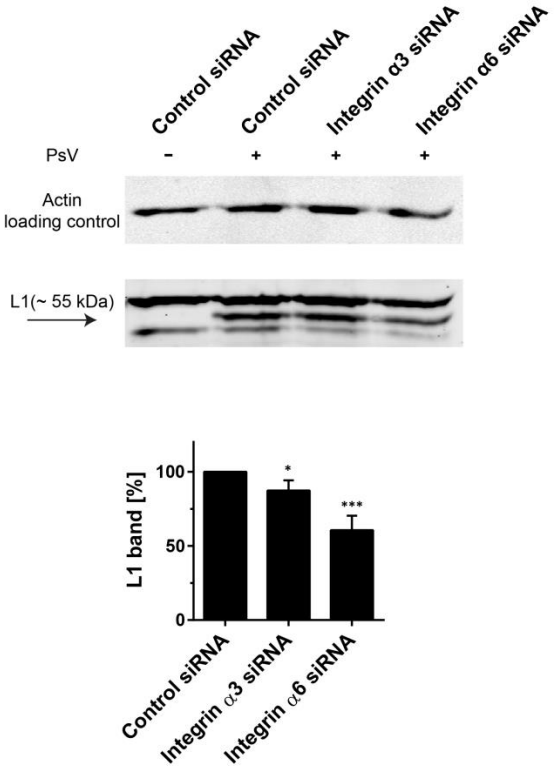

Figure 5.15 Knockdown of integrin α6 but not of integrin α3 strongly inhibits PsV binding

Two days after siRNA transfection, cells were incubated for 1 h at 0 °C with HPV16 PsVs, scraped from the substrate, washed, lysed and analyzed by Western blot. Binding of viral particles was assayed by quantification of the L1 ~55 kDa band. The control value was set to 100 % and used for normalization. The CamVir1 anti-L1 antibody detects some unspecific bands (compare control cells treated with and without PsVs). Values are given as means ± SD (n = 4 independent experiments). Unpaired Student's t-test, comparing control to knockdown conditions (***p < 0.001; *p < 0.05). Figure taken, legend taken and modified from reference [130].

5.3 Characterization of HPV16 viral entry platform

HPV16 PsVs associate with CD151 nanodomains on the cell surface (Figure 5.7). They also associate with nanodomains defined by tetraspanin CD151 in the plasma membrane. These local CD151 maxima also associate with integrins α3 and α6 maxima (Figure 5.4). The results described above confirmed that integrins α3 and α6 are functionally relevant during HPV16 cell entry (section 5.2). Yet, several questions remain unanswered. Do viral particles preferentially associate with one of the components? What is the local maxima composition at PsV attachment sites? Can an entry platform be defined?

In order to be able to analyse the PsV attachment site under non-overexpression conditions in a triple staining (viral particle, CD151 and integrins), it was not possible to visualize PsVs by antibody staining. This is because the available anti-HPV16 antibodies are either mouse or rabbit antibodies just like the best working anti-CD151 and anti-integrin antibodies. Therefore, so-called EdU modified PsVs were employed in these experiments. These pseudoviral particles contain a reporter plasmid where the thymidine analogue EdU is incorporated into the DNA. Thereby, the reporter plasmid DNA can be labelled directly with a fluorophore, in this case fluorescein, via click chemistry.

5.3.1 Association of PsVs with CD151 and integrin α6

HaCaT cells were seeded onto PLL-coated glass coverslips and incubated with EdU PsVs for 5 h. Thereafter, membrane sheets were generated. Samples were fixed, permeabilized, click-labeled with fluorescein and immunostained. Imaging was performed using STED microscopy. As can be seen, PsVs often overlapped with or were close to maxima positive for CD151 and/or integrin α6 (Figure 5.16 A, indicated by white circles). To confirm this visual impression, the PCC between PsVs and CD151 and

between PsVs and integrin α6 was calculated, respectively. As a control, the image of one channel within the analysed region of interest was flipped vertically and horizontally to mimic a random relationship between the channels. This value was then compared to the value obtained from the original image. While the PCC was quite low for both proteins (~ 0.07 and 0.05 for PsVs/CD151 and PsVs/integrin α6, respectively), the values were significantly higher than in the control, confirming the visual impression of specific association (Figure 5.16 B). To analyse the spatial relationship, the distance of a PsV to its nearest CD151 and integrin α6 maximum was determined. For individual PsVs pooled from all analysed membrane sheets, distances to CD151 and integrin α6 maxima were plotted against each other (Figure 5.16 C). In most cases, PsVs showed distances closer than 250 nm to their next maxima. Interestingly the distribution of very short distances appeared to be similar for both maxima types, suggesting none of them is preferred for association.

In recent years, it has been shown that proteins concentrate in protein clusters that contain many copies of a protein and have a size range of 100-200 nm [85,134,135]. The maxima observed in this study have a similar size and could represent clustered proteins. Are all detected maxima protein clusters? It is possible that especially the dimmer maxima originate from background signal, like trapped antibody complexes that could not be washed off. Moreover, some of them may also arise from single molecules. When analysing the local composition of the PsV binding sites with reference to the association of PsVs with protein clusters, the many maxima not arising from protein clusters make it difficult to recognize specific association.

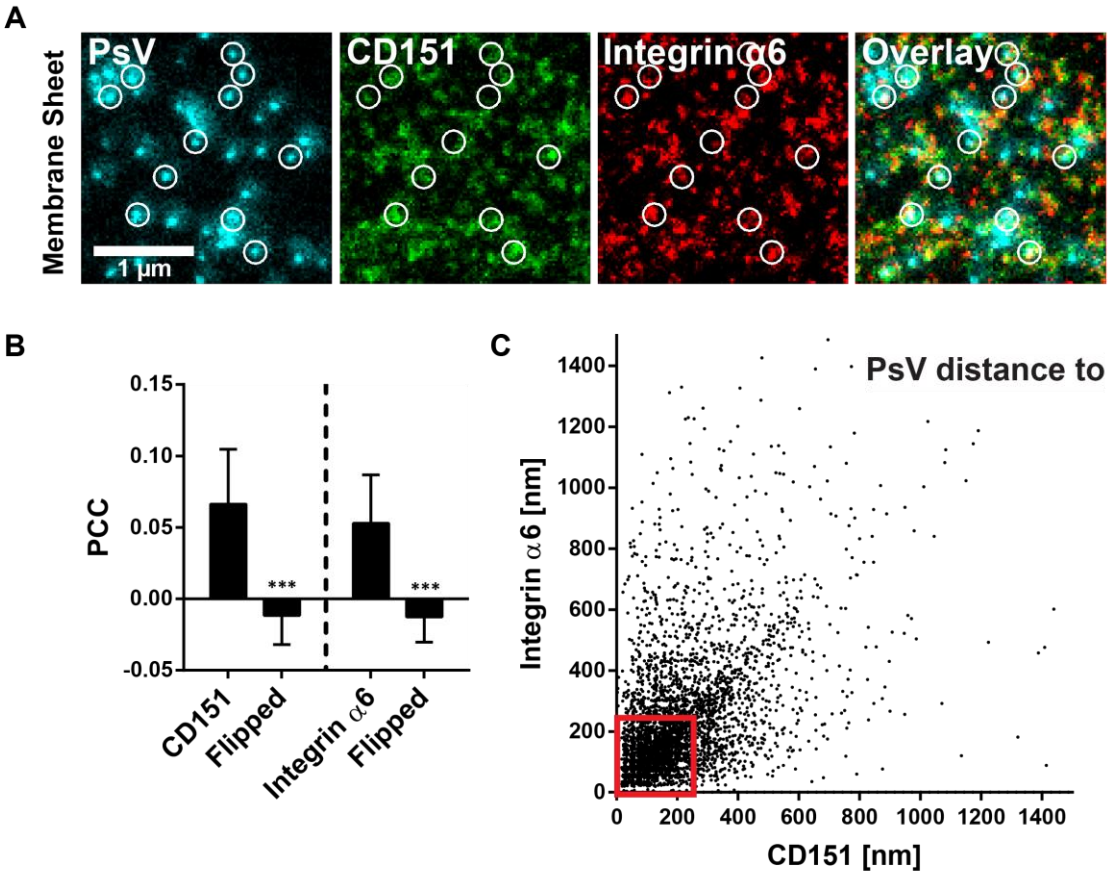

Figure 5.16 Viral particle distance to CD151 and integrin α6 maxima
Membrane sheets were generated from HaCaT cells treated for 5 h with EdU-PsVs. They were stained for EdU-PsVs (cyan lookup table; click-labelled with fluorescein), CD151 (green lookup table; immunostaining) and integrin α6 (red lookup table; immunostaining), followed by STED microscopy imaging. (A) Images from the three channels and an overlay are shown and displayed at arbitrary intensity scalings (linear lookup tables). Circles mark identical pixel locations. (B) Pearson correlation coefficient between PsVs and CD151 (left) and integrin α6 (right). A control value for randomized distribution ('flipped') was calculated after flipping of one channel. Values are given as means ± SD (n = 57 membrane sheets collected from three biological replicates). (C) For individual PsVs, the nearest distance to a CD151 and an integrin α6 maximum was plotted (the analysis includes 4452 PsVs from 57 membrane sheets collected from three biological replicates). Statistical analysis was performed employing the unpaired Student's t-test comparing the original to the flipped images (***$p < 0.001$). Red boxes frame viral particles potentially used for further analysis of the platform area (Fig. 5.17). For this, only PsVs closer than 250 nm to bright CD151/integrin maxima were considered. Figure and legend both taken and modified from reference [130].

Indeed, in an initial analysis including all maxima, only little specific association was observed. Therefore, the data were filtered for more intense maxima. The assumption that the entry platform is defined by more intense maxima is supported by the data described above, where CD151 signal at PsV location increased during the infection process (Figure 5.7). Consequently, further analysis of the HPV16 entry platform was performed focussing on the 10-20 % most intense maxima that were assumed to be protein clusters. An entry platform is supposed to contain the components required for cell entry. Therefore, PsVs were considered to be potentially associated with an entry platform when they were closer than 250 nm to both, a CD151 cluster and an integrin α6 cluster. These PsVs were then used for further analysis of the composition of the entry platform. Within a 1 µm x 1 µm region centred to the PsV position, the numbers of CD151 and integrin α6 clusters were counted and regarded as the platform area composition (Figure 5.17 A, B). How do these regions differ from randomly chosen areas? To answer this question, the images from the CD151 and integrin α6 channels were flipped vertically and horizontally to create a random relationship to PsVs. For the same viral particles, the cluster densities in the randomized areas were quantified. In randomized areas, 1.5 CD151 clusters and 2.1 integrin clusters were found on average per μm^2, whereas platform areas contained on average 3.9 CD151 clusters and 4.9 integrin α6 clusters (Figure 5.17 B).

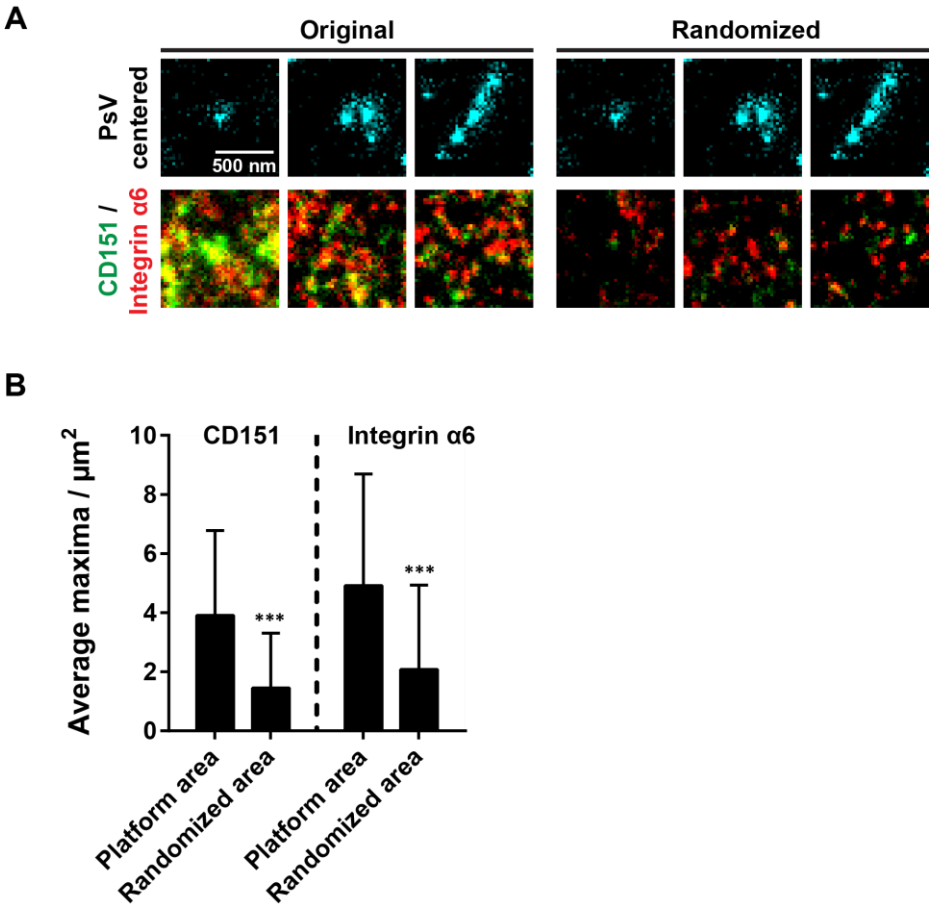

Figure 5.17 Local crowding of CD151 and integrin α6 clusters at PsV attachment sites

To characterize the anatomy of a possibly forming viral platform area, those PsVs from Figure 5.16 with a distance smaller than 250 nm to both a bright CD151 and integrin α6 maximum (for examples, see centrally located PsVs in the left panels in A) were selected. In a PsV centred 1 µm × 1 µm ROI the number of bright maxima (see methods) in the CD151 and integrin channels were counted. The same was performed after flipping the CD151/integrin channels, causing a randomized relationship between PsV-attachment sites and maxima (A, right panels). In the original images more closely associated maxima are present at sites of PsV-attachment. Images are displayed in cyan (PsV), green (CD151) and red (integrin) at arbitrary intensity scalings (linear lookup tables). (B) Quantification of the bright maxima in the 1 µm × 1 µm ROI. Values are given as means ± SD (n = 283 1 µm × 1 µm ROIs). Statistical analysis was performed employing the unpaired Student's t-test comparing the original to the randomized condition (***p < 0.001). The number of clusters per attachment site was highly variable. Figure and legend both taken and modified from reference [130].

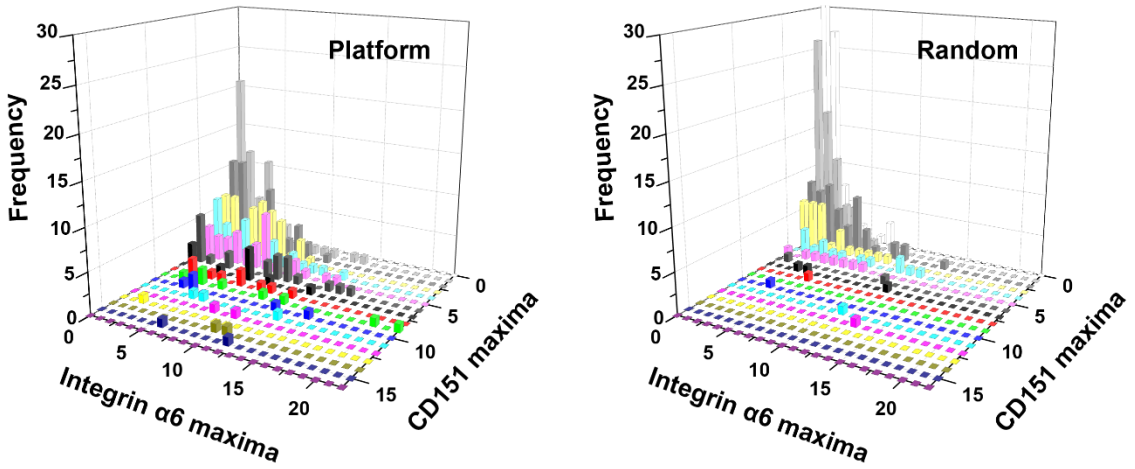

Figure 5.18 Histograms illustrating the variability of the number of CD151 and integrin α6 clusters in the platform area
Individual maxima/µm^2 from Figure 5.17 plotted as 2D histograms. For each presumed viral particle attachment site (283 PsVs), the number of bright integrin α6 maxima is plotted versus the number of bright CD151 maxima. Plots are shown for the platform and the randomized area. The histogram of the randomized areas is truncated at low count bins. The value at the zero/zero count bin reaches 68. Figure and legend both taken and modified from reference [130].

It should be noted that the composition of individual platforms was highly variable (Figure 5.18). Platform areas contained between 2 and 31 CD151 and integrin α6 clusters in total. Randomized areas comprised 25 clusters at most while a large part (43 %) contained less than two clusters. According to our definition, the platform has to contain at least 2 clusters (1 of each type), a restriction which does not apply to the randomized area. However, most platform areas consisted of 8 clusters or more (51 % of analysed platform areas). For randomized areas, this applied to only 13 % of all analysed areas.

5.3.2 Association of PsVs with CD151 and integrin α3

The relative association of PsVs to CD151 and integrin α3 was analysed in the same way as for integrin α6. HaCaT cells were plated onto PLL-coated glass coverslips and incubated with EdU PsVs for 5 h. Immunostaining of CD151 was performed using an alternative antibody (rabbit monoclonal) because the available anti-integrin α3 antibody was raised in mice, just like the anti-CD151 antibody used in all other experiments. Cells were fixed and permeabilised using methanol as according to the manufacturer's instruction the rabbit anti-CD151 antibody requires this fixation method for proper epitope binding. It was not possible to efficiently screen the samples for membrane sheets due to the low staining intensities of the CD151 and integrin α3 antibodies. Therefore, the analysis was performed on intact cells as identification was possible due to intracellular signal. Just like for integrin α6, PsVs often overlapped with or were close to maxima positive for CD151 and/or integrin α3 (Figure 5.19 A, indicated by white circles). Again, the PCC between PsVs/CD151 and PsVs/integrin α3 was calculated, respectively (Figure 5.19 B). The PCC between PsVs and CD151 was comparable (0.05) to the value previously found on membrane sheets. However, the correlation coefficient for integrin α3 (0.12) was substantially higher than for the other two components. Both values were significantly higher than for randomized images, again confirming a specific association. The nearest distances of individual PsVs to both proteins pooled from all analysed cells were calculated and plotted against each other (Figure 5.19 C). Just like for membrane sheets, most distances to integrin α3 and CD151 were shorter than 250 nm. Again, the distribution of very short distances appeared to be similar for both maxima types.

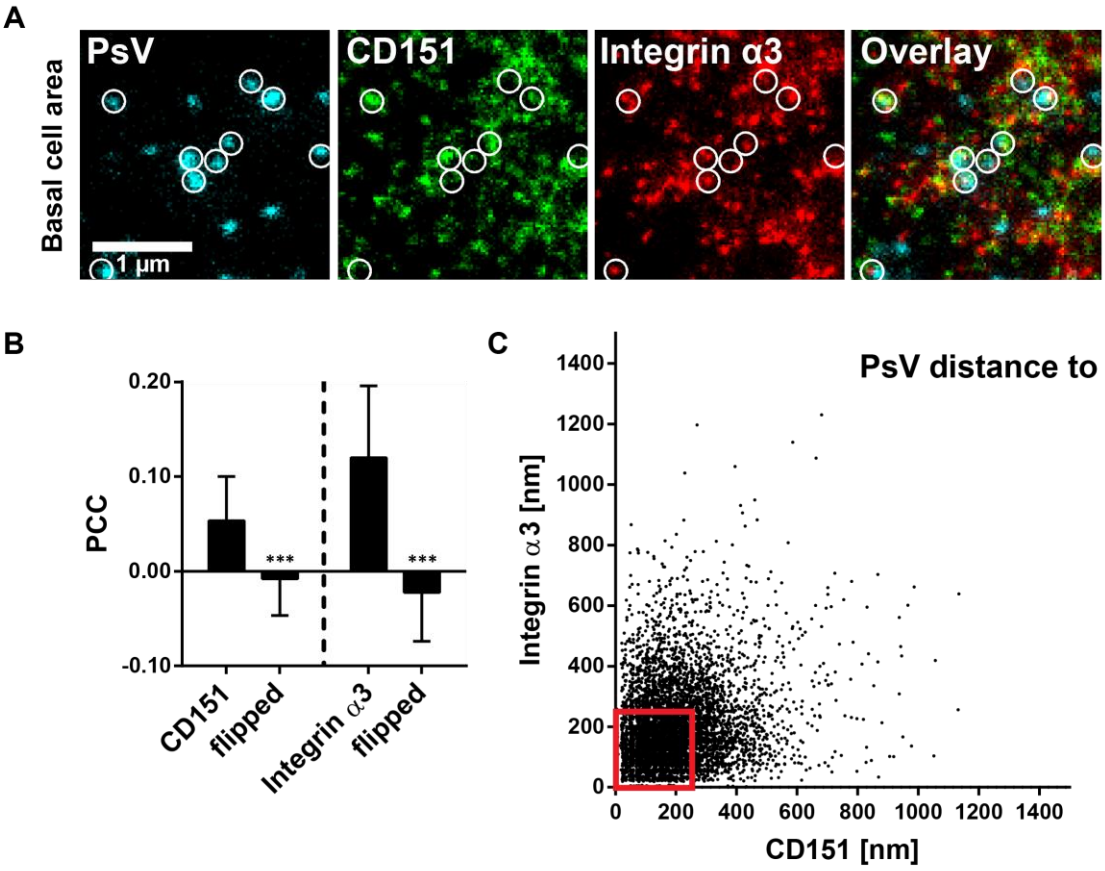

1Figure 5.19 Viral particle distance to CD151 and integrin α3 maxima
HaCaT cells were treated for 5 h with EdU-PsVs. They were stained for EdU-PsVs (cyan lookup table; click-labelled with fluorescein), CD151 (green lookup table; immunostaining) and integrin α3 (red lookup table; immunostaining), followed by STED microscopy imaging. (A) Images from the three channels and an overlay are shown and displayed at arbitrary intensity scalings (linear lookup tables). Circles mark identical pixel locations. (B) Pearson correlation coefficient between PsVs and CD151 (left) and integrin α3 (right). A control value for randomized distribution ('flipped') was calculated after flipping of one channel. Values are given as means ± SD (n = 60 cells collected from three biological replicates). (C) For individual PsVs, the nearest distance to a CD151 and an integrin α3 maximum was plotted (the analysis includes 8519 PsVs from 60 cells collected from three biological replicates). Statistical analysis was performed employing the unpaired Student's t-test comparing the original to the flipped images (***$p < 0.001$). Red box frames viral particles potentially used for further analysis of the platform area (Fig. 5.20). For this, only PsVs closer than 250 nm to bright CD151/integrin maxima were considered. Figure and legend both taken and modified from reference [130].

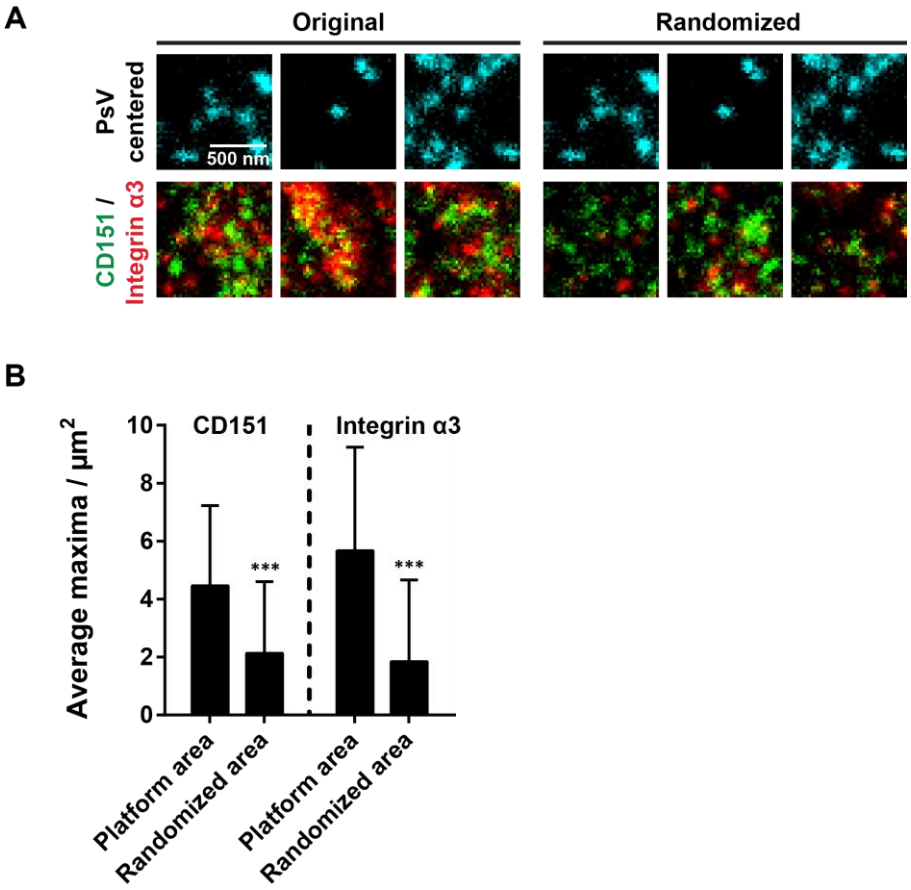

Figure 5.20 Local crowding of CD151 and integrin α3 clusters at PsV attachment site

To characterize the anatomy of a possibly forming viral platform area, those PsVs from Figure 5.19 with a distance smaller than 250 nm to both a bright CD151 and integrin α3 maximum (for examples see centrally located PsVs in the left panels in A) were selected. In a PsV centred 1 µm × 1 µm ROI the number of bright maxima (see methods) in the CD151 and integrin channels were counted. The same was performed after flipping the CD151/integrin channels, causing a randomized relationship between PsV-attachment sites and maxima (A, right panels). In the original images more closely associated maxima are present at sites of PsV-attachment. Images are displayed in cyan (PsV), green (CD151) and red (integrin) at arbitrary intensity scalings (linear lookup tables). (B) Quantification of the bright maxima in the 1 µm × 1 µm ROI. Values are given as means ± SD (n = 678 1 µm × 1 µm ROIs). Statistical analysis was performed employing the unpaired Student's t-test comparing the original to the randomized condition (***$p < 0.001$). Please note, that the number of clusters per attachment site was highly variable. Figure and legend both taken and modified from reference [130].

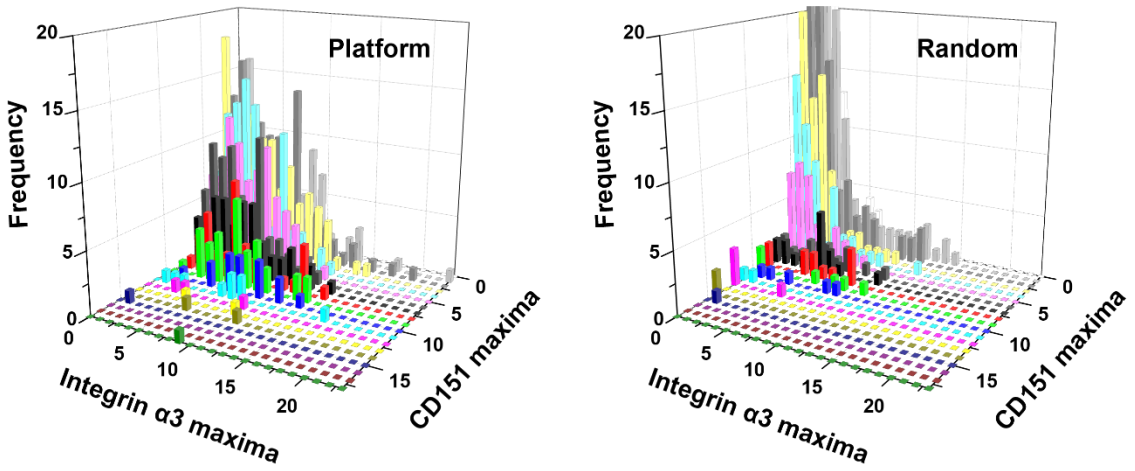

Figure 5.21 Histograms illustrating the variability of the number of CD151 and integrin α3 clusters in the platform area
Individual maxima/µm^2 from Figure 5.20 plotted as 2D histograms. For each presumed viral particle attachment site (678 PsVs), the number of bright integrin α3 maxima is plotted versus the number of bright CD151 maxima. Plots are shown for the platform and the randomized area. The histogram of the randomized areas is truncated at low count bins. The value at the zero/zero count bin reaches 139. Figure and legend both taken and modified from reference [130].

For description of the anatomy of the entry platform with regard to CD151 and integrin α3, images obtained from the cells immunostained for CD151 and integrin α3 were processed in the same way as for the membrane sheets stained for CD151 and integrin α6. Thus, the data from Figure 5.19 were filtered for intense maxima that were regarded as protein clusters. Again, PsVs were assumed to possibly be attached to an entry platform if they were closer than 250 nm to both cluster types. The entry platforms were characterised by counting the cluster numbers of both proteins within a 1 µm x 1 µm region centred to the PsV position. Platform areas were compared to randomized areas created by flipping the CD151 and integrin α3 channels, therefore creating random relationships with regard to the PsV position (Figure 5.20 A, B). In randomized areas, 2.1 and 1.8 clusters per µm^2 were found for CD151 and integrin α3, respectively (Figure 5.20 B). These values are comparable to those previously found on randomized areas from membrane sheets stained for CD151 and integrin α6. Platform

areas contained an average of 4.5 CD151 clusters per μm^2 and for integrin α3 an average of 5.7 clusters per μm^2.

As already observed for CD151/integrin α6 platforms, individual CD151/integrin α3 entry platforms were highly variable in their composition (Figure 5.21). Platform areas contained between 2 and 28 clusters (per definition, platform areas contain at least one cluster of each type), which is comparable to CD151/integrin α6 platforms. Randomized areas contained a maximum of 22 clusters while a large part (38 %) contained less than two clusters. However, most platform areas (51 %) contained 10 clusters or more. For randomized areas, this applied to only 12 % of analysed areas.

Taken together, comparable results were obtained for the characterization of the viral entry platform area for both, CD151/integrin α6 on membrane sheets and CD151/integrin α3 on intact cells. By using the above definition for HPV16 platform areas, they are characterized by a region of the plasma membrane with a roughly 2.5-fold higher density of CD151 and integrin clusters compared to randomized regions.

It should be noted that the analysis of intact cells included almost twice as much PsVs as on membrane sheets. This may be due to the sheeting process. HaCaT membrane sheets are much smaller than intact cells, probably due to applying several ultrasound pulses to the coverslip. As PsVs often concentrate at cellular edges (see also Figure 5.22 A), it is possible that edge regions are often ripped off and by this reduce the PsV density on membrane sheets. Interestingly, integrin α3 concentrated in the same area as PsVs on numerous occasions, seemingly following the pattern of PsV distribution (Figure 5.22 A). To a lower extent, CD151 was distributed in a similar fashion. The same observation, albeit less frequently, was made on membrane sheets originated from HaCaT cells overexpressing CD151-GFP and fixed with PFA instead of methanol, suggesting that the observation is independent of the fixation method and sample preparation (Figure 5.22 B). This was not noted in the case of integrin α6. However, this should be verified using intact cells with intact cellular periphery.

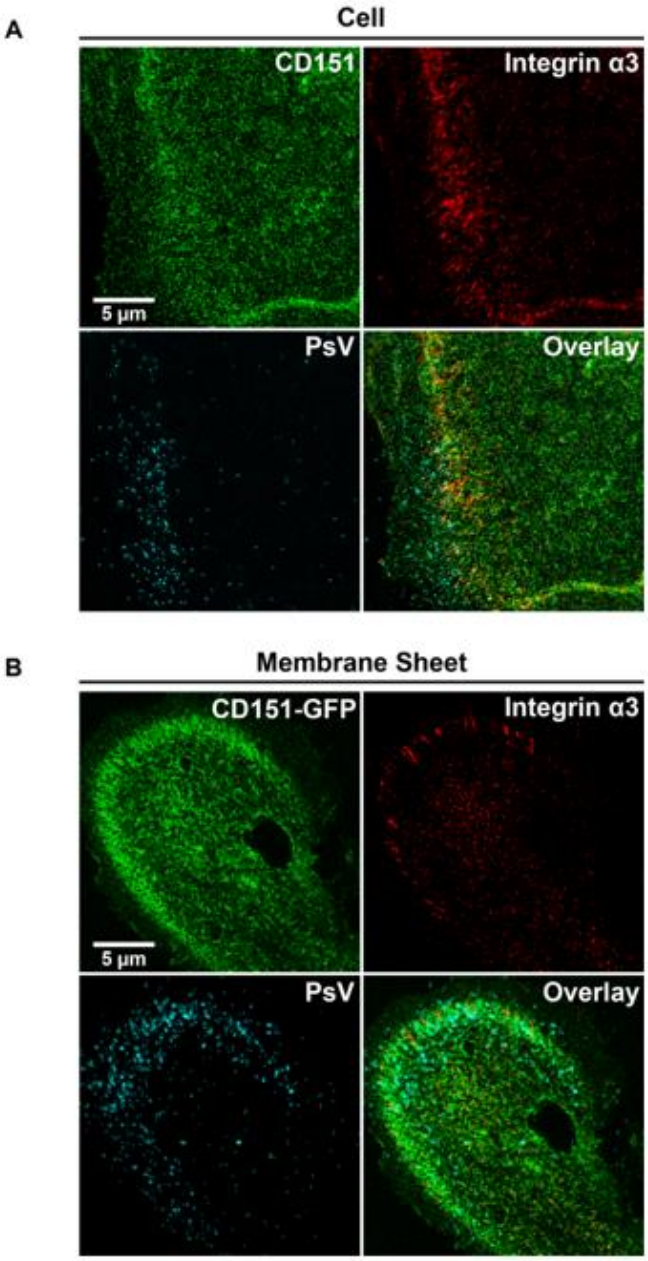

Figure 5.22 PsV binding pattern imaged on intact cells or membrane sheets from cells overexpressing CD151-GFP
(A) Basal membrane of a HaCaT cell fixed with methanol (from the experiment shown in Figure 5.19). (B) Membrane sheet generated from a HaCaT cell overexpressing CD151-GFP and incubated with PsVs for 5 h before membrane sheets preparation. Sheets were fixed, permeabilized, and fluorescently labelled. PsVs (cyan) and integrin α3 (red) were immunostained and CD151-GFP (green)

was enhanced with GFP nanobodies. Examplary images illustrate that independent from the fixation protocol and sample preparation in many cases integrin α3 (linear red lookup table) enriches at the cell periphery (B). In particular viral particles (linear cyan lookup table), but also CD151 (linear green lookup table), accumulate at the cell periphery. Images are displayed at arbitrary intensity scalings. Figure taken, legend taken and modified from reference [130].

5.3.3 Connection of the entry platform to the cytoskeleton

As pictured above, HPV16 PsVs associate with areas of the plasma membrane characterized by crowded TEM components. However, it remains unclear whether the virus targets entry platforms, which are already present on the cell surface, or if HPVs actively create their entry platforms by themselves. Do platforms mark viral attachment sites, or are bound viral particles transported to the platforms?

A previous study employing TIRF microscopy on living cells suggests that only PsVs that are associated with CD151 assemblies are internalized [48]. From this study, the Florin group made some of the recorded TIRF movies available for the analysis of PsV and CD151-assembly mobility. There, HeLa cells were transfected with CD151-CFP and incubated for 1.5 h to 4 h with HPV16 PsVs labelled directly with Alexa488 via Alexa Fluor 488 succinimidylester. Cells were imaged for CD151-CFP and PsVs with TIRF microscopy by recording one image every six seconds (Figure 5.23 A and B). The TIRF movies were analysed for the mobility of PsVs and CD151-CFP assemblies at the plasma membrane. Here, the CD151 pattern is not well-resolved due to diffraction-limited resolution. Viral particles and CD151 structures were randomly chosen and tracked over a period of up to 180 s (Figure 5.23 B, C). Most PsVs were immobile on the cell surface. CD151 assemblies, however, displayed a much higher mobility and moved across the cell surface in many cases. The mean square displacement (MSD) for CD151 and PsV were calculated and plotted versus the time intervals, thereby highlighting the great mobility difference between both type of objects (Figure 5.23 D). In contrast to PsVs, the plot suggests a unidirectional flow for CD151-CFP.

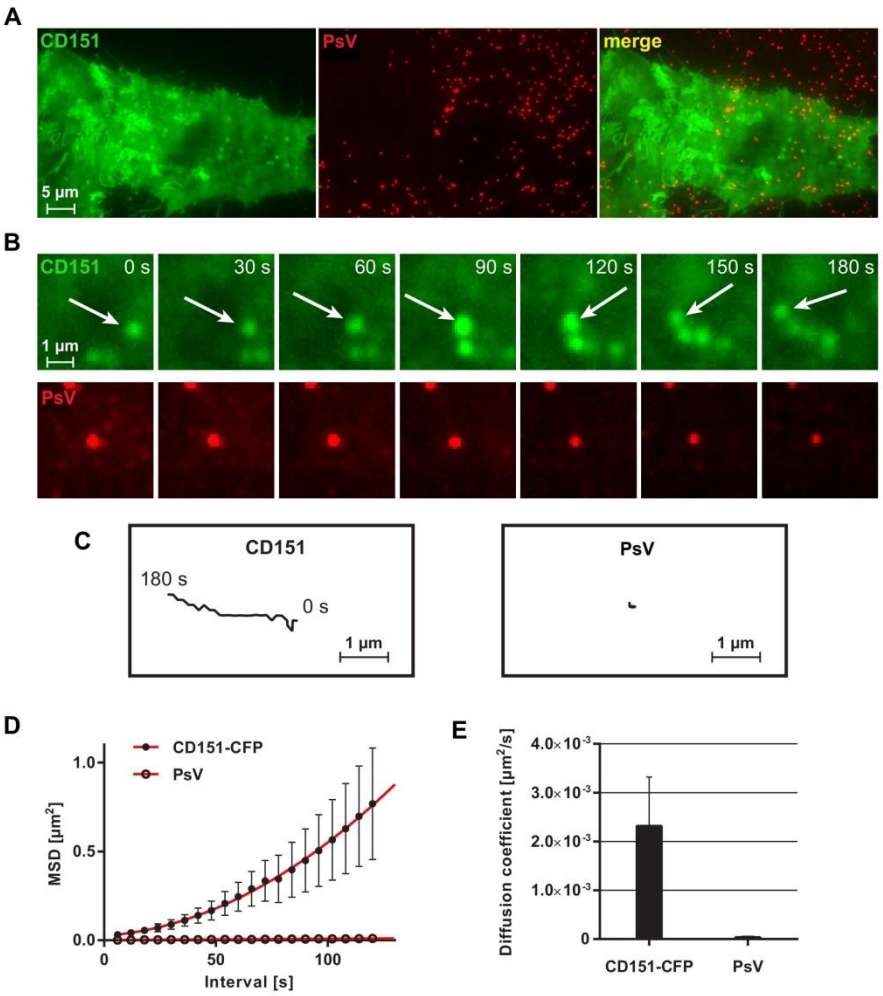

Figure 5.23 Viral particle mobility
For the analysis, five movies were analyzed that were already published in part in reference [48]. HeLa cells were transfected with CD151-CFP (shown in green) and incubated with Alexa Fluor 488 (AF488)-labelled HPV16 PsVs (shown in red) for 1.5–4 h, followed by imaging for 3 min at 0.166 Hz employing TIRF microscopy. (A) Overview from the two channels and overlay. The CD151 cluster pattern is not well resolved due to diffraction-limited resolution. (B) Magnified views (upper and lower rows are not the same field of view). Images taken from a 180 s sequence show the lateral mobility of a CD151-CFP particle (upper row) and PsV particle (lower row). Spherical CD151 structures often move directional. (C) Tracks of the object marked with an arrow in (B) and the centered viral particle in (B). (D) Mean squared displacement (MSD) plotted against time interval (n = 14–15 particles per channel) for CD151-CFP and PsV particles, respectively. (E) Diffusion coefficients for CD151-CFP and PsV particles. All values are given as means ± SEM. Figure and legend both taken and modified from reference [51].

This suggests an active transport of CD151, possibly linking the assemblies to motor proteins and cytoskeletal movement. For simplicity, the diffusion coefficients were calculated assuming random diffusion coefficients D. Diffusion coefficients were determined for each individual track and an average diffusion coefficient was calculated ($D = 9*10^{-6}$ $\mu m^2/s$ for PsVs and $D = 2.3*10^{-3}$ $\mu m^2/s$ for CD151-CFP assemblies, Figure 5.23 D). While individual diffusion coefficients for CD151 were highly variable, it can be concluded that these assemblies are much more mobile than viral particles, which remained almost immobile on the cell surface. The less mobile viruses combined with the fact that more viruses are associated with CD151 over time (Figure 5.7) suggest that platforms are forming around viruses rather than the viral particle being transported to the platform.

No matter if viruses bind to preformed structures or actively induce their formation, the entry platform needs to be connected in some way to intracellular dynamics to support the viral cell entry. Previous reports confirmed that HPV infection is dependent on actin dynamics [31,108,109]. Noteworthy, a study performed by Shigeta *et al*. made a connection between CD151 and the actin cytoskeleton [113]. In this study, antibody induced aggregation of CD151 resulted in the occurrence of aggregated actin at sites of patched CD151 signal. Interestingly, incubating the cells with anti-integrin α3 antibody had the same effect. Thus, it is tempting to speculate that HPV16 entry platforms defined by CD151 are connected to actin reorganization.

To further clarify whether PsV entry platforms are associated with the actin cytoskeleton, HaCaT cells were transfected with CD151-GFP and incubated with or without HPV16 PsVs for 3 h, followed by membrane sheet preparation. Samples were fixed, permeabilized, PsVs and F-actin and GFP signal was enhanced using nanobodies. Images were recorded via confocal microscopy (Figure 5.24 A). Large assemblies of CD151 were observed to colocalize with aggregated actin. Therefore, the fraction of CD151-GFP that colocalized with actin signal was calculated (Figure 5.24 B). Incubation

with PsVs increased the ratio of colocalizing CD151-GFP/actin to total CD151-GFP from 0.2 to 0.3. On many occasions, PsVs could be observed at the edge or within such CD151-actin colocalizing structures (see magnified views of the PsV condition, Figure 5.24 A). Consequently, the data suggest a connection between CD151 platforms and the actin cytoskeleton.

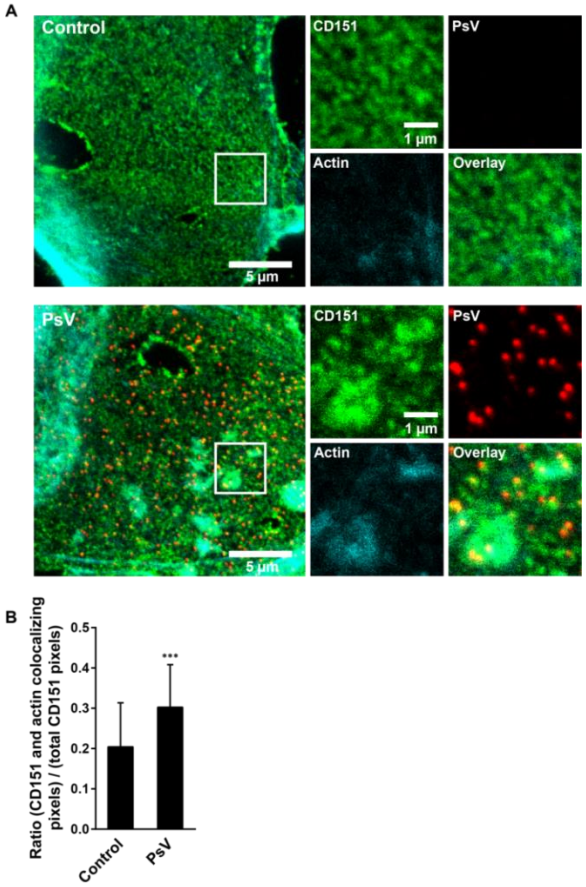

Figure 5.24 Large CD151 assemblies coincide with intracellular actin accumulations
CD151-GFP transfected HaCaT cells were treated for 3 h without or with PsVs. Membrane sheets were generated, stained and imaged by confocal microscopy. Green (CD151-GFP; GFP signal was enhanced by nanobodies), red (PsVs visualized by L1 antibody labeling) and cyan (filamentous actin; fluorescently labelled phalloidin). Images are displayed using a linear lookup table. For each channel, the same arbitrary scaling was applied. (A) For each condition a membrane sheet is shown. Magnified views of the white boxes are shown, illustrating the

individual channels. (B) For the CD151 and the actin channels, within a freehand ROI excluding membrane edges, the pixels with an intensity higher than the average ROI intensity were selected. Then, the number of pixels positive in both channels was related to the number of all positive pixels in the CD151 channel. Values are given as means ± SD (n = 45 membrane sheets collected from three biological replicates). Unpaired Student's t-test (***p < 0.001). Figure and legend both taken from reference [130].

5.3.4 Additional components and 3D morphology of the entry platform

Apart from CD151 and integrins, more proteins are expected to be part of the entry platform. One of these candidates is the tetraspanin CD63. It was shown to be required for infection with HPV and it colocalizes with CD151 [31]. Its role is supposed to be controlling intracellular trafficking of viral particles [112]. Large CD63 assemblies were observed on keratinocyte membrane sheets where they were observed to colocalize with HPV16 PsVs [111].

In the present study, the effect of PsV incubation on the aggregation of CD63 was investigated. Therefore, HaCaT cells were transfected with CD63-GFP and incubated with or without HPV16 PsVs for 3 h. Cells were fixed, permeabilized and stained for PsVs, GFP and F-actin. Images of the basal membrane were recorded via confocal microscopy (Figure 5.25). As can be seen, assemblies of CD63-GFP are already visible in the absence of PsVs. Viral particles concentrated predominantly at the cell periphery. Occasionally, PsVs crowded at CD63-GFP assemblies, which colocalized with actin, sometimes forming a ring-like pattern around these structures (Figure 5.25, left magnified view of the PsV condition). The number of CD63-GFP and actin assemblies was counted manually. PsVs barely increased the amount of CD63-GFP or actin assemblies found per cell (Figure 5.26 A and B).

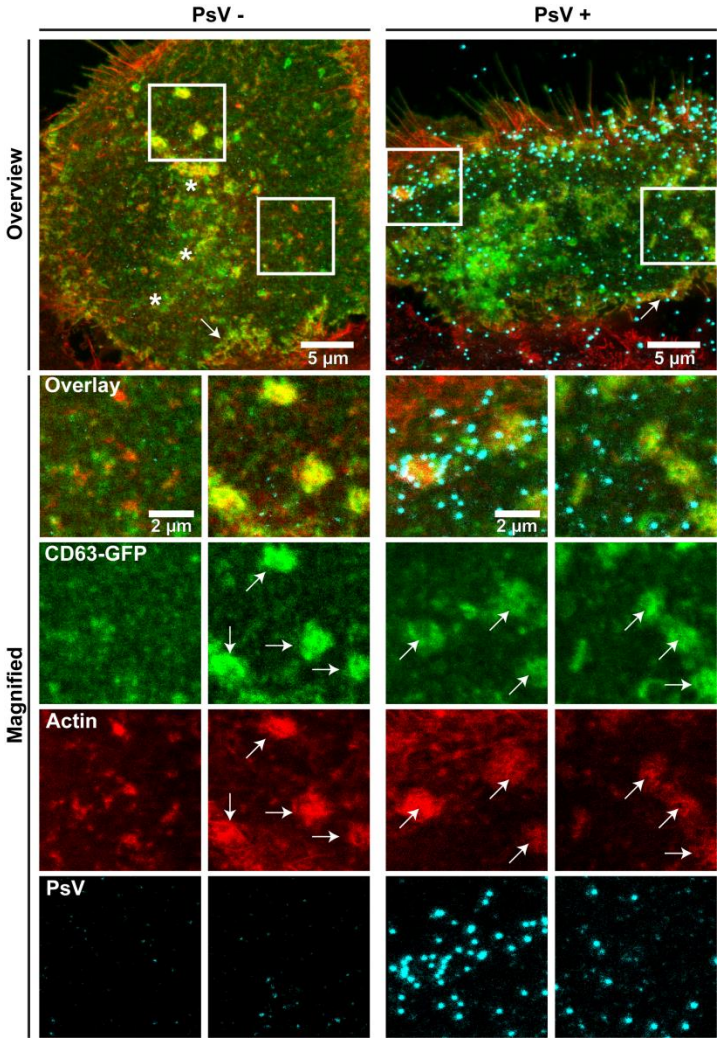

Figure 5.25 CD63/actin positive structures in HaCaT cells in the absence and presence of PsVs

HaCaT cells were transfected with CD63-GFP and one day later incubated for 3 h at 37 °C without (left panels) or with (right panels) PsVs. Cells were fixed and stained for PsVs and actin with an antibody and fluorescently labeled phalloidin, respectively, and GFP signal was enhanced by nanobodies. Confocal scans from the basal cell membrane were recorded. The linear lookup tables illustrate the channels for CD63-GFP, actin and PsVs in green, red and cyan, respectively. Overlap between green and red is illustrated in yellow and overlap between all three channels in white. Examples of patched structures counted as assemblies in Fig. 5.26 are marked by arrows in the magnified views. For Fig. 5.26, assemblies were counted per cell base. Large continuous structures, like those often found at the cell periphery (see arrows in overview images) or CD63-vesicular structures in the perinuclear region (see asterisks) were excluded from the analysis. Figure taken, legend taken and modified from reference [136].

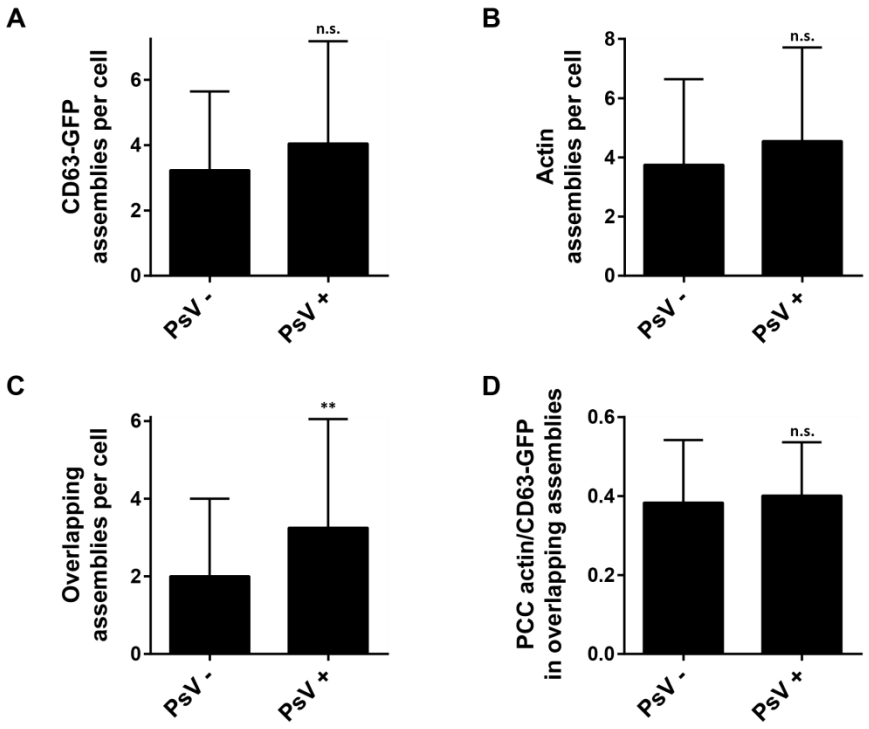

Figure 5.26 Quantification of CD63/actin positive assemblies in PsV treated and untreated HaCaT cells
The number of CD63 (A), actin assemblies (B) and of assemblies with overlapping CD63 and actin signals (C), which are a subset of (A) and (B), was counted manually in cells as shown in Fig. 1. (D) Regions of interest (ROIs) were placed on CD63/actin positive assemblies from PsV treated and untreated cells and the Pearson correlation coefficient (PCC) within the ROIs was calculated. Values are given as means ± SD (For A-C: n = 59 - 60 basal membranes collected from 3 biological replicates; for D: n = 120 - 195 overlapping assemblies as counted for C). Unpaired Student's t-test, comparing PsV treated to untreated cells (**, $p < 0.01$). Data analysis and plotting was performed by Lisa Hitschler (AG Thorsten Lang). Figure and legend both taken and modified from reference [136].

However, the amount of assemblies, which were positive for both proteins, increased significantly by about 50 % (Figure 5.26 C). The PCC between CD63-GFP and actin signal was calculated within ROIs placed on colocalizing assemblies from cells treated with or without PsVs. The overlap of these colocalizing assemblies did not differ between the two conditions (Figure 5.26 D). The results indicate that the PsVs increase the occurrence of organelles positive for CD63 and coated with actin.

The experiments above (Figure 5.24) showed that colocalization between CD151 and actin on membrane sheets even increased after PsV incubation. Consequently, the CD63/actin-rich structures may also contain the tetraspanin CD151. To clarify this, HaCaT cells were co-transfected with CD151-RFP and CD63-GFP. Cells were incubated with PsVs for 3 h in order to promote the occurrence of CD63/actin colocalizing assemblies. Cells were fixed, permeabilized and stained for GFP, RFP and F-actin. It was also speculated that these assemblies might represent large membrane invaginations. Therefore, a set of five confocal scans, each separated by 400 nm axial distance, was recorded for each cell starting at the basal membrane. As seen in the example shown in Figure 5.27, assemblies are spherical in shape with diameters in the range of a few micrometres. The assembly marked by an arrow has a strong tetraspanin signal at the basal membrane that remains intense until the + 800 nm section. Another assembly, marked by an asterisk, is barely visible at the basal membrane and displays increased signal in the above lying cell sections. This indicates that this assembly marks an organelle that might have already separated from the plasma membrane. The staining intensity of assemblies positive for CD151/CD63/actin was quantified at the basal membrane. Plotting the intensities of all three components against each other for individual assemblies revealed that in general, intensities correlate suggesting that the components depend on each other (Figure 5.28). The PCCs within the assemblies were calculated, yielding 0.44 ± 0.14 (CD63/actin), 0.39 ± 0.15 (CD63/CD151), and 0.41 ± 0.14 (CD151/actin). The high coefficients suggest that all three components are enriched to a comparable extent.

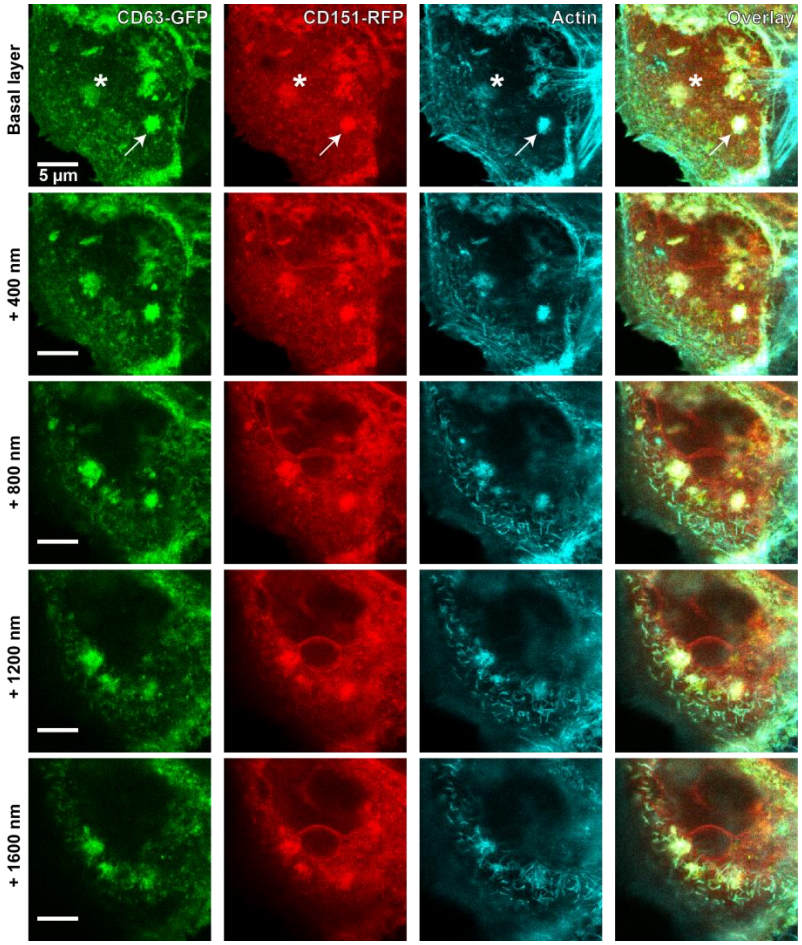

Figure 5.27 Assemblies enriched in CD63, CD151 and actin
HaCaT cells were transfected with CD63-GFP and CD151-RFP, and one day later incubated for 3 h at 37 °C with PsVs. Cells were fixed and stained for actin by fluorescently labelled phalloidin, and GFP- and RFP-signal was enhanced by nanobodies. An image stack was recorded starting at the basal cell membrane, with 400 nm axial distances between the optical sections. The linear lookup tables illustrate the channels for CD63-GFP, CD151-RFP and actin in green, red and cyan, respectively. Overlap between all three channels is illustrated in white. See Fig. 5.28 for the analysis of the relationship between the signals. An assembly marked by an arrow has an intense staining intensity in the lower optical sections. An asterisk marks an assembly barely visible in the basal section that shows increased staining intensity in the above lying optical sections. Figure taken, legend taken and modified from reference [136].

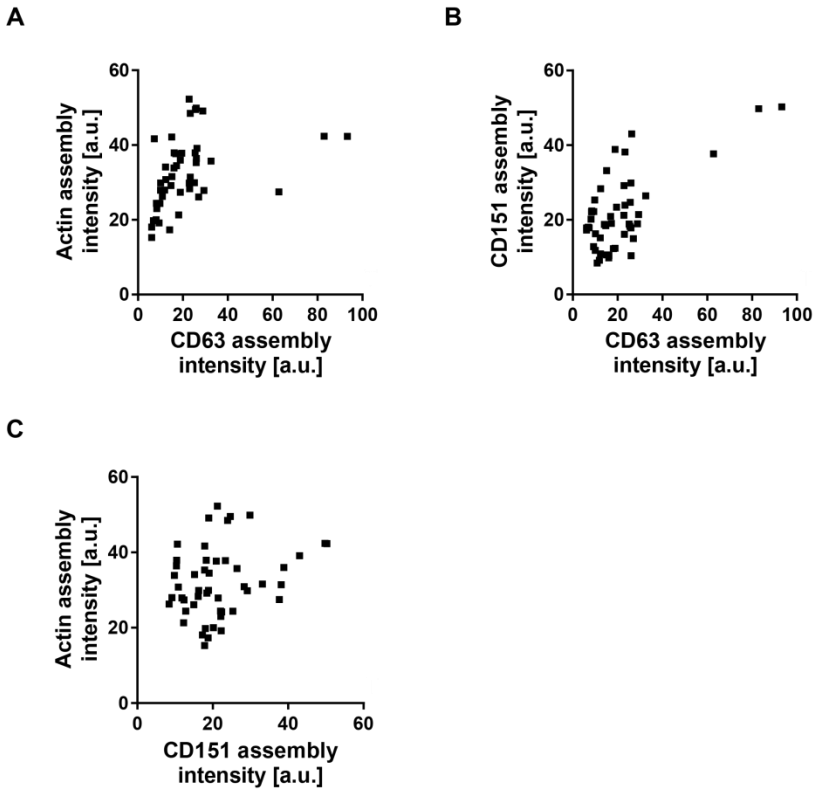

Figure 5.28 Relationship between CD63, CD151 and actin signals
Analysis of aggregated assemblies shown in Fig. 5.27. The average intensities of actin and CD63 (A), CD151 and CD63 (B) and actin and CD151 (C) in assemblies recorded at the basal layer were plotted against each other. From the same regions the Pearson correlation coefficients (PCCs) were determined obtaining 0.44 ± 0.14 (CD63/actin), 0.39 ± 0.15 (CD63/CD151), and 0.41 ± 0.14 (CD151/actin) (values are given as means ± SD). (A-C: n = 49 assemblies from 20 cells collected from 3 biological replicates). Data analysis and plotting was performed by Lisa Hitschler (AG Thorsten Lang). Figure and legend both taken and modified from reference [136].

5.3.4 Link to intracellular dynamics

A direct interaction between tetraspanins and filamentous actin has not yet been reported. However, patched tetraspanins clearly overlapped with intense actin staining. This suggests that a molecular link between the components must exist. OBSL1, thought to be a cytoskeletal adaptor protein closely related to obscurin [117], may represent such a molecular linker because OBSL1 was shown to interact with the HPV16 minor capsid protein L2 and to be required for efficient internalization and infection by the virus [118].

Thus, it was hypothesized that OBSL1 is also enriched in aggregated actin assemblies. For verification, HaCaT cells were transfected with V5-OBSL1 and incubated with HPV16 PsVs for 3 h to promote assembly formation. Cells were stained for V5 and F-actin and imaged via confocal microscopy. V5-OBSL1 seemed to overlap with actin especially where the actin staining had a more aggregated pattern and at cell-cell contact sites (Figure 5.29). The colocalization between OBSL1 and actin was analysed by calculating the PCC, differentiating between aggregated actin signal and more filamentous actin structures usually found at the cell periphery. The analysis revealed a striking difference between the two pools of actin, confirming the visual impression and suggesting OBSL1 has a strong preference for aggregated actin structures.

The question arises whether PsVs would be present at sites where actin and OBSL1 are co-enriched at the plasma membrane, possibly defining sites of endocytosis. In order to ensure that only early plasma membrane structures are imaged, membrane sheets were employed. Because the V5-OBSL1 construct does not express well in HaCaT cells and this cell line is very inefficient for the preparation of membrane sheets, HepG2 cells were used in this experiment. HepG2 cells were transfected with V5-OBSL1 and incubated with PsVs for 3 h followed by membrane sheet preparation. Samples were fixed, permeabilized and stained for V5-tag, PsVs and F-actin. Images were recorded via STED microscopy and screened for sites at which PsVs are in close proximity to

actin and OBSL1. Figure 5.30 shows the largest structure that could be found. In this image, the microscope resolves a central hole within an elongated filamentous actin structure. The OBSL1 signal overlapped quite well with the actin signal. Strikingly, several PsVs were present at the inner side of the ring-like structure. This example suggests that the extensive overlap between OBSL1 and actin, already observed in the previous experiment, occurs already at the plasma membrane.

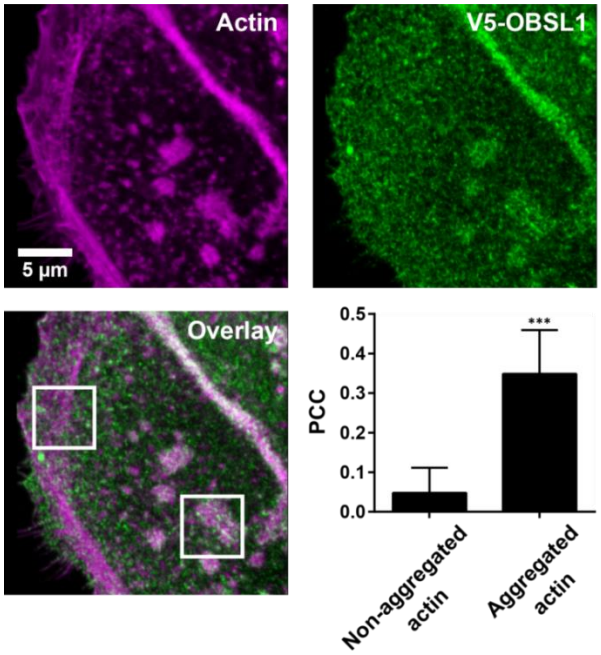

Figure 5.29 Overlap between actin and OBSL1
HaCaT cells were transfected with V5-OBSL1 and one day post transfection cells were incubated with PsVs for 3 h, fixed and stained for V5 with an antibody and for actin with phalloidin conjugated to a fluorophore. The linear lookup tables illustrate the channels for V5-OBSL1 and actin in green and magenta, respectively. The similarity between the OBSL1 and actin signals was quantified by calculation of the Pearson Correlation Coefficient (PCC) using squared ROIs placed on non-aggregated or aggregated actin structures. Values are shown as means ± SD (n = 21-27 ROIs collected from 39 cells pooled from 4 biological replicates). Unpaired Student's t-test, comparing aggregated to non-aggregated actin (***, $p < 0.001$). Figure taken, legend taken and modified from reference [136].

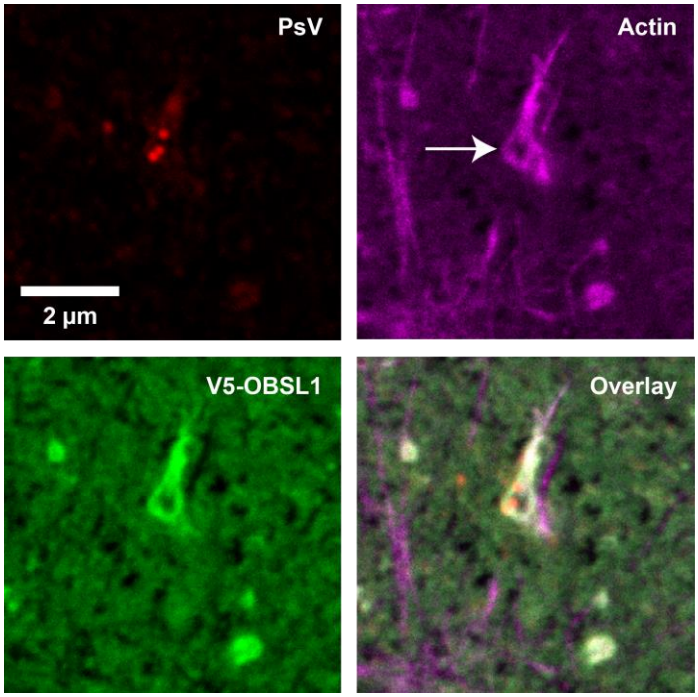

Figure 5.30 Morphology of endocytic organelles
HepG2 cells were transfected with V5-OBSL1. One day post transfection, cells were incubated with PsVs for 3 h and then exposed to a brief ultrasound pulse, which removes the upper parts of the cells leaving behind the basal cell membranes. The linear lookup tables illustrate the channels for PsV, V5-OBSL1 and actin in red, green and magenta, respectively. Images were screened for locations at which PsVs are close to actin and OBSL1 positive structures. Shown is the largest example found. Figure and legend both taken and modified from reference [136].

6 Discussion

Infection by papillomavirus is a slow and asynchronous process involving many steps with entry kinetics in the range of several hours. While different cellular factors involved in the infection process have been identified, it remains largely unclear how they cooperate with each other to enable infection. Moreover, the precise role of numerous host factors remains in the dark. In this study, the functional and spatial relationship between several membrane proteins, which were shown to be involved in the HPV16 infection process (CD151, integrin α3, integrin α6), was investigated. The cellular proteins CD151, integrin α3 and integrin α6 were shown to form closely associated complexes on the cell surface, thereby forming functional entities. All three components were shown to cluster together at sites close to cell surface bound viral particles thus forming what can be defined as a viral entry platform. The tetraspanin CD151 could be regarded as the central membrane organizer that recruits the functional components for viral entry. These platforms were identified as sites of rearrangement of the actin cytoskeleton. In addition, two further possible components of the entry platform were identified, CD63 and OBSL1, the latter possibly representing the physical link between the cytoskeleton and the entry platform. Since numerous viruses make use of TEMs for endocytosis or exocytosis, the concept proposed in this study with one or more tetraspanins concentrating several host factors related to infection, may be a general mechanism for various viral infections.

6.1 Plasma membrane distribution of CD151 and integrins

In recent years, the amount of studies that reported a role for tetraspanins in viral infections increased. While some viruses bind directly to tetraspanins, like hepatitis C virus to CD81 [96], involvement in other viral infections seems to be more indirect. In

MERS coronavirus and influenza A virus infections, host cell factors were concentrated in TEMs defined by CD9 [94]. Regarding HPV16 infection, CD151 was shown to be required for efficient infection of different cell lines [31,48,110]. Moreover, it was shown to colocalize with viral particles during infection [31]. Additionally, only viral particles associated with CD151 assemblies are internalized [48]. However, no direct interaction between CD151 and HPV was reported to date. Based on current knowledge, it can be speculated that CD151 may organize a specialized type of TEMs containing one or several entry factors required for infection. Laminin binding integrins α3 and α6 are prominent candidates for such viral host cell factors, as they interact with CD151 [137] and especially integrin α6 is known to be required for HPV infection [47,48]. The role of integrin α3 is controversial since, according to Aksoy *et al.*, this integrin is not required for HPV infection of HaCaT cells [138] while Scheffer *et al*. found reduced infectivity in integrin α3 depleted HeLa cells [48]. To examine a possible formation of TEMs containing laminin-binding integrins in keratinocytes, the spatial distribution of CD151, integrin α3 and integrin α6 in the plasma membrane of the keratinocyte HaCaT cells was investigated employing STED microscopy (section 5.1.2).

In this experiment, overexpressed CD151-GFP was used. The Florin group verified the functionality of CD151-GFP for HPV16 infection. This was done by performing infectivity rescue experiments by overexpressing CD151-GFP in cells depleted of endogenous CD151. The experiment confirmed that overexpressed CD151-GFP restored infectivity to the same extent as overexpressed wildtype CD151 [130].

In order to ensure that only plasma membrane distribution was analysed, membrane sheets were used. None of the three proteins was uniformly distributed across the plasma membrane. Instead, they seemed to concentrate in nanodomains quantified as local signal maxima displaying apparent diameters of about 100 – 200 nm (Figure 5.4). However, determining the exact size of the protein entities is challenging. Maxima sizes are assumed to be enlarged by the use of antibody labelling itself rendering size

measurement difficult. The labelled proteins are coated by a shell of antibodies, therefore increasing the real size. A previous study analysing microtubuli estimated that labelling with primary-secondary antibodies enlarges the diameter of the observed structure by about 20 nm [133].

The lognormal distribution of the maxima sizes (Figure 5.5) led to the assumption that the small maxima sizes were not resolved properly, which would also corrupt measured sizes. This effect was particularly visible in integrin α3, which had the lowest average maxima size (Figure 5.4). This assumption was confirmed when estimating the PSF of the STED microscope. This was done by measuring the apparent size of antibody-labelled HPV16 PsVs. They can be used as standard due to their constant size, employing the same imaging conditions and considering the shell of fluorophores of about 20 nm. The images are blurred by PSFs of 64 – 97 nm. Therefore, the resolution is in the range of the smallest maxima. The signal-to-noise ratio is an additional factor that likely influences the observed maxima sizes. Samples displaying a low staining intensity, as was the case for CD151-GFP, also lead to an overestimation of the maxima size because small maxima, presumably containing less protein, may not be detected. Taken together, these technical issues all lead to an overestimation of the average maxima size. However, a large fraction of the maxima is clearly above the resolution limit and therefore does most likely not arise from single molecules but from protein clusters, which are often found to be in the same size range as in this study [85,134,135].

Of higher relevance than the exact sizes is the distance between the protein maxima, as this parameter helps figuring out if different maxima types are distinct segregated structures or arise from the same assembly where the individual components are evenly mixed. If maxima are distinct entities, the distance between neighbouring maxima is expected to be in the range of their sizes or above. For direct contact, the distance needs to be at least the sum of the radii of the respective maxima. If components are evenly mixed and maxima originate from the same entity, maxima

should be located at the very same position and display very short inter-maxima distances. In this study, the average distance between maxima was about 100 – 300 nm while distances differed greatly between the different maxima types (Figure 5.4). The nearest distances of CD151-GFP to integrin α3 and integrin α6 are 144 nm and 107 nm, respectively. With respect to the measured maxima sizes (Figure 5.4), these short distances, averaging even below the sum of the radii, would allow for mutual penetration and interaction of the maxima, especially in the case of integrin α6/CD151. However, as already discussed above, maxima sizes are corrupted. Therefore, it cannot be precisely concluded to which extent the maxima are mutually penetrating. Nevertheless, the average inter maxima distances strongly deviate from zero and are therefore not homogeneous mixtures of the components. The maxima originate from distinct separated entities that probably have contact at their edges, possibly mutually penetrating to some extent.

6.2 Influence of the CD151 expression level on cluster anatomy

Since CD151 was overexpressed for some experiments, it becomes important to discuss what this implies for the cell surface distribution and anatomy of TEMs. With respect to HPV infection, CD151-GFP was shown to be as functional as the wildtype form [130]. Therefore, CD151-GFP is likely incorporated into the same domains as the endogenous tetraspanins. For verification, membrane sheets from CD151-GFP expressing HaCaT cells were stained with anti-CD151 antibody (Figure 5.3) and the calculated PCC (0.75) for GFP/antibody is even higher than the value previously found for a double-tagged protein (0.63) [132]. Consequently, it can be safely concluded that CD151-GFP mixes with wildtype CD151 in the same domains.

Overexpression led to an average increase in CD151 plasma membrane level by 2.5-fold, (Figure 5.3). An increased CD151-level was accompanied by an increased density

of detected nanodomains (Figure 5.4). To a lower extent, the size of the maxima was also enlarged. The same trend was observed in cells with endogenous and reduced cell surface levels of CD151 (Figure 5.11), where density and size of CD151 domains were again dependent on the individual expression level. Hence, wildtype CD151 and CD151-GFP display the same clustering behaviour. Moreover, CD151 nanodomains seem to be dynamic entities, as their size and number depend on the overall CD151 level. This clustering behaviour may be a general feature of protein clusters, as similar trends are observed for other proteins [77,134].

While the CD151 level has an impact on the CD151 maxima characteristics, it becomes interesting to know if the tetraspanin level also has an influence on TEM components.

When overexpressing CD151-GFP, average staining intensity of integrin α6 was also increased. This finding might indicate a cotransport of CD151 and integrin α6 to the plasma membrane. In accordance with the idea of a cotransport, CD151 was found to bind integrin α6 precursor forms [139]. The mutual dependence is further supported by the decrease of cell-surface CD151 after integrin α6 knockdown (Figure 5.11). This has interesting implications for HPV infection. It was reported that CD151 overexpression increases the susceptibility of cells for HPV16 infection [48]. The effect may be explained by an increased number of TEMs containing viral host cell factors, such as integrin α6 on the cell surface thereby promoting cell entry.

6.3 Different roles for CD151, integrin α3 and integrin α6 in HPV16 infection

Integrin α6 is accepted to be a host cell factor required for infection by papillomaviruses [47,48]. Flow cytometry experiments showed that the expression level of different cell lines correlates with the amount of bound HPV particles [49]. Moreover, anti-integrin α6 antibodies are able to reduce virus binding to cells [45,49] and overexpression of integrin α6 was shown to confer HPV binding to receptor-negative

cells [46]. Immunoprecipitation suggests that binding occurs directly [45]. On the other hand, it is widely assumed that the HPV main receptors are HSPGs [38,40,140].

In this study, depletion of integrin α6 strongly reduced PsV binding to HaCaT cells in both biochemical and microscopic experiments (Figure 5.15 and 5.11). In line with this, all investigated post-binding steps were likewise reduced after depletion: intracellular processing of the capsid (Figure 5.13 and 5.14), cointernalization of CD151 (Figure 5.11) and expression of the reporter plasmid (performed by the Florin group [130]). Taken together, the experiments confirm that integrin α6 is an important cellular factor for HPV attachment to host cells. Nevertheless, despite a relative high knockdown efficiency (Figure 5.9), roughly half of the PsVs remained bound to the cells. This fraction may represent PsVs bound to other cellular factors like the above-mentioned HSPGs. Other HPV binding proteins may be considered, such as growth factor receptors [43] or laminin, the latter one having been shown to be able to act as primary attachment site [44].

In this study, depletion of integrin α3 resulted in a strong reduction of all viral post-binding steps. The Florin group could also show that integrin α3 knockdown severely reduced infectivity with HPV16 PsVs [130]. However, integrin α3 depletion hardly reduced primary binding of PsVs in Western blot quantification (Figure 5.15). Likewise, PsV density at the basal membrane was not significantly affected by knockdown (Figure 5.10). Consequently, the role of integrin α3 seems to be in virus internalization rather than in virus binding. Integrins appear to be involved in signalling during HPV infection [47,115,141], including activation of focal adhesion kinase (FAK) and phosphoinositide-3- kinase (PI3K). Therefore, integrin α3 may be an indirect effector required for internalization. Activity of FAK is necessary for HPV uptake to early endosomes [47]. Moreover, adenoviruses internalization is known to be dependent on integrin αv and PI3K [142]. Recently, integrin α3 was shown to modulate EGFR expression [143]. This is particularly interesting in the context of HPV infection because EGFR binds

to HPV [43] and entry platform formation was shown to be dependent on EGFR signalling [51]. On the other hand, our findings contradict a study by Aksoy *et al.* where integrin α3 knockdown had no effect on HPV infectivity [138]. The discrepancy may result from the use of a much lower multiplicity of infection and a different infectivity-reporter system (GFP based reporter plasmid, quantification by flow cytometry) in the mentioned study.

Integrin α3 and integrin α6 may also have roles beyond the cell entry of HPV16. The Florin group, who performed the luciferase based infectivity measurements, used a reporter plasmid containing the HPV16 long control region. Noteworthy, depletion of integrin α3 inhibited promoter activity while it was strongly increased by integrin α6 knockdown [130]. This suggests that integrins may not only be important for HPV16 cell entry but could also be important modulators of viral gene expression during the viral replication.

Previous TIRF life-imaging experiments employing CD151-CFP and fluorescently labelled PsVs showed that only PsVs, which were associated with larger CD151-CFP assemblies (here, assemblies were not resolved to cluster crowds), were internalized [48]. This further emphasizes that HPV16 entry platforms are defined by CD151 cluster crowds.

The role of CD151 is most likely to incorporate integrins into TEMs [139,144,145]. To date, CD151 was not shown to interact directly with HPV16. However, infectivity rescue experiments performed with CD151 mutants that do not associate with laminin-binding integrins, confirmed that the interaction between CD151 and integrins is crucial for HPV infection [48]. Moreover, as already discussed above, CD151 could act as a carrier molecule by co-transporting host cell receptors like integrin α6 to the cell surface.

6.4 Association of viral particles with CD151/integrin defined entry platforms

If CD151 and associated integrins are involved in the entry process of HPV16 cell entry, viral particles should get in close proximity to these proteins on the cell surface during infection. Therefore, the spatial relationship between PsVs and CD151/integrin immunostaining was quantified.

Using EdU-PsVs, the association between viral particles and CD151/integrin α6 was investigated on membrane sheets (Figure 5.16). The calculation of the PCC between PsVs and CD151/integrin α6 was used to quantify the colocalization. Indeed, the PCC of both proteins was significantly higher than compared to randomized images, confirming a specific association. Albeit this, the PCC value was relatively low. One reason for this could be the use of STED-microscopy itself. Using this method, fluorescent signal is resolved into smaller entities. Therefore, staining that seems to overlap in diffraction-limited microscopy may be resolved into smaller domains that are in very close proximity, maybe even getting in contact, but not being located at the very same place, therefore reducing the overlap. Thus, as another parameter, the distance between PsVs and CD151/integrin maxima was considered. Most distances were in the range of a few hundred nanometres and PsVs were not specifically closer to integrin α6 maxima than to CD151 maxima. One explanation for this is that protein clusters only represent the non-interacting protein pool. In this case, clusters could act as a reservoir [146] for receptor molecules and release single molecules into the cluster area to which viral particles could bind. Alternatively, a technical explanation might account for the observations. By binding to its receptor, viral particle could reduce the antigen accessibility to antibody staining. However, this possibility is not very likely as PsV binding in the integrin knockdown condition (Figure 5.10) does not reduce CD151 staining and CD151 intensity at PsV location increased over time (Figure 5.7). Moreover, integrin maxima are still occasionally visible at the very same location of the

PsVs (see immunostaining in section 5.3), which should not occur if PsV binding systematically shields the epitope of the antibody.

It is more likely that the observations mentioned above (low PCC and most PsV distances a few hundred nanometre away from the next maximum) may be due to the complex HPV16 entry process. The viral cell surface dynamics are incredibly slow and unsynchronized [31,55,61,109]. A fraction of the PsVs could therefore be bound to other types of receptors like HSPGs [40,140], laminin [44] and growth factor receptors [43]. Cell surface events also include capsid conformational changes and processing by cell surface cyclophilins and proteases [58,60]; consequently viral particles must interact with these molecules at some point. PsVs being bound to other molecules would also explain why roughly half of the viral particles were still bound to the cells after integrin α6 depletion in both biochemical and microscopic experiments (Figure 5.15 and 5.11) despite a relatively high knockdown efficiency (Figure 5.9). However, the experiments in this study do not allow for differentiating between the binding states of the virus.

For association with CD151/integrin α3, an alternative anti-CD151 antibody was used (rabbit monoclonal instead of mouse monoclonal). Because of the low staining intensity of this antibody and of the anti-integrin α3 antibody, it was necessary to image intact cells, which are easier to identify due to intracellular staining, as it was not possible to screen for membrane sheets efficiently. Despite these differences in sample preparation, the PCC for CD151/PsV was comparable to the previous experiment and specific association was confirmed again. The PCC for integrin α3/PsV was substantially higher as for CD151/PsV and integrin α6/PsV, in accordance with the visual impression that the integrin α3 pattern follows the pattern of PsV distribution (Figure 5.22). However, PsVs were not specifically closer to integrin α3 than to CD151 or integrin α6 and again most distances were in the range of a few hundred nanometres.

Regardless of whether viral particles bind directly to protein clusters or to single molecules released to the surroundings, PsVs that are associated with the entry platform should be located in the proximity of respective protein clusters. As initially mentioned in section 5.3.1, some detected maxima, especially dimmer maxima, may not represent protein clusters but could arise from single molecules or trapped antibody complexes. Moreover, it was observed that the staining intensity of CD151 at PsV positions increased with rising incubation time (Figure 5.7). Consequently, the analysis focussed on the ~ 10 – 20 % brightest maxima for the description of the platform area. PsVs were considered to be potentially platform associated when they were closer than 250 nm to both the next CD151 and integrin cluster. The cluster density was then measured in a 1 µm x 1 µm square centred to these presumed platform associated PsVs. Compared to randomly chosen areas, the density of bright maxima for the three protein types was roughly 2-3-fold higher in platform areas. This suggests that HPV16 preferentially associates with cluster crowds that organize in an entry platform. However, the individual composition of the cluster crowds was highly variable (Figure 5.18 and 5.21). This may be explained by the analysis covering a wide range of binding states caused by the slow and unsynchronized infection process. Smaller cluster crowds could therefore be early stage platforms, while fully formed platforms may be best represented by the most densely packed platforms, in extreme cases containing more than 30 clusters. The platforms are likely even more densely packed, as in the triple stainings (PsV/CD151/integrin) only one of the integrins could be stained.

Moreover, additional components are expected to be present in these cluster crowds, as for example EGFR that is colocalized with CD151 and HPV16 [51] and other integrins, as they exist as heterodimers.

6.5 Additional platform components and link to intracellular dynamics

The entry platform likely contains components other than CD151, integrin α3 and integrin α6. Beside EGFR that was already shown to colocalize with CD151 and PsVs [51] the platform is expected to also contain other tetraspanins. One additional component of the entry platform could be CD63 as it was shown to be required for infection with several HPV subtypes in different cell lines [110,112]. Moreover, it colocalizes with HPV and CD151 during infection [31]. However, it does not appear to have a role in the cell surface events of HPV infection as its knockdown does not prevent viral particles to be internalized [112]. Instead, CD63 controls the post-endocytic trafficking of HPV in a complex with syntenin-1 [112] with which it interacts through its cytoplasmic tail [90]. CD63 was shown to form assemblies colocalizing with PsVs on membrane sheets [111], similarly to those observed for CD151 in this study. Therefore, it was speculated that these assemblies would also colocalize with assemblies of actin. Indeed, similar tetraspanin/actin assemblies were found employing overexpressed CD63-GFP. These assemblies often contained HPV16 PsVs or were framed by viral particles that occasionally formed ring-like structures (Figure 5.25). In double transfection experiments together with CD151-RFP, it could be shown that both tetraspanins are co-enriched in the same assemblies overlapping with actin. Taken together, it can be concluded that CD63 is also part of the viral entry platform.

6.6 Link of the platform to intracellular dynamics

In order to be able to enter the cell, platforms must be linked to intracellular dynamics. HPV enters the cell via a clathrin- and caveolin-independent but actin dependent entry pathway[31,108,109]. Therefore, it is likely that HPV16 entry platforms are related to actin dynamics. Indeed, assemblies of CD151-GFP were found to colocalize with assemblies of filamentous actin. The overall colocalization even increased after incubation with

HPV16 PsVs (Figure 5.24). The association of platforms with actin most likely accompanies the maturation process on the plasma membrane as these colocalizing assemblies were observed on membrane sheets. These findings draw interesting parallels to a study performed by Shigeta *et al*. In the mentioned study, incubation of A431 cells overexpressing CD151-GFP with antibody raised against CD151 resulted in aggregation of the tetraspanin [113]. These assemblies also colocalized with assemblies of actin, similarly to the structures observed here in the context of HPV infection. Interestingly, incubation with anti-integrin α3 antibody resulted in the very same phenotype [113], indicating that the antibody crosslinks the same entities.

This suggests that the accumulation and aggregation of CD151 nanodomains on the cell surface could trigger intracellular signalling pathways that are required for cytoskeletal actin reorganization. In this context, HPV may promote this aggregation and cytoskeletal reorganization by crosslinking several CD151 nanodomains via binding to integrin α6. These CD151/actin assemblies may be structures related to focal adhesions, connecting extracellular components to the cytoskeleton [147]. The fact that FAK signalling is activated during HPV infection supports this idea [47]. It was suggested that laminin-5 binding to laminin-binding integrins is supported by CD151 and leads to the activation of FAK [148]. HPV was shown to be able to bind laminin-5 as well as integrin α6. It is conceivable that HPV could promote the formation of focal adhesions by supporting the binding of laminin to integrins, thereby activating FAK.

Although not being an absolute requirement for infection, it was also observed that HPV particles induce the formation of filopodia that facilitate infection of cells [47,149,150]. The formation of filopodia requires the activation of Cdc42 [151]. It has been shown that CD151 is able to mediate activation of Cdc42 via laminin-binding integrins [113,114]. Even more remarkable is that plating cells on substrate coated with anti-CD151 or anti-integrin α3 resulted in extensive formation of filopodia [113]. Taken together, these observations suggest that HPV utilize and activate focal adhesion related signalling

structures in a CD151 and integrin dependent manner, leading to cytoskeletal reorganization and filopodia formation.

Furthermore, physically linking the entry platform to the cytoskeleton needs to be achieved. OBSL1 is a poorly characterized cytosolic protein that is thought to be a cytoskeletal adaptor protein, based on structural and functional homology to the closely related protein obscurin [117,152]. It is mainly known for its role in the 3-M syndrome [127]. It was recently shown to interact with the HPV L2-protein and to be involved in endocytosis of viral particles [118]. While OBSL1 does not seem to be involved in cell surface attachment of viral particles, it was shown to colocalize with CD151 and PsVs [118]. Hence, OBSL1 is a strong candidate for linking the viral entry platform to the cytoskeleton during endocytosis. In accordance with this idea, V5-OBSL1 was observed to have a strong preference for association with aggregated actin structures similar to those found in the entry platforms (Figure 5.29). Moreover, preliminary observations indicate that OBSL1 can be found in early endocytic structures at the plasma membrane, also containing viral particles and actin (Figure 5.30). However, these HPV associated endocytic plasma membrane structures were only observed in HepG2 cells. This was due to a very low transfection efficiency of the V5-OBSL1 construct in association with the fact that HaCaT cells are quite resistant to membrane sheet generation. Hence, these findings need to be verified in keratinocytes. Nevertheless, it can be assumed that OBSL1 associates with the HPV entry platform and could act as the linker to the cytoskeleton.

6.7 Caught in the web or spinning the web?

HPV16 PsVs associate with large tetraspanins and integrin cluster crowds on the cell surface that colocalize with patched assemblies of actin. However, it is not fully resolved whether PsVs actively induce this patching process or bind to structures that

are already present on the cell surface. Under endogenous conditions, the occurrence of very large entry platforms was rather low. As already mentioned, HPV internalization is an asynchronous and very slow process with internalization half-times in the range of several hours [55]. The low number of large platforms could be explained by a slow platform maturation process resulting in only few fully formed platforms after several hours. Therefore the data may cover a wide range of binding states. Alternatively, the observation could also be explained by platforms being quickly internalized after full maturation. Hence, the fraction of functional platforms would disappear from the plasma membrane, leaving behind only the smaller immature platforms. A former TIRF study suggests that only viral particles associated with CD151 assemblies are internalized [48]. Most viral particles associated with assemblies were internalized within a time frame of a few minutes [48].

It was observed that most PsVs remained nearly immobile at the cell base (Figure 5.23), confirming previous findings [149], whereas in general, CD151 moved more quickly through the cell base. This is in line with the idea that a fully formed platform would quickly disappear from the plasma membrane. Therefore, it is more likely that the platforms slowly form at PsV attachment sites, especially as the CD151 staining intensity at PsV binding sites gradually increases during the infection process (Figure 5.7). However, this does not exclude that PsV can bind directly to functional platforms. The fact that the majority of PsVs remains immobile on the cell body could point to the involvement of components of the extracellular matrix, like laminin-5 [153], and laminin-binding integrins [137].

The idea of assemblies being actively formed by viral particles was initially suggested in studies employing overexpressed tetraspanins [77,111]. Indeed, the observation of large tetraspanin crowds was most prominent in the experiments relying on tetraspanin overexpression. Here, PsVs were shown to enhance the colocalization of CD151-GFP and actin on membrane sheets (Figure 5.24). Moreover, incubation with viral particles

increased the occurrence of CD63-GFP/actin overlapping assemblies. However, tetraspanins, actin and even colocalizing assemblies were already present without addition of PsVs. But why are more large platforms visible upon overexpression? The size and frequency of these structures could be influenced by the availability of components. The CD151 maxima size and density was shown to be dependent on the expression level (Figure 5.3 and 5.11) and integrin α6 cell surface level and cluster density was also influenced by CD151 overexpression. It is noteworthy that CD151 overexpression was shown to enhance the activation of Cdc42 [113], which is required for filopodia formation [151]. Therefore, it is conceivable that tetraspanin overexpression promotes the growth of focal adhesion related entry platforms.

The assemblies observed in overexpression experiments seem to reach diameters of a few micrometres. However, earlier experiments employing electron microscopy suggest that early endocytic structures are rather in the size range of a few hundred nanometres [109]. These only grew larger when actin polymerization was inhibited using cytochalisin D, thereby forming tubular structures around one micrometre in size. Another study also suggests that intracellular trafficking vesicles are quite variable in size, occasionally reaching the micrometre range [112]. However, the tetraspanin assemblies observed in those studies are much smaller than those observed in our overexpression experiments. It is possible that the size of endocytic structures is limited by the availability of platform components and that overexpression thereby greatly emphasizes an otherwise modest viral patching effect.

It is unlikely that HPV create a new type of cellular structure. Even if they seem to increase the occurrence of tetraspanin/actin assemblies in overexpression experiments, these structures can already be observed in the absence of viral particles and they could be related to focal adhesions. However, there is some evidence that HPVs seem to be able to actively spin their own tetraspanin web for endocytosis. The colocalization of CD151 and actin was enhanced upon PsV incubation, just like the

occurrence of CD63/actin structures. Moreover, if viral particles can promote the formation of their entry platform, they could thereby activate signalling pathways promoting cytoskeletal dynamics. Indeed, several observations point towards this possibility. HPVs actively induce the formation of filopodia in infected cells [47,150]. Moreover, viral particles induce the activation of FAK [47] and PI3K [115] in an integrin dependent manner and HPV was reported to activate EGFR phosphorylation [43]. If HPVs were passively endocytosed by being caught in the tetraspanin web, no activation of signalling pathways would be expected. Engagement of CD151 and integrin α3 with antibodies was previously shown to lead to cytoskeletal reorganization and filopodia formation [113]. Engagement of CD151 also led to an activation of Cdc42 [113,114], which is a prerequisite for filopodia formation [151]. Based on analogy, HPV particles could exhibit a crosslinking activity on tetraspanin/integrin nanodomains similar to these antibody-engagement effects, thereby promoting the formation of focal adhesion-like structures. This promoting activity could in turn be dependent on the concentration of TEM components on the cell-surface, which would explain why large tetraspanin/actin assemblies are especially visible in cells overexpressing tetraspanins. In conclusion, several observation indicate that HPV are able to spin their own tetraspanin web for endocytosis. Yet, this does not exclude the possibility that they are able to use functional platforms already present on the cell surface. To what extent HPVs contribute to the patching of TEMs and the formation of focal adhesion-like structures on the cell surface during cell entry, especially under endogenous conditions, needs to be investigated in more detail. Therefore, the question if HPV are caught in the tetraspanin web or spinning their own web cannot yet be fully answered.

6.8 Tetraspanin entry platforms in the infection by other pathogens

In this study, the anatomy and functionalization of the HPV16 entry platform was investigated and CD151 was found to recruit several proviral factors required for infection. These findings have direct implications for the infection process of cytomegalovirus, as similarities to HPV infection can be observed (Figure 6.1). IN CMV infection, CD151 was shown to have a role in cellular entry, despite not appearing to be a direct viral receptor [154]. In contrast to HPV, CMV is an enveloped DNA virus [111]. A general CMV receptor has not been identified to date. However, several host cell factors are discussed to be possible receptors, including integrins [155–157], EGFR [158] and HSPGs [159,160], that may be organized in TEMs [161]. Based on this analogy, it is possible that CMV uses the same entry platform as HPV to get access into host cells.

In a more general view, it is possible that the concept of a tetraspanin organizing all components required for viral cell entry or exit, may be a blueprint for numerous other viral infections. As already mentioned above, host cell receptors for MERS coronavirus and influenza A virus were shown to be concentrated in TEMs, as well as pseudoviral particles [94]. Several other viruses also utilize TEMs during infection [92,162]. CD81 not only mediates direct binding to HCV [96], it also associates with other HCV entry factors like Claudin-1, the GTPase HRas, Rap2B and integrin β1 [163,164]. In HIV infection, tetraspanins CD81 and CD9 modulate membrane fusion and thereby cell entry by co-clustering of receptor CD4 and coreceptor CXCR4 [97]. In infections by Lujo virus, CD63 was found to mediate fusion of virus and host cell membrane [165]. Although its precise role remains unclear, TSPAN9 was shown to promote infection of several alphaviruses [166].

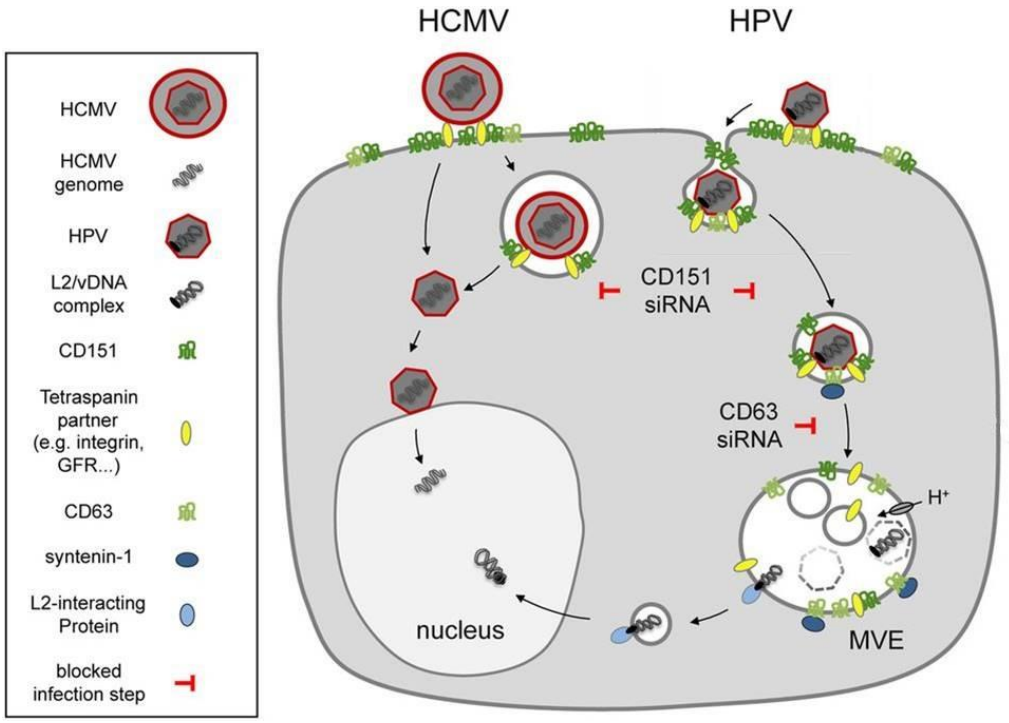

Figure 6.1 Tetraspanins involved in infections by human cytomegalo- and papillomaviruses
Model for the cell entry of HCMV and HPV. Both viruses are thought to enter the host cell via TEMs defined by CD151. CD151 knockdown was reported to inhibit cell entry of both pathogens. The enveloped HCMV virus releases its capsid in the cytosol either after direct fusion at the plasma membrane or in endocytosed vesicles. The capsid is routed to the nucleus where the viral DNA is uncoated. The non-enveloped HPV is taken up into endosomes in a CD151 dependent manner. Endosomes are routed in a CD63/syntenin-1 dependent manner to multivesicular endosomes where uncoating occurs and the L2/viral DNA complex is released. The L2/vDNA complex then translocates to the nucleus. Figure taken and modified from reference [111].

Besides their role in promoting cell entry of numerous viruses, tetraspanins were also reported to modulate viral exit. The budding of enveloped viruses occurs at cellular membranes and was reported to be organized by tetraspanins for several viral infections. In HSV-1 infection, the viral protein VP26 interacts with TSPAN7. This interaction is required for viral particles being able to exit the cell [167]. For influenza A, CD81 is not only required for viral entry but also for viral exit. CD81 is recruited into

large assemblies at the viral budding sites and is required for the release of viruses, as CD81 depletion impairs the scission of viruses from the plasma membrane [168]. In a similar fashion, CD81 and CD9 are recruited to the sites were the HIV Gag protein is inserted to the plasma membrane and tetraspanins are incorporated in the budding virions [169–171].

However, the involvement of tetraspanins is not restricted to viral infections, but a role in infections by bacterial pathogens was also reported. For example, the FimH adhesin of uropathogenic *E. coli* directly interacts with TSPAN21, also known as uroplakin Ia [172]. Moreover, CD81 is required for cellular invasion of *Listeria monocytogenes* and tetraspanins are recruited to the bacterial entry site [173]. Tetraspanins, notably CD151, CD63 and CD9, promote adherence of *Neisseria meningitides* to host cells and similar effects were observed for several other bacterial species [174].

6.9 Viral entry platforms as targets for therapeutics

All these reports emphasize one substantial aspect: tetraspanins are involved in a wide variety of infections by bacterial and viral pathogens. This makes them very interesting as potential targets for therapeutic broad range drugs. Targeting host cell factors also has the advantage of avoiding the build-up of resistance mechanisms in pathogens. In fact, tetraspanins are currently investigated as targets for therapeutic mAbs in the treatment of cancer [175] and targeting of CD37 already moved on to clinical trials in humans [176]. Similar approaches could be used for antiviral treatments, especially where therapeutic options are limited like it is the case for CMV [177]. At least for HCV, treatment with anti-CD81 antibody was shown to prevent infection in an *in vivo* mouse model [178]. However, mAbs targeting tetraspanins are not widely investigated in clinical studies for viral infections.

Another approach could be the use of small peptides as antiviral drugs. Treatment of cells with small peptides comprising the C-terminal or LEL part of tetraspanins exhibited inhibitory effects on infection of HPV and CMV [110]. Pretreatment of cells with recombinant proteins containing the LEL part of tetraspanins also reduced the adherence of *Neisseria meningitides* to host cells, which could be reproduced for several other bacterial species [174]. Thus, small peptides derived from tetraspanins could be a promising broad range therapeutic option for the treatment of many viral and bacterial infections involving TEMs.

6.10 Conclusions and implications of the study

Regardless of their involvement in viral entry or viral exit, tetraspanins do not have a catalytic activity of their own. In contrast, their promoting activity seem to rely on their ability to interact with numerous other partner proteins, either by binding directly to viral proteins or by gathering several host cell factors required for viral infection.

The HPV internalization is a complex and not fully understood process involving many steps. Here, we were able to show that viral particles associate with large assemblies of CD151 consisting of several nanodomains. These assemblies are functionalized by at least two components: integrin α6 for virus binding and integrin α3 for virus endocytosis. Furthermore, the assemblies seem to contain CD63 and to be sites of actin accumulation possibly promoted by virus-cell contact. The entry platforms apparently extend into the cell interior and could be possibly linked to the cytoskeleton via the adaptor protein OBSL1. However, the platforms do not seem to be a new type of structure per se, but to be related to focal adhesions. Since CD151 interacts with numerous proteins, the entry platform likely contains additional components. In fact, it is noteworthy that numerous observations related to HPV binding and internalization can be related directly or indirectly to CD151 (for a

schematic overview, see Figure 6.2). Laminin-5 can act as a transient HPV receptor [44]. Through its interaction with laminin-binding integrins, which are associated with CD151 [137], it could facilitate the transfer of viral particles to the entry platform. CD63, which was shown to interact with HPV16 PsV in a complex with syntenin-1 [112], was also observed to colocalize with CD151 [31]. As it is required for intracellular trafficking of the virus, it may connect the entry platforms to intracellular dynamics. The cytoskeletal adaptor protein OBSL1 is also colocalized with CD151 and interacts with the viral L2 capsid protein [118]. Therefore, it may couple the entry platform to reorganization of the actin cytoskeleton required for internalization. HPV was observed to greatly induce the formation of filopodia which in turn enhance infectivity of host cells [149,150]. Engagement of CD151 and integrin α3 was also shown to induce filopodia formation [113], likely via activation of Cdc42 [113,114]. HPV was further observed to bind and activate EGFR [43], which colocalizes with CD151 and viral particles [51]. Direct interaction of CD151 and EGFR was also reported [119]. It is well established that HPV uses HSPGs as receptor [38,39], notably Syndecan-1 and Syndecan-4 [40,50]. Interestingly, Syndecan-1 and Syndecan-4 interact with integrin α6β4 via cytoplasmic interactions with the β4 subunit [179]. Activation of FAK, which is required for infection, is reported to be dependent on integrin α6 [47], just like activation of PI3K [115].

HPV associates with annexin A2 heterotetramer at the cell surface through interaction with the L2 capsid protein [120,122]. L2 exposure requires conformational changes of the capsid, which is facilitated by the activity of Cyclophilin B [60]. In addition, Kallikrein-8, a secreted serine-protease, was shown to cleave L1 in the extracellular space, which is also thought to contribute to L2-exposure [58]. L2-exposure in turn is also needed for cleavage of the minor capsid protein via furin, a step required for HPV infection [180].

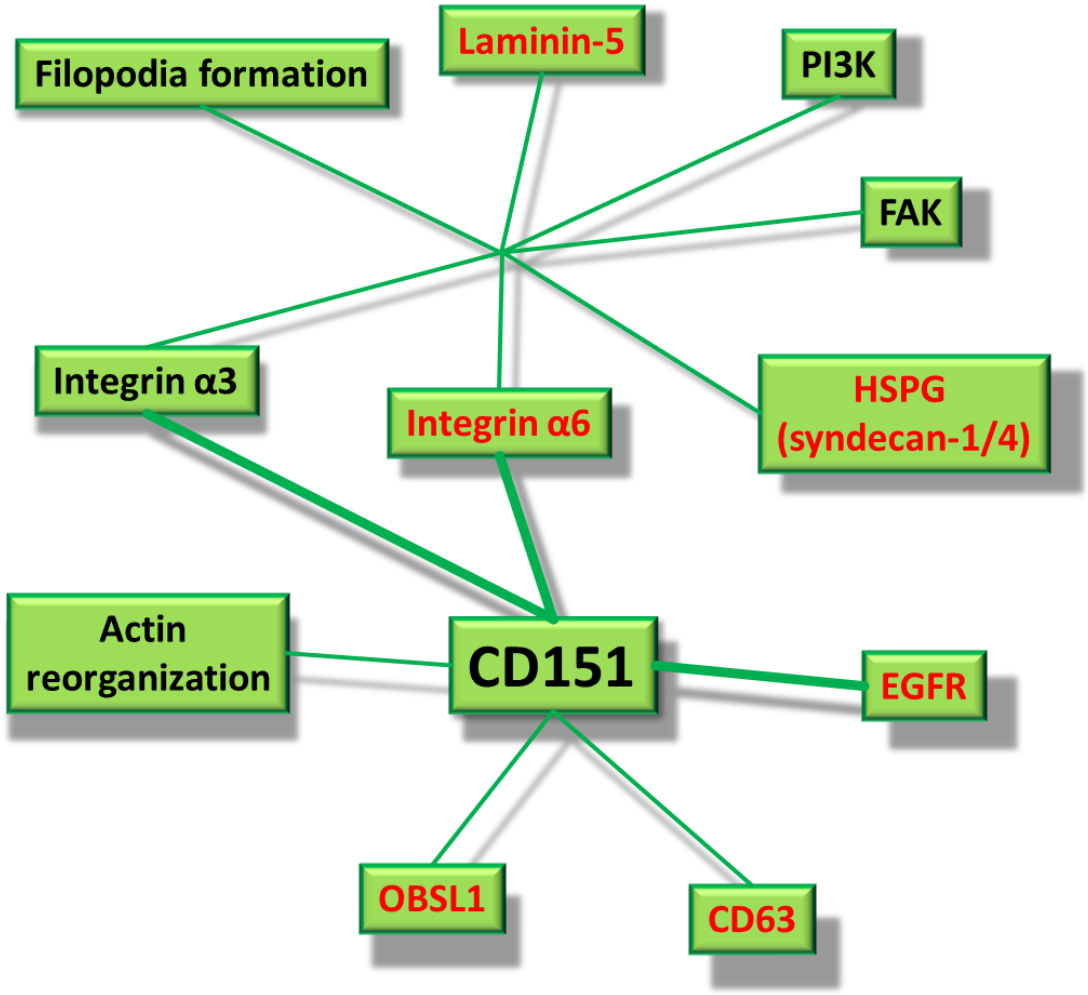

Figure 6.2 The HPV related CD151 web
Schematic representation of HPV interaction partners, molecules activated during HPV infection or cellular functionalities promoting/required for HPV infection that can be related directly or indirectly via associated integrins to CD151 (see text). HPV interaction partners are indicated in red. Thick lines represent reported direct interactions of CD151.

However, it is not clear whether all these steps occur in TEMs organized by CD151. Therefore, more work is needed in order to investigate if all host cell effectors of HPV infection are indeed present in the viral entry platform defined by CD151. Another question that remains to be answered deals with the coordination of the association with tetraspanins and viral particles in time and space. It is conceivable that the

different molecules enter the platform at different time points and distinct maturation stages can be distinguished, which has to be assessed in the future. With all these observations that can be related to CD151, it is tempting to speculate that CD151 may not just organize a single step in the entry pathway, but could in fact be able to form a platform containing all required components for HPV binding and internalization.

In conclusion, the model proposed here, a viral entry platform organized by a tetraspanin recruiting several host cell factors required for the different steps of pathogen internalization, could be a general building principle applicable to many other viruses and other pathogens. However, more work is needed to identify more components of the tetraspanin-based HPV16 entry platform and how the components coordinate in time and space during infection.

7 References

1. Tischer, I., Gelderblom, H., Vettermann, W. & Koch, M. A. A very small porcine virus with circular single-stranded DNA. *Nature* **295,** 64–66; 10.1038/295064a0 (1982).
2. Rodrigues, R. A. L., Mougari, S., Colson, P., La Scola, B. & Abrahão, J. S. "Tupanvirus", a new genus in the family Mimiviridae. *Archives of virology* **164,** 325–331; 10.1007/s00705-018-4067-4 (2019).
3. Nasir, A., Kim, K. M. & Caetano-Anollés, G. Viral evolution: Primordial cellular origins and late adaptation to parasitism. *Mobile Genetic Elements* **2,** 247–252; 10.4161/mge.22797 (2012).
4. Doorbar, J. *et al.* The biology and life-cycle of human papillomaviruses. *Vaccine* **30 Suppl 5,** F55-70; 10.1016/j.vaccine.2012.06.083 (2012).
5. Willemsen, A. & Bravo, I. G. Origin and evolution of papillomavirus (onco)genes and genomes. *Philosophical transactions of the Royal Society of London. Series B, Biological sciences* **374,** 20180303; 10.1098/rstb.2018.0303 (2019).
6. Egawa, N. & Doorbar, J. The low-risk papillomaviruses. *Virus research* **231,** 119–127; 10.1016/j.virusres.2016.12.017 (2017).
7. Martel, C. de, Plummer, M., Vignat, J. & Franceschi, S. Worldwide burden of cancer attributable to HPV by site, country and HPV type. *International Journal of Cancer* **141,** 664–670; 10.1002/ijc.30716 (2017).
8. Stanley, M. A. Epithelial cell responses to infection with human papillomavirus. *Clinical microbiology reviews* **25,** 215–222; 10.1128/CMR.05028-11 (2012).
9. Mikuličić, S. & Florin, L. The endocytic trafficking pathway of oncogenic papillomaviruses. *Papillomavirus research (Amsterdam, Netherlands)* **7,** 135–137; 10.1016/j.pvr.2019.03.004 (2019).

10. Doorbar, J., Egawa, N., Griffin, H., Kranjec, C. & Murakami, I. Human papillomavirus molecular biology and disease association. *Reviews in Medical Virology* **25,** 2–23; 10.1002/rmv.1822 (2015).
11. Pyeon, D., Pearce, S. M., Lank, S. M., Ahlquist, P. & Lambert, P. F. Establishment of Human Papillomavirus Infection Requires Cell Cycle Progression. *PLoS Pathogens* **5**; 10.1371/journal.ppat.1000318 (2009).
12. Aydin, I. *et al.* Large scale RNAi reveals the requirement of nuclear envelope breakdown for nuclear import of human papillomaviruses. *PLoS Pathogens* **10,** e1004162; 10.1371/journal.ppat.1004162 (2014).
13. Bergvall, M., Melendy, T. & Archambault, J. The E1 proteins. *Virology* **445,** 35–56; 10.1016/j.virol.2013.07.020 (2013).
14. Graham, S. V. Human papillomavirus: gene expression, regulation and prospects for novel diagnostic methods and antiviral therapies. *Future microbiology* **5,** 1493–1506; 10.2217/fmb.10.107 (2010).
15. Zheng, Z.-M. & Baker, C. C. PAPILLOMAVIRUS GENOME STRUCTURE, EXPRESSION, AND POST-TRANSCRIPTIONAL REGULATION. *Frontiers in bioscience : a journal and virtual library* **11,** 2286–2302 (2006).
16. Yim, E.-K. & Park, J.-S. The role of HPV E6 and E7 oncoproteins in HPV-associated cervical carcinogenesis. *Cancer research and treatment : official journal of Korean Cancer Association* **37,** 319–324; 10.4143/crt.2005.37.6.319 (2005).
17. Doorbar, J. The E4 protein; structure, function and patterns of expression. *Virology* **445,** 80–98; 10.1016/j.virol.2013.07.008 (2013).
18. Venuti, A. *et al.* Papillomavirus E5: the smallest oncoprotein with many functions. *Molecular cancer* **10,** 140; 10.1186/1476-4598-10-140 (2011).
19. Cerqueira, C. & Schiller, J. T. Papillomavirus assembly: an overview and perspectives. *Virus research* **231,** 103–107; 10.1016/j.virusres.2016.11.010 (2016).

20. Conway, M. J. *et al.* Tissue-spanning redox gradient-dependent assembly of native human papillomavirus type 16 virions. *Journal of Virology* **83,** 10515–10526; 10.1128/JVI.00731-09 (2009).
21. Kirnbauer, R., Booy, F., Cheng, N., Lowy, D. R. & Schiller, J. T. Papillomavirus L1 major capsid protein self-assembles into virus-like particles that are highly immunogenic. *Proceedings of the National Academy of Sciences of the United States of America* **89,** 12180–12184; 10.1073/pnas.89.24.12180 (1992).
22. Baker, T. S. *et al.* Structures of bovine and human papillomaviruses. Analysis by cryoelectron microscopy and three-dimensional image reconstruction. *Biophysical journal* **60,** 1445–1456 (1991).
23. Buck, C. B., Day, P. M. & Trus, B. L. The Papillomavirus Major Capsid Protein L1. *Virology* **445,** 169–174; 10.1016/j.virol.2013.05.038 (2013).
24. Modis, Y., Trus, B. L. & Harrison, S. C. Atomic model of the papillomavirus capsid. *The EMBO journal* **21,** 4754–4762; 10.1093/emboj/cdf494 (2002).
25. Wolf, M., Garcea, R. L., Grigorieff, N. & Harrison, S. C. Subunit interactions in bovine papillomavirus. *Proceedings of the National Academy of Sciences of the United States of America* **107,** 6298–6303; 10.1073/pnas.0914604107 (2010).
26. Sapp, M., Fligge, C., Petzak, I., Harris, J. R. & Streeck, R. E. Papillomavirus Assembly Requires Trimerization of the Major Capsid Protein by Disulfides between Two Highly Conserved Cysteines. *Journal of Virology* **72,** 6186–6189 (1998).
27. Buck, C. B., Thompson, C. D., Pang, Y.-Y. S., Lowy, D. R. & Schiller, J. T. Maturation of Papillomavirus Capsids. *Journal of Virology* **79,** 2839–2846; 10.1128/JVI.79.5.2839-2846.2005 (2005).
28. Guan, J. *et al.* Cryoelectron Microscopy Maps of Human Papillomavirus 16 Reveal L2 Densities and Heparin Binding Site. *Structure (London, England : 1993)* **25,** 253–263; 10.1016/j.str.2016.12.001 (2017).

29. Chen, X. S., Garcea, R. L., Goldberg, I., Casini, G. & Harrison, S. C. Structure of Small Virus-like Particles Assembled from the L1 Protein of Human Papillomavirus 16. *Molecular cell* **5,** 557–567; 10.1016/S1097-2765(00)80449-9 (2000).
30. Christensen, N. D. *et al.* Surface conformational and linear epitopes on HPV-16 and HPV-18 L1 virus-like particles as defined by monoclonal antibodies. *Virology* **223,** 174–184; 10.1006/viro.1996.0466 (1996).
31. Spoden, G. *et al.* Clathrin- and caveolin-independent entry of human papillomavirus type 16--involvement of tetraspanin-enriched microdomains (TEMs). *PloS one* **3,** e3313; 10.1371/journal.pone.0003313 (2008).
32. Wang, J. W. & Roden, R. B. S. L2, the minor capsid protein of papillomavirus. *Virology* **445,** 175–186; 10.1016/j.virol.2013.04.017 (2013).
33. Buck, C. B., Pastrana, D. V., Lowy, D. R. & Schiller, J. T. Efficient intracellular assembly of papillomaviral vectors. *Journal of Virology* **78,** 751–757; 10.1128/jvi.78.2.751-757.2004 (2004).
34. Day, P. M., Thompson, C. D., Schowalter, R. M., Lowy, D. R. & Schiller, J. T. Identification of a Role for the trans-Golgi Network in Human Papillomavirus 16 Pseudovirus Infection. *Journal of Virology* **87,** 3862–3870; 10.1128/JVI.03222-12 (2013).
35. Campos, S. K. Subcellular Trafficking of the Papillomavirus Genome during Initial Infection: The Remarkable Abilities of Minor Capsid Protein L2. *Viruses* **9**; 10.3390/v9120370 (2017).
36. Marušič, M. B., Ozbun, M. A., Campos, S. K., Myers, M. P. & Banks, L. Human Papillomavirus L2 facilitates viral escape from late endosomes via Sorting Nexin 17. *Traffic (Copenhagen, Denmark)* **13,** 455–467; 10.1111/j.1600-0854.2011.01320.x (2012).

37. Kämper, N. *et al.* A membrane-destabilizing peptide in capsid protein L2 is required for egress of papillomavirus genomes from endosomes. *Journal of Virology* **80,** 759–768; 10.1128/JVI.80.2.759-768.2006 (2006).
38. Raff, A. B. *et al.* The evolving field of human papillomavirus receptor research: a review of binding and entry. *Journal of Virology* **87,** 6062–6072; 10.1128/JVI.00330-13 (2013).
39. Ozbun, M. A. Extracellular events impacting human papillomavirus infections: Epithelial wounding to cell signaling involved in virus entry. *Papillomavirus research (Amsterdam, Netherlands)* **7,** 188–192; 10.1016/j.pvr.2019.04.009 (2019).
40. Shafti-Keramat, S. *et al.* Different heparan sulfate proteoglycans serve as cellular receptors for human papillomaviruses. *Journal of Virology* **77,** 13125–13135; 10.1128/jvi.77.24.13125-13135.2003 (2003).
41. Knappe, M. *et al.* Surface-exposed amino acid residues of HPV16 L1 protein mediating interaction with cell surface heparan sulfate. *The Journal of biological chemistry* **282,** 27913–27922; 10.1074/jbc.M705127200 (2007).
42. Joyce, J. G. *et al.* The L1 major capsid protein of human papillomavirus type 11 recombinant virus-like particles interacts with heparin and cell-surface glycosaminoglycans on human keratinocytes. *The Journal of biological chemistry* **274,** 5810–5822; 10.1074/jbc.274.9.5810 (1999).
43. Surviladze, Z., Dziduszko, A. & Ozbun, M. A. Essential roles for soluble virion-associated heparan sulfonated proteoglycans and growth factors in human papillomavirus infections. *PLoS Pathogens* **8,** e1002519; 10.1371/journal.ppat.1002519 (2012).
44. Culp, T. D., Budgeon, L. R., Marinkovich, M. P., Meneguzzi, G. & Christensen, N. D. Keratinocyte-secreted laminin 5 can function as a transient receptor for human papillomaviruses by binding virions and transferring them to adjacent cells. *Journal of Virology* **80,** 8940–8950; 10.1128/JVI.00724-06 (2006).

45. Evander, M. *et al.* Identification of the alpha6 integrin as a candidate receptor for papillomaviruses. *Journal of Virology* **71,** 2449–2456 (1997).
46. McMillan, N. A., Payne, E., Frazer, I. H. & Evander, M. Expression of the alpha6 integrin confers papillomavirus binding upon receptor-negative B-cells. *Virology* **261,** 271–279; 10.1006/viro.1999.9825 (1999).
47. Abban, C. Y. & Meneses, P. I. Usage of heparan sulfate, integrins, and FAK in HPV16 infection. *Virology* **403,** 1–16; 10.1016/j.virol.2010.04.007 (2010).
48. Scheffer, K. D. *et al.* Tetraspanin CD151 Mediates Papillomavirus Type 16 Endocytosis. *Journal of Virology* **87,** 3435–3446; 10.1128/JVI.02906-12 (2013).
49. Yoon, C. S., Kim, K. D., Park, S. N. & Cheong, S. W. alpha(6) Integrin is the main receptor of human papillomavirus type 16 VLP. *Biochemical and biophysical research communications* **283,** 668–673; 10.1006/bbrc.2001.4838 (2001).
50. Surviladze, Z., Sterkand, R. T. & Ozbun, M. A. Interaction of human papillomavirus type 16 particles with heparan sulfate and syndecan-1 molecules in the keratinocyte extracellular matrix plays an active role in infection. *The Journal of general virology* **96,** 2232–2241; 10.1099/vir.0.000147 (2015).
51. Mikuličić, S. *et al.* ADAM17-dependent signaling is required for oncogenic human papillomavirus entry platform assembly. *eLife* **8**; 10.7554/eLife.44345 (2019).
52. Patterson, N. A., Smith, J. L. & Ozbun, M. A. Human papillomavirus type 31b infection of human keratinocytes does not require heparan sulfate. *Journal of Virology* **79,** 6838–6847; 10.1128/JVI.79.11.6838-6847.2005 (2005).
53. Day, P. M., Lowy, D. R. & Schiller, J. T. Heparan sulfate-independent cell binding and infection with furin-precleaved papillomavirus capsids. *Journal of Virology* **82,** 12565–12568; 10.1128/JVI.01631-08 (2008).
54. Day, P. M., Gambhira, R., Roden, R. B. S., Lowy, D. R. & Schiller, J. T. Mechanisms of human papillomavirus type 16 neutralization by l2 cross-neutralizing and l1 type-

specific antibodies. *Journal of Virology* **82,** 4638–4646; 10.1128/JVI.00143-08 (2008).

55. Selinka, H.-C., Giroglou, T., Nowak, T., Christensen, N. D. & Sapp, M. Further evidence that papillomavirus capsids exist in two distinct conformations. *Journal of Virology* **77,** 12961–12967; 10.1128/jvi.77.24.12961-12967.2003 (2003).
56. Richards, K. F., Bienkowska-Haba, M., Dasgupta, J., Chen, X. S. & Sapp, M. Multiple Heparan Sulfate Binding Site Engagements Are Required for the Infectious Entry of Human Papillomavirus Type 16. *Journal of Virology* **87,** 11426–11437; 10.1128/JVI.01721-13 (2013).
57. Cerqueira, C. *et al.* Heparin increases the infectivity of Human Papillomavirus type 16 independent of cell surface proteoglycans and induces L1 epitope exposure. *Cellular microbiology* **15,** 1818–1836; 10.1111/cmi.12150 (2013).
58. Cerqueira, C., Samperio Ventayol, P., Vogeley, C. & Schelhaas, M. Kallikrein-8 Proteolytically Processes Human Papillomaviruses in the Extracellular Space To Facilitate Entry into Host Cells. *Journal of Virology* **89,** 7038–7052; 10.1128/JVI.00234-15 (2015).
59. Dasgupta, J. *et al.* Structural Basis of Oligosaccharide Receptor Recognition by Human Papillomavirus*. *The Journal of biological chemistry* **286,** 2617–2624; 10.1074/jbc.M110.160184 (2010).
60. Bienkowska-Haba, M., Patel, H. D. & Sapp, M. Target cell cyclophilins facilitate human papillomavirus type 16 infection. *PLoS Pathogens* **5,** e1000524; 10.1371/journal.ppat.1000524 (2009).
61. Becker, M., Greune, L., Schmidt, M. A. & Schelhaas, M. Extracellular Conformational Changes in the Capsid of Human Papillomaviruses Contribute to Asynchronous Uptake into Host Cells. *Journal of Virology* **92**; 10.1128/JVI.02106-17 (2018).

62. Selinka, H.-C. *et al.* Inhibition of transfer to secondary receptors by heparan sulfate-binding drug or antibody induces noninfectious uptake of human papillomavirus. *Journal of Virology* **81,** 10970–10980; 10.1128/JVI.00998-07 (2007).
63. Horvath, C. A. J., Boulet, G. A. V., Renoux, V. M., Delvenne, P. O. & Bogers, J.-P. J. Mechanisms of cell entry by human papillomaviruses: an overview. *Virology journal* **7,** 11; 10.1186/1743-422X-7-11 (2010).
64. Charrin, S., Jouannet, S., Boucheix, C. & Rubinstein, E. Tetraspanins at a glance. *Journal of cell science* **127,** 3641–3648; 10.1242/jcs.154906 (2014).
65. Haeuw, J.-F., Goetsch, L., Bailly, C. & Corvaia, N. Tetraspanin CD151 as a target for antibody-based cancer immunotherapy. *Biochemical Society transactions* **39,** 553–558; 10.1042/BST0390553 (2011).
66. van Deventer, S. J., Dunlock, V.-M. E. & van Spriel, A. B. Molecular interactions shaping the tetraspanin web. *Biochemical Society transactions* **45,** 741–750; 10.1042/BST20160284 (2017).
67. Berditchevski, F., Zutter, M. M. & Hemler, M. E. Characterization of novel complexes on the cell surface between integrins and proteins with 4 transmembrane domains (TM4 proteins). *Molecular Biology of the Cell* **7,** 193–207; 10.1091/mbc.7.2.193 (1996).
68. Serru, V. *et al.* Selective tetraspan-integrin complexes (CD81/alpha4beta1, CD151/alpha3beta1, CD151/alpha6beta1) under conditions disrupting tetraspan interactions. *Biochemical Journal* **340,** 103–111 (1999).
69. Hemler, M. E. Tetraspanin functions and associated microdomains. *Nature reviews. Molecular cell biology* **6,** 801–811; 10.1038/nrm1736 (2005).
70. Yauch, R. L., Kazarov, A. R., Desai, B., Lee, R. T. & Hemler, M. E. Direct Extracellular Contact between Integrin α 3 β 1 and TM4SF Protein CD151. *The Journal of biological chemistry* **275,** 9230–9238; 10.1074/jbc.275.13.9230 (2000).

71. Stipp, C. S., Kolesnikova, T. V. & Hemler, M. E. EWI-2 is a major CD9 and CD81 partner and member of a novel Ig protein subfamily. *The Journal of biological chemistry* **276,** 40545–40554; 10.1074/jbc.M107338200 (2001).
72. Horváth, G. *et al.* CD19 is linked to the integrin-associated tetraspans CD9, CD81, and CD82. *The Journal of biological chemistry* **273,** 30537–30543; 10.1074/jbc.273.46.30537 (1998).
73. Claas, C., Stipp, C. S. & Hemler, M. E. Evaluation of prototype transmembrane 4 superfamily protein complexes and their relation to lipid rafts. *The Journal of biological chemistry* **276,** 7974–7984; 10.1074/jbc.M008650200 (2001).
74. Charrin, S. *et al.* Lateral organization of membrane proteins: tetraspanins spin their web. *The Biochemical journal* **420,** 133–154; 10.1042/BJ20082422 (2009).
75. Zimmerman, B. *et al.* Crystal Structure of a Full-Length Human Tetraspanin Reveals a Cholesterol-Binding Pocket. *Cell* **167,** 1041-1051.e11; 10.1016/j.cell.2016.09.056 (2016).
76. Homsi, Y. & Lang, T. The specificity of homomeric clustering of CD81 is mediated by its δ-loop. *FEBS open bio* **7,** 274–283; 10.1002/2211-5463.12187 (2017).
77. Homsi, Y. *et al.* The extracellular δ-domain is essential for the formation of CD81 tetraspanin webs. *Biophysical journal* **107,** 100–113; 10.1016/j.bpj.2014.05.028 (2014).
78. Kovalenko, O. V., Metcalf, D. G., DeGrado, W. F. & Hemler, M. E. Structural organization and interactions of transmembrane domains in tetraspanin proteins. *BMC structural biology* **5,** 11; 10.1186/1472-6807-5-11 (2005).
79. Yang, X. *et al.* Palmitoylation of Tetraspanin Proteins: Modulation of CD151 Lateral Interactions, Subcellular Distribution, and Integrin-dependent Cell Morphology. *Molecular Biology of the Cell* **13,** 767–781; 10.1091/mbc.01-05-0275 (2002).

80. Charrin, S. *et al.* Differential stability of tetraspanin/tetraspanin interactions: role of palmitoylation. *FEBS Letters* **516,** 139–144; 10.1016/s0014-5793(02)02522-x (2002).
81. Odintsova, E. *et al.* Gangliosides play an important role in the organization of CD82-enriched microdomains. *The Biochemical journal* **400,** 315–325; 10.1042/BJ20060259 (2006).
82. Levy, S. & Shoham, T. Protein-protein interactions in the tetraspanin web. *Physiology (Bethesda, Md.)* **20,** 218–224; 10.1152/physiol.00015.2005 (2005).
83. Seigneuret, M., Delaguillaumie, A., Lagaudrière-Gesbert, C. & Conjeaud, H. Structure of the tetraspanin main extracellular domain. A partially conserved fold with a structurally variable domain insertion. *The Journal of biological chemistry* **276,** 40055–40064; 10.1074/jbc.M105557200 (2001).
84. Yauch, R. L., Berditchevski, F., Harler, M. B., Reichner, J. & Hemler, M. E. Highly Stoichiometric, Stable, and Specific Association of Integrin α3β1 with CD151 Provides a Major Link to Phosphatidylinositol 4-Kinase, and May Regulate Cell Migration. *Molecular Biology of the Cell* **9,** 2751–2765 (1998).
85. Zuidscherwoude, M. *et al.* The tetraspanin web revisited by super-resolution microscopy. *Scientific reports* **5,** 12201; 10.1038/srep12201 (2015).
86. Charrin, S. *et al.* A physical and functional link between cholesterol and tetraspanins. *European journal of immunology* **33,** 2479–2489; 10.1002/eji.200323884 (2003).
87. Yang, X. *et al.* Palmitoylation supports assembly and function of integrin–tetraspanin complexes. *J Cell Biol* **167,** 1231–1240; 10.1083/jcb.200404100 (2004).
88. Zuidscherwoude, M. *et al.* Tetraspanin microdomains control localized protein kinase C signaling in B cells. *Science signaling* **10**; 10.1126/scisignal.aag2755 (2017).

89. Tejera, E. *et al.* CD81 regulates cell migration through its association with Rac GTPase. *Molecular Biology of the Cell* **24,** 261–273; 10.1091/mbc.E12-09-0642 (2013).
90. Latysheva, N. *et al.* Syntenin-1 is a new component of tetraspanin-enriched microdomains: mechanisms and consequences of the interaction of syntenin-1 with CD63. *Molecular and cellular biology* **26,** 7707–7718; 10.1128/MCB.00849-06 (2006).
91. Monk, P. N. & Partridge, L. J. Tetraspanins: gateways for infection. *Infectious disorders drug targets* **12,** 4–17 (2012).
92. Florin, L. & Lang, T. Tetraspanin Assemblies in Virus Infection. *Frontiers in immunology* **9,** 1140; 10.3389/fimmu.2018.01140 (2018).
93. Earnest, J. T. *et al.* The tetraspanin CD9 facilitates MERS-coronavirus entry by scaffolding host cell receptors and proteases. *PLoS Pathogens* **13,** e1006546; 10.1371/journal.ppat.1006546 (2017).
94. Earnest, J. T., Hantak, M. P., Park, J.-E. & Gallagher, T. Coronavirus and influenza virus proteolytic priming takes place in tetraspanin-enriched membrane microdomains. *Journal of Virology* **89,** 6093–6104; 10.1128/JVI.00543-15 (2015).
95. Bruening, J. *et al.* Hepatitis C virus enters liver cells using the CD81 receptor complex proteins calpain-5 and CBLB. *PLoS Pathogens* **14,** e1007111; 10.1371/journal.ppat.1007111 (2018).
96. Pileri, P. *et al.* Binding of hepatitis C virus to CD81. *Science (New York, N.Y.)* **282,** 938–941; 10.1126/science.282.5390.938 (1998).
97. Gordón-Alonso, M. *et al.* Tetraspanins CD9 and CD81 modulate HIV-1-induced membrane fusion. *Journal of immunology (Baltimore, Md. : 1950)* **177,** 5129–5137; 10.4049/jimmunol.177.8.5129 (2006).
98. Li, G. *et al.* The dual role of tetraspanin CD63 in HIV-1 replication. *Virology journal* **11,** 23; 10.1186/1743-422X-11-23 (2014).

99. Pols, M. S. & Klumperman, J. Trafficking and function of the tetraspanin CD63. *Experimental cell research* **315,** 1584–1592; 10.1016/j.yexcr.2008.09.020 (2009).

100. Flannery, A. R., Czibener, C. & Andrews, N. W. Palmitoylation-dependent association with CD63 targets the Ca2+ sensor synaptotagmin VII to lysosomes. *The Journal of cell biology* **191,** 599–613; 10.1083/jcb.201003021 (2010).

101. Martinez, I. *et al.* Synaptotagmin VII regulates Ca(2+)-dependent exocytosis of lysosomes in fibroblasts. *J Cell Biol* **148,** 1141–1149; 10.1083/jcb.148.6.1141 (2000).

102. Yoshida, T. *et al.* A CD63 mutant inhibits T-cell tropic human immunodeficiency virus type 1 entry by disrupting CXCR4 trafficking to the plasma membrane. *Traffic (Copenhagen, Denmark)* **9,** 540–558; 10.1111/j.1600-0854.2007.00700.x (2008).

103. Duffield, A., Kamsteeg, E.-J., Brown, A. N., Pagel, P. & Caplan, M. J. The tetraspanin CD63 enhances the internalization of the H,K-ATPase beta-subunit. *Proceedings of the National Academy of Sciences of the United States of America* **100,** 15560–15565; 10.1073/pnas.2536699100 (2003).

104. Sincock, P. M. *et al.* PETA-3/CD151, a member of the transmembrane 4 superfamily, is localised to the plasma membrane and endocytic system of endothelial cells, associates with multiple integrins and modulates cell function. *Journal of cell science* **112 (Pt 6),** 833–844 (1999).

105. Liu, L. *et al.* Tetraspanin CD151 promotes cell migration by regulating integrin trafficking. *The Journal of biological chemistry* **282,** 31631–31642; 10.1074/jbc.M701165200 (2007).

106. Haining, E. J. *et al.* The TspanC8 subgroup of tetraspanins interacts with A disintegrin and metalloprotease 10 (ADAM10) and regulates its maturation and cell surface expression. *The Journal of biological chemistry* **287,** 39753–39765; 10.1074/jbc.M112.416503 (2012).

107. Prox, J. *et al.* Tetraspanin15 regulates cellular trafficking and activity of the ectodomain sheddase ADAM10. *Cellular and molecular life sciences : CMLS* **69,** 2919–2932; 10.1007/s00018-012-0960-2 (2012).

108. Spoden, G. *et al.* Human Papillomavirus Types 16, 18, and 31 Share Similar Endocytic Requirements for Entry. *Journal of Virology* **87,** 7765–7773; 10.1128/JVI.00370-13 (2013).

109. Schelhaas, M. *et al.* Entry of Human Papillomavirus Type 16 by Actin-Dependent, Clathrin- and Lipid Raft-Independent Endocytosis. *PLoS Pathogens* **8**; 10.1371/journal.ppat.1002657 (2012).

110. Fast, L. A. *et al.* Inhibition of Tetraspanin Functions Impairs Human Papillomavirus and Cytomegalovirus Infections. *International journal of molecular sciences* **19**; 10.3390/ijms19103007. (2018).

111. Fast, L. A., Lieber, D., Lang, T. & Florin, L. Tetraspanins in infections by human cytomegalo- and papillomaviruses. *Biochemical Society transactions* **45,** 489–497; 10.1042/BST20160295 (2017).

112. Gräßel, L. *et al.* The CD63-Syntenin-1 Complex Controls Post-Endocytic Trafficking of Oncogenic Human Papillomaviruses. *Scientific reports* **6,** 32337; 10.1038/srep32337 (2016).

113. Shigeta, M. *et al.* CD151 regulates epithelial cell–cell adhesion through PKC- and Cdc42-dependent actin cytoskeletal reorganization. *J Cell Biol* **163,** 165–176; 10.1083/jcb.200301075 (2003).

114. Hong, I.-K., Jeoung, D.-I., Ha, K.-S., Kim, Y.-M. & Lee, H. Tetraspanin CD151 Stimulates Adhesion-dependent Activation of Ras, Rac, and Cdc42 by Facilitating Molecular Association between β1 Integrins and Small GTPases*. *The Journal of biological chemistry* **287,** 32027–32039; 10.1074/jbc.M111.314443 (2012).

115. Fothergill, T. & McMillan, N. A. J. Papillomavirus virus-like particles activate the PI3-kinase pathway via alpha-6 beta-4 integrin upon binding. *Virology* **352,** 319–328; 10.1016/j.virol.2006.05.002 (2006).

116. Sala-Valdés, M. *et al.* EWI-2 and EWI-F link the tetraspanin web to the actin cytoskeleton through their direct association with ezrin-radixin-moesin proteins. *The Journal of biological chemistry* **281,** 19665–19675; 10.1074/jbc.M602116200 (2006).

117. Geisler, S. B. *et al.* Obscurin-like 1, OBSL1, is a novel cytoskeletal protein related to obscurin. *Genomics* **89,** 521–531; 10.1016/j.ygeno.2006.12.004 (2007).

118. Wüstenhagen, E. *et al.* The Cytoskeletal Adaptor Obscurin-Like 1 Interacts with the Human Papillomavirus 16 (HPV16) Capsid Protein L2 and Is Required for HPV16 Endocytosis. *Journal of Virology* **90,** 10629–10641; 10.1128/JVI.01222-16 (2016).

119. Kgk, D., Kumari, S., G, S. & Malla, R. R. Marine natural compound cyclo(L-leucyl-L-prolyl) peptide inhibits migration of triple negative breast cancer cells by disrupting interaction of CD151 and EGFR signaling. *Chemico-biological interactions* **315,** 108872; 10.1016/j.cbi.2019.108872 (2020).

120. Woodham, A. W. *et al.* The S100A10 subunit of the annexin A2 heterotetramer facilitates L2-mediated human papillomavirus infection. *PloS one* **7,** e43519; 10.1371/journal.pone.0043519 (2012).

121. Bharadwaj, A., Bydoun, M., Holloway, R. & Waisman, D. Annexin A2 heterotetramer: structure and function. *International journal of molecular sciences* **14,** 6259–6305; 10.3390/ijms14036259 (2013).

122. Dziduszko, A. & Ozbun, M. A. Annexin A2 and S100A10 Regulate Human Papillomavirus Type 16 Entry and Intracellular Trafficking in Human Keratinocytes. *Journal of Virology* **87,** 7502–7515; 10.1128/JVI.00519-13 (2013).

123. Taylor, J. R. *et al.* Heterotetrameric annexin A2/S100A10 (A2t) is essential for oncogenic human papillomavirus trafficking and capsid disassembly, and protects

virions from lysosomal degradation. *Scientific reports* **8,** 11642; 10.1038/s41598-018-30051-2 (2018).

124. Broniarczyk, J. *et al.* The VPS4 component of the ESCRT machinery plays an essential role in HPV infectious entry and capsid disassembly. *Scientific reports* **7,** 45159; 10.1038/srep45159 (2017).

125. Broniarczyk, J., Bergant, M., Goździcka-Józefiak, A. & Banks, L. Human papillomavirus infection requires the TSG101 component of the ESCRT machinery. *Virology* **460-461,** 83–90; 10.1016/j.virol.2014.05.005 (2014).

126. Larios, J., Mercier, V., Roux, A. & Gruenberg, J. ALIX- and ESCRT-III-dependent sorting of tetraspanins to exosomes. *The Journal of cell biology* **219**; 10.1083/jcb.201904113 (2020).

127. Hanson, D. *et al.* The primordial growth disorder 3-M syndrome connects ubiquitination to the cytoskeletal adaptor OBSL1. *American journal of human genetics* **84,** 801–806; 10.1016/j.ajhg.2009.04.021 (2009).

128. Bergsdorf, C., Beyer, C., Umansky, V., Werr, M. & Sapp, M. Highly efficient transport of carboxyfluorescein diacetate succinimidyl ester into COS7 cells using human papillomavirus-like particles. *FEBS Letters* **536,** 120–124; 10.1016/S0014-5793(03)00039-5 (2003).

129. Sapp, M. *et al.* Analysis of type-restricted and cross-reactive epitopes on virus-like particles of human papillomavirus type 33 and in infected tissues using monoclonal antibodies to the major capsid protein. *The Journal of general virology* **75 (Pt 12),** 3375–3383; 10.1099/0022-1317-75-12-3375 (1994).

130. Finke, J. *et al.* Anatomy of a viral entry platform differentially functionalized by integrins α3 and α6. *Scientific reports* **10,** 5356; 10.1038/s41598-020-62202-9 (2020).

131. Zhang, X. A. *et al.* Function of the Tetraspanin CD151–α6β1 Integrin Complex during Cellular Morphogenesis. *Molecular Biology of the Cell* **13,** 1–11; 10.1091/mbc.01-10-0481 (2002).

132. Sieber, J. J., Willig, K. I., Heintzmann, R., Hell, S. W. & Lang, T. The SNARE Motif Is Essential for the Formation of Syntaxin Clusters in the Plasma Membrane. *Biophysical journal* **90,** 2843–2851; 10.1529/biophysj.105.079574 (2006).

133. Aquino, D. *et al.* Two-color nanoscopy of three-dimensional volumes by 4Pi detection of stochastically switched fluorophores. *Nature methods* **8,** 353–359; 10.1038/nmeth.1583 (2011).

134. Merklinger, E. *et al.* The packing density of a supramolecular membrane protein cluster is controlled by cytoplasmic interactions. *eLife* **6**; 10.7554/eLife.20705 (2017).

135. Willig, K. I., Rizzoli, S. O., Westphal, V., Jahn, R. & Hell, S. W. STED microscopy reveals that synaptotagmin remains clustered after synaptic vesicle exocytosis. *Nature* **440,** 935–939; 10.1038/nature04592 (2006).

136. Finke, J., Hitschler, L., Boller, K., Florin, L. & Lang, T. HPV caught in the tetraspanin web? *Medical microbiology and immunology*; 10.1007/s00430-020-00683-1 (2020).

137. Stipp, C. S. Laminin-binding integrins and their tetraspanin partners as potential antimetastatic targets. *Expert reviews in molecular medicine* **12,** e3; 10.1017/S1462399409001355 (2010).

138. Aksoy, P., Abban, C. Y., Kiyashka, E., Qiang, W. & Meneses, P. I. HPV16 infection of HaCaTs is dependent on β4 integrin, and α6 integrin processing. *Virology* **449,** 45–52; 10.1016/j.virol.2013.10.034 (2013).

139. Kazarov, A. R., Yang, X., Stipp, C. S., Sehgal, B. & Hemler, M. E. An extracellular site on tetraspanin CD151 determines α3 and α6 integrin–dependent cellular morphology. *J Cell Biol* **158,** 1299–1309; 10.1083/jcb.200204056 (2002).

140. Giroglou, T., Florin, L., Schäfer, F., Streeck, R. E. & Sapp, M. Human Papillomavirus Infection Requires Cell Surface Heparan Sulfate. *Journal of Virology* **75,** 1565–1570; 10.1128/JVI.75.3.1565-1570.2001 (2001).

141. Payne, E., Bowles, M. R., Don, A., Hancock, J. F. & McMillan, N. A. Human papillomavirus type 6b virus-like particles are able to activate the Ras-MAP kinase pathway and induce cell proliferation. *Journal of Virology* **75,** 4150–4157; 10.1128/JVI.75.9.4150-4157.2001 (2001).

142. Li, E., Stupack, D., Klemke, R., Cheresh, D. A. & Nemerow, G. R. Adenovirus endocytosis via alpha(v) integrins requires phosphoinositide-3-OH kinase. *Journal of Virology* **72,** 2055–2061 (1998).

143. Lee, J., Lee, J., Choi, C. & Kim, J. H. Blockade of integrin α3 attenuates human pancreatic cancer via inhibition of EGFR signalling. *Scientific reports* **9,** 2793; 10.1038/s41598-019-39628-x (2019).

144. Yang, X. H. *et al.* CD151 accelerates breast cancer by regulating alpha 6 integrin function, signaling, and molecular organization. *Cancer research* **68,** 3204–3213; 10.1158/0008-5472.CAN-07-2949 (2008).

145. Berditchevski, F. *et al.* Analysis of the CD151-alpha3beta1 integrin and CD151-tetraspanin interactions by mutagenesis. *The Journal of biological chemistry* **276,** 41165–41174; 10.1074/jbc.M104041200 (2001).

146. Lang, T. & Rizzoli, S. O. Membrane protein clusters at nanoscale resolution: more than pretty pictures. *Physiology (Bethesda, Md.)* **25,** 116–124; 10.1152/physiol.00044.2009 (2010).

147. Ivaska, J. Unanchoring integrins in focal adhesions. *Nature cell biology* **14,** 981–983; 10.1038/ncb2592 (2012).

148. Yang, X. H. *et al.* Disruption of laminin-integrin-CD151-focal adhesion kinase axis sensitizes breast cancer cells to ErbB2 antagonists. *Cancer research* **70,** 2256–2263; 10.1158/0008-5472.CAN-09-4032 (2010).

149. Schelhaas, M. *et al.* Human papillomavirus type 16 entry: retrograde cell surface transport along actin-rich protrusions. *PLoS Pathogens* **4,** e1000148; 10.1371/journal.ppat.1000148 (2008).

150. Smith, J. L., Lidke, D. S. & Ozbun, M. A. Virus activated filopodia promote human papillomavirus type 31 uptake from the extracellular matrix. *Virology* **381,** 16–21; 10.1016/j.virol.2008.08.040 (2008).

151. Nobes, C. D. & Hall, A. Rho, rac, and cdc42 GTPases regulate the assembly of multimolecular focal complexes associated with actin stress fibers, lamellipodia, and filopodia. *Cell* **81,** 53–62; 10.1016/0092-8674(95)90370-4 (1995).

152. Blondelle, J. *et al.* Murine obscurin and Obsl1 have functionally redundant roles in sarcolemmal integrity, sarcoplasmic reticulum organization, and muscle metabolism. *Communications biology* **2,** 178; 10.1038/s42003-019-0405-7 (2019).

153. Aumailley, M., El Khal, A., Knöss, N. & Tunggal, L. Laminin 5 processing and its integration into the ECM. *Matrix biology : journal of the International Society for Matrix Biology* **22,** 49–54; 10.1016/s0945-053x(03)00013-1 (2003).

154. Hochdorfer, D., Florin, L., Sinzger, C. & Lieber, D. Tetraspanin CD151 Promotes Initial Events in Human Cytomegalovirus Infection. *Journal of Virology* **90,** 6430–6442; 10.1128/JVI.00145-16 (2016).

155. Feire, A. L., Roy, R. M., Manley, K. & Compton, T. The Glycoprotein B Disintegrin-Like Domain Binds Beta 1 Integrin To Mediate Cytomegalovirus Entry ▿. *Journal of Virology* **84,** 10026–10037; 10.1128/JVI.00710-10 (2010).

156. Feire, A. L., Koss, H. & Compton, T. Cellular integrins function as entry receptors for human cytomegalovirus via a highly conserved disintegrin-like domain. *Proceedings of the National Academy of Sciences of the United States of America* **101,** 15470–15475; 10.1073/pnas.0406821101 (2004).

157. Wang, X., Huang, D. Y., Huong, S.-M. & Huang, E.-S. Integrin alphavbeta3 is a coreceptor for human cytomegalovirus. *Nature medicine* **11,** 515–521; 10.1038/nm1236 (2005).

158. Wang, X., Huong, S.-M., Chiu, M. L., Raab-Traub, N. & Huang, E.-S. Epidermal growth factor receptor is a cellular receptor for human cytomegalovirus. *Nature* **424,** 456–461; 10.1038/nature01818 (2003).

159. Compton, T., Nowlin, D. M. & Cooper, N. R. Initiation of human cytomegalovirus infection requires initial interaction with cell surface heparan sulfate. *Virology* **193,** 834–841; 10.1006/viro.1993.1192 (1993).

160. Kari, B. & Gehrz, R. A human cytomegalovirus glycoprotein complex designated gC-II is a major heparin-binding component of the envelope. *Journal of Virology* **66,** 1761–1764 (1992).

161. Viswanathan, K., Verweij, M. C., John, N., Malouli, D. & Früh, K. Quantitative membrane proteomics reveals a role for tetraspanin enriched microdomains during entry of human cytomegalovirus. *PloS one* **12,** e0187899; 10.1371/journal.pone.0187899 (2017).

162. Hantak, M. P., Qing, E., Earnest, J. T. & Gallagher, T. Tetraspanins: Architects of Viral Entry and Exit Platforms. *Journal of Virology* **93**; 10.1128/JVI.01429-17 (2019).

163. Harris, H. J. *et al.* Claudin Association with CD81 Defines Hepatitis C Virus Entry. *The Journal of biological chemistry* **285,** 21092–21102; 10.1074/jbc.M110.104836 (2010).

164. Zona, L. *et al.* HRas signal transduction promotes hepatitis C virus cell entry by triggering assembly of the host tetraspanin receptor complex. *Cell host & microbe* **13,** 302–313; 10.1016/j.chom.2013.02.006 (2013).

165. Raaben, M. *et al.* NRP2 and CD63 Are Host Factors for Lujo Virus Cell Entry. *Cell host & microbe* **22,** 688-696.e5; 10.1016/j.chom.2017.10.002 (2017).

166. Stiles, K. M. & Kielian, M. Role of TSPAN9 in Alphavirus Entry and Early Endosomes. *Journal of Virology* **90,** 4289–4297; 10.1128/JVI.00018-16 (2016).

167. Wang, Z. *et al.* (Alpha)3(beta)1 integrin regulates epithelial cytoskeletal organization. *Journal of cell science* **112 (Pt 17),** 2925–2935 (1999).

168. He, J. *et al.* Dual Function of CD81 in Influenza Virus Uncoating and Budding. *PLoS Pathogens* **9**; 10.1371/journal.ppat.1003701 (2013).

169. Jolly, C. & Sattentau, Q. J. Human immunodeficiency virus type 1 assembly, budding, and cell-cell spread in T cells take place in tetraspanin-enriched plasma membrane domains. *Journal of Virology* **81,** 7873–7884; 10.1128/JVI.01845-06 (2007).

170. Krementsov, D. N. *et al.* HIV-1 Assembly Differentially Alters Dynamics and Partitioning of Tetraspanins and Raft Components. *Traffic (Copenhagen, Denmark)* **11,** 1401–1414 (2010).

171. Hogue, I. B., Grover, J. R., Soheilian, F., Nagashima, K. & Ono, A. Gag induces the coalescence of clustered lipid rafts and tetraspanin-enriched microdomains at HIV-1 assembly sites on the plasma membrane. *Journal of Virology* **85,** 9749–9766; 10.1128/JVI.00743-11 (2011).

172. Zhou, G. *et al.* Uroplakin Ia is the urothelial receptor for uropathogenic Escherichia coli: evidence from in vitro FimH binding. *Journal of cell science* **114,** 4095–4103 (2001).

173. Tham, T. N. *et al.* Tetraspanin CD81 is required for Listeria monocytogenes invasion. *Infection and immunity* **78,** 204–209; 10.1128/IAI.00661-09 (2010).

174. Green, L. R. *et al.* Cooperative role for tetraspanins in adhesin-mediated attachment of bacterial species to human epithelial cells. *Infection and immunity* **79,** 2241–2249; 10.1128/IAI.01354-10 (2011).

175. Vences-Catalán, F. & Levy, S. Immune Targeting of Tetraspanins Involved in Cell Invasion and Metastasis. *Frontiers in immunology* **9**; 10.3389/fimmu.2018.01277 (2018).

176. Pagel, J. M. *et al.* Otlertuzumab (TRU-016), an anti-CD37 monospecific ADAPTIR(™) therapeutic protein, for relapsed or refractory NHL patients. *British journal of haematology* **168,** 38–45; 10.1111/bjh.13099 (2015).

177. Lurain, N. S. & Chou, S. Antiviral drug resistance of human cytomegalovirus. *Clinical microbiology reviews* **23,** 689–712; 10.1128/CMR.00009-10 (2010).

178. Meuleman, P. *et al.* Anti-CD81 antibodies can prevent a hepatitis C virus infection in vivo. *Hepatology (Baltimore, Md.)* **48,** 1761–1768; 10.1002/hep.22547 (2008).

179. Wang, H., Jin, H., Beauvais, D. M. & Rapraeger, A. C. Cytoplasmic domain interactions of syndecan-1 and syndecan-4 with α6β4 integrin mediate human epidermal growth factor receptor (HER1 and HER2)-dependent motility and survival. *The Journal of biological chemistry* **289,** 30318–30332; 10.1074/jbc.M114.586438 (2014).

180. Day, P. M. & Schiller, J. T. The role of furin in papillomavirus infection. *Future microbiology* **4,** 1255–1262; 10.2217/fmb.09.86 (2009).

8 Acknowledgements

I would like to thank Prof. Dr. Thorsten Lang for giving me the opportunity to work in his group and on this very interesting and relevant topic. I am grateful for his constant support, supervision and for the fruitful discussions, we had.

I also want to thank Dr. Luise Florin and her lab, especially Snježana Mikuličić, for the collaboration on this project. Without their contribution, support and know-how about HPV, this work would never have been possible.

I would like to thank all current and former members of the Lang group for the great and enjoyable working atmosphere. Special thanks go to Dennis de Coninck, Dr. Yahya Homsi and Dr. Elisa Merklinger for getting me started in this new field and to new methods. Thanks a lot also to Dr. Gero Schlötel for his constant technical advices with the STED microscope. Thanks to my lab companions Nikolas Hochheimer, Lisa Hitschler, Dominik Sons, Jasmin Mertins, Ricarda Sies and Vivien Averesch for the help, advices, fruitful discussions and particularly for the great atmosphere in and outside the lab.

I owe a lot to Lisa Hitschler and Dominik Sons who helped me out with data acquisition and analysis (see Figure 5.7, 5.26 and 5.28) during the stressful times of revisions and contributed to the success of this study.

Thanks a lot to Christina Sagorny and Lisa Hitschler for the time and effort you spent on boring task of proof-reading this thesis!

And of course, I want to thank all members of the LIMES institute for the help, support and sharing of instruments.

I am grateful for the funding of the DFG that allowed me to conduct the research necessary for this work.

I would like to thank my friends outside the institute for their support, friendship and helping me through the good and the bad times of the PhD. I don’t know, if I would have made it without you!

And last but not least I want to thank my family for their constant support. I am especially grateful to my parents, Evelyne Laval-Finke and Eckhardt Finke, who made all this possible in the first place. Your love and unshakable belief in me helped me making it through and keeping me motivated and grounded.